Geir Watterud

Determination of oxygen transport coefficients in perovskites and perovskite related materials with mixed conductivity

Doctoral thesis
for the degree of doktor ingeniør

Trondheim, July 2005

Norwegian University of Science and Technology
Faculty of Natural Sciences and Technology
Department of Materials
Science and Engineering

NTNU
Innovation and Creativity

IMT-Report 2005:73
IUK-Thesis 115

NTNU
Norwegian University of Science and Technology
Doctoral thesis
for the degree of doktor ingeniør
Faculty of Natural Sciences and Technology
Department of Materials Science and Engineering

ISBN 82-471-7275-5 (printed vers.)
ISBN 82-471-7274-7 (electronic vers.)
ISSN 1503-8181

Doctoral theses at NTNU, 2005:191
IMT-Report 2005:73
IUK-Thesis 115

Printed by NTNU-trykk

PREFACE

First of all, I want to thank my main supervisor Associated Professor Kjell Wiik for the guidance and support and for all the good discussions about oxygen transport in perovskites during my period as a Ph.D. student. This has been invaluable for my work. I would also like to thank my co-supervisor Dr. Techn. Stein Julsrud whose experience and knowledge has been of great help to fulfil this thesis. Next, I would like to thank Professor Tor Grande and Professor Mari-Ann Einarsrud for being interested in my work and answering questions about all the small matters that lies underneath this work.

I would also like to thank the rest of the "uorganisk" part of the Department of Materials Science and Engineering, fellow Ph.D. students, technical staff and others for making a fun working environment, for all the non-official coffee breaks and for all the relevant and irrelevant discussions.

Financial support from Norsk Hydro is appreciated.

Finally I would like to thank my family for the support and my three children Sander, Otilie and Ingard for never asking me about oxygen transport but: "Can we play, dad?" My biggest gratitude goes to my dear wife Stine, I could not have done this without you.

Trondheim, July 2005

Geir Watterud

TABLE OF CONTENT

SCIENTIFIC PAPERS

APPENDICES

LIST OF ACRONYMS

CD	Crystallographic density
LC	$LaCoO_3$
LSC-02	$La_{0.8}Sr_{0.2}CoO_{3-\delta}$
LSC-05	$La_{0.5}Sr_{0.5}CoO_{3-\delta}$
MIEC	Mixed Ionic and Electronic Conductivity
OPM	Oxygen Permeable Membrane
P_{O2}	Partial pressure of oxygen (O_2)
SEM	Scanning Electron Microscopy
SOFC	Solid Oxide Fuel Cell
ST	$SrTiO_3$
STA-02	$SrTi_{0.98}Al_{0.02}O_3$
STA-05	$SrTi_{0.95}Al_{0.05}O_3$
XRD	X-Ray Diffraction
YSZ	Yttria-Stabilized Zirconia

1 SUMMARY

Perovskites and perovskite related materials are materials that are candidates for applications such as oxygen permeable membranes, cathodes for SOFC and high-temperature oxygen sensors. This arises from the potential high ionic conductivity and the chemical stability even at low partial pressures of oxygen. From an application point of view, it is important to have knowledge about the oxygen transport properties in these materials. Oxygen transport in mixed conducting oxides involves two inherently different processes; oxygen exchange between bulk gas and surface and solid state diffusion. The objective of this work has been to obtain fundamental understanding of these transport properties in mixed ionic and electronic conductors. For that purpose two materials systems with significant differences in electronic conductivty and oxygen vacancy concentration were chosen as objectives for the investigation, viz.: Sr-substituted $LaCoO_3$ and Al-substituted $SrTiO_3$.

All transport properties (diffusion and surface exchange) have been assessed by electrical conductivity relaxation, and the work also evaluate the pros and cons using this specific method to obtain transport data for the materials in question.

In the first two papers (Paper 1 and Paper 2) transport properties are derived for $La_{1-x}Sr_xCoO_{3-\delta}$ (x=0 (LC), 0.2 (LSC-02) and 0.5 (LSC-05)). In Paper 1 "chemical transport coefficients", D_{chem} and k_{chem}, are reported. More fundamental transport coefficients, such as oxygen component diffusion coefficient (D_O) and vacancy diffusion coefficients (D_V), are also deduced and discussed. Activation energies for D_O and D_V, were determined. The activation energies for D_O varies from 279 kJ/mol for LC to 174-222 kJ/mol for LSC-02 and 90-105 kJ/mol for LSC-05, decreasing with increasing Sr-content. The activation energies for the vacancy diffusion coefficient, D_V, are smaller than for the component diffusion coefficients and typical values are 77 kJ/mol for LC, 85 kJ/mol for LSC-02 and 75 kJ/mol for LSC-05, that is, almost independent of Sr-content. The enthalpies of vacancy formation decreases with increasing Sr content. The values are 206 kJ/mol for LC, 75 kJ/mol for LSC-02 and 15 kJ/mol for LSC-05, which agrees well with values reported in the literature. However, the vacancy diffusion coefficient showed an unexpected increase at high concentrations of oxygen vacancies, corresponding to δ=0.27-0.30. The phenomena with a P_{O2} dependent D_V is discussed.

In Paper 2, the oxygen surface exchange coefficient, k_0, is derived from "chemical values" reported in Paper 1, and used as a basis to deduce probable reaction mechanisms associated with surface exchange. The temperature dependency plots showed that for the composition with x = 0.5, the k_0 made a shift in activation energy from ~120 kJ/mol to ~15 kJ/mol above 950 °C. It is suggested that this significant shift in activation energy might be due to an oxygen adsorption/desorption mechanism on the surface becoming rate controlling at high temperatures. The composition with x=0.2 did not show this shift in activation energy. Relations between possible rate controlling reactions and reaction rates (k_0) were established, and formed the basis for discussions on probable rate controlling processes. There are reasons to assume that for oxidation prosesses a rate controlling reaction involving a direct "installation" of an oxygen molecule into two vacancies is dominating, while a dissociation of an oxygen molecule generally gives a better description for a reduction process.

In Paper 3 the oxygen transport properties in $SrTi_{1-x}Al_xO_3$ (x=0 (ST), 0.02 (STA-02) and 0.05 (STA-05)) were determined in O_2/N_2 mixtures. In this contribution the electrical conductivity is also presented in a large P_{O2}-interval (O_2/N_2- and CO/CO_2-mixtures). Electrical conductivity for pure $SrTiO_3$ (ST) in terms of P_{O2} applied well with defect chemistry reported in the literature. For the two Al-substituted compositions the electrical conductivity followed predicted behaviour at high and low P_{O2}'s. However, in the medium P_{O2} range we were not able to describe the conductivity behaviour in terms of classical defect chemistry. Reasons for the discrepancy is discussed.

D_{chem} for ST and STA-02 are reported and are, along with their corresponding activation energies, 187 and 104-180 kJ/mol, respectively, in good accordance with values from literature. Furthermore, values for the component diffusion coefficient, D_O, and the vacancy diffusion coefficient, D_V, are reported for ST at 950 °C, the only composition where oxygen vacancy concentrations are available in the literature. Values for k_{chem} in STA-02 and STA-05 are also reported, and show pronounced P_{O2} dependencies. For STA-05 the activation energy for k_{chem} is found to vary between 90 and 105 kJ/mol. Due to a high uncertainty, activation energies are not reported for STA-02.

Reported D_{chem} and k_{chem} values for related materials in literature indicate increasing numeric values with decreasing concentration of oxygen vacancies. It is reasoned that this is due to an ever increasing termodynamic

factor with decreasing population of vacancies. The implications for the component diffusion coefficient is discussed.

In Paper 4 the oxygen transport properties in $SrTiO_3$ pure and with Al were investigated in mixtures of CO/CO_2. D_{chem} are reported for ST and STA-02 while k_{chem} are reported for ST, STA-02 and STA-05. The D_{chem} showed a P_{O2}-dependency, which can be explained by the variation in the thermodynamic factor. The introduction of Al in the sample increases the value of D_{chem}, probably due to the introduction of more oxygen vacancies. STA-02 showed a discrete increase in D_{chem} in the CO-rich atmospheres, this may be due to phase transition or phase separation at $P_{O2} \sim 10^{-17}$ atm. The k_{chem} showed a maximum at $P_{CO}/P_{CO2} = 1$ for STA-02 and STA-05. This behaviour corresponds well with a rate controlling reaction involving a charged and adsorbed CO_2 molecule. The same maximum is also reported in the literature for $BaTiO_3$ wihtout and with 1.8 % Al and for $La_{0.9}Sr_{0.1}FeO_3$.

This work has examined chemical diffusion and surface exchange coefficients with electrical conductivity relaxation in two material systems with distinct differences in electrical conductivity and oxygen vacancy concentrations. The main focus has been to elucidate properties of the transport coefficients based on own measurements, but also include transport coefficients from other material systems from literature as references. The vacancy diffusion coefficients have been examined, showing that they increase with increasing concentration of oxygen vacancies in materials where the concentration of vacancies is high. No obvious reason for this behaviour has been found, however, it may be related to a change in activation energy. It is rather well established in the literature that for materials where the concentration of vacancies may be characterized as dilute, we should expect a D_V independent of the population of vacancies. Finally, based on own results and data reported in the literature it appears that with respect to the oxygen surface flux the oxygen vacancy concentration seems to be the property of most importance. That is, for oxidation processes the oxygen exchange flux will increase with vacancy population.

2 INTRODUCTION

2.1 Background

The large natural gas reserves in Norway and other oil-producing countries combined with the increasing demand of electrical energy and the generally decreasing oil reserves worldwide have lead to an extensive research into new and alternative methods for power generation as well as methods for upgrading natural gas to value-added products. Some of the technologies corresponding to these methods are technologies utilising Solid Oxide Fuel Cells (SOFC) and Oxygen Permeable Membranes (OPM).

2.1.1 Reformation of natural gas

Although natural gas reserves already exceed the oil reserves, only a small fraction of natural gas is being used as feed stock in the petro-chemical industry. During the last years a lot of research has been performed in order to convert the most abundant component in natural gas, methane, to value-added products. In the conventional route for converting methane to methanol, syngas ($CO + H_2$) is produced in the first stage by partial oxidation of methane, and processes with methane conversion efficiencies higher than 99% [1] has been reported. Also, large amounts of purified oxygen are needed and a significant cost is associated with the production of pure oxygen. A possible low cost route for production of oxygen is via an OPM-system.

2.1.2 Solid Oxide Fuel cells

SOFCs are devices that can convert chemical energy from natural gas directly to DC electricity and with the large resources of natural gas there is a potential of exploitation of this technology. The theoretical advantages of this technology are low emissions of NO_x and SO_x, high efficiency and fuel adaptability [2]. There are however practical issues to solve [3].

SOFCs consist of a dense oxygen-ion-conducting electrolyte with two porous electrodes made of mixed ionic-electronic conductor (MIEC) on each side. The SOFC operation principle is presented in Fig.1.

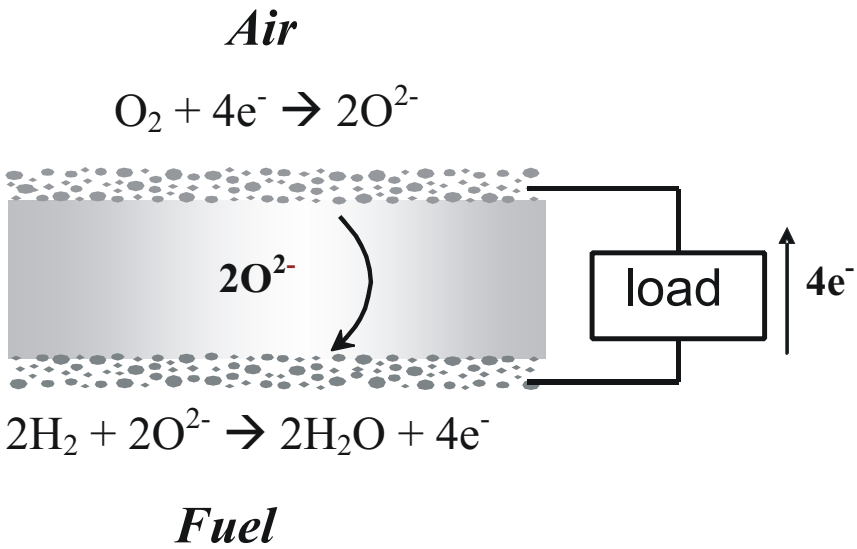

Fig. 1. The principle of a Solid Oxide Fuel Cell. Reduction of oxygen occurs at the cathode (air side), while oxidation of H_2 (or a natural gas) occurs at the anode (fuel side). The electrons flow in an external circuit. Figure from Wærnhus [54].

In a SOFC molecular oxygen is reduced at the cathode (air electrode) by electrons supplied from an external circuit, and form oxygen ions (O^{2-}) through a surface reaction. The oxygen ions diffuse through the solid electrolyte to the anode (fuel electrode) and oxidise the fuel liberating electrons.

A number of different design approaches have been put forward during the years including planar-, monolithic-, segment-cell-series- and tubular geometries [4, 5, 6]. A number of material requests must be fulfilled for the cell components (anode, interconnecting material, electrolyte and cathode) comprising chemical, phase, morphological and dimensional stability in oxidising and/or reducing environments. They also need to be chemically compatible with the other components in order to avoid growth of secondary phases at the interfaces. In addition the materials should have similar coefficient of thermal expansion to avoid separation and cracking during fabrication and operation.

The main functional property for the dense electrolyte is high ionic conductivity. Traditionally the most used material is stabilised zirconia (ZrO_2), especially yttria-stabilized zirconia (YSZ), because of its level of ionic conductivity at around 1000°C and the stability in both oxidising and reducing environments. During the last decade lanthanum gallate ($LaGaO_3$) substituted with Mg and Sr has shown higher ionic conductivity than the

YSZ and is therefore also an electrolyte candidate material [7]. The properties of stabilised zirconia have been extensively studied [8,9,10]. Because of the high operating temperature only noble metals or electronically conducting oxides can be used as a cathode material in combination with YSZ. However, noble metals such as platinum, palladium and silver are unsuitable because of prohibitive cost. Several substituted oxides and mixed oxides have been proposed and investigated [11,12]. The disadvantages for most of these materials are thermal expansion mismatch, incompatibility with the electrolyte and poor conductivity. The electrodes need to have high electronic conductivity and sufficient porosity to promote transport of reactants and products in and out of from the interface between the electrode and the electrolyte, where the incorporation of oxygen is believed to take place on the triple-phase boundary. As a cathode material lanthanum manganites substituted with Sr and/or Ca are most commonly used [12], due to their high electronic conductivity, stability in both oxidising and reducing environments and relatively good compatibility with YSZ. Because of the reducing conditions of the fuel gas, metals may be used as SOFC anode materials. Nickel is most used because of its low cost. To maintain the porous structure and to provide a thermal expansion coefficient acceptably close to those of the other cell components, nickel metal is often dispersed on the surface of an YSZ support (nickel/YSZ cermet). Due to the strict requirements for the interconnect material in the SOFC (i.e. chemical, mechanical and functional stability) only a few oxide systems are relevant. Lanthanum chromites ($LaCrO_3$), with Sr and Ca, are particularly suitable with respect to the requirement of a high electronic conductivity in both reducing and oxidising atmosphere. The compound also possesses an excellent stability and is compatible with other cell components. Currently $LaCrO_3$ is the most common material for interconnect in SOFC's. However by lowering the operational temperature, metals may become candidate materials as interconnect [14].

2.1.3 Oxygen permeable membranes (OPM)

Several perovskites exhibit mixed electronic and oxygen ionic conductivity (MIEC). These materials are receiving considerable attention due to their possible applications in oxygen separation and partial oxidation of natural gas [15,16,17,18,19]. The advantage of a MIEC compared to a pure ionic conductor such as YSZ, is that no external electrodes is required for operation. If the partial pressure gradient of oxygen across the membrane is sufficient (driving potential of transport), oxygen is spontaneously transferred from the high P_{O2} side to the low P_{O2} side. Several different designs have been proposed for the OPM: hollow-tubes, honeycomb or disk reactors. Regardless of the design, a gas-tight seal between the membrane

and the surrounding material(s) is essential. The sealing material should be chemically inert to the other materials and have good sealing properties in a wide temperature range.

The transport of oxygen through an OPM involves similar processes as for a SOFC. The oxygen transport consists of two inherently different processes; oxygen exchange between bulk gas and surface and solid state diffusion. The surface reaction may involve a number of steps, which from an oxidation point of view may comprise adsorption, charge transfer, dissociation and finally "installation" in a vacancy.

Perovskite-related oxides are one material group that has attracted a lot of attention due to their suitable transport properties and stability under different atmospheres [18,19,20,21,22,23]. By substitution of the cations on the A site and/or the B site, the materials can be tailored for the desired functional properties (e.g. electronic and ionic conductivity). The material system La-M-Fe-Co-O (M= Sr, Ba, Ca) with various compositions at the A- and B-site in the perovskite exhibits high oxygen permeation fluxes and appreciable electronic conductivity at 800 ºC [24,25,26,27,28]. These materials are thus candidate materials for dense oxygen permeable membranes.

2.1.4 Other applications for oxygen conducting materials

Perovskite materials such as $La_{1-x}Sr_xFeO_3$ are candidate materials for conductometric oxygen sensors, since their electrical conductivity depends on oxygen partial pressure and temperature. The material is also stable in a wide range of oxygen partial pressure [29,30]. Oxygen sensors most commonly used, such as stabilized ZrO_2 [31], requires a reference partial pressure of oxygen which is not necessary for the application of mixed conducting perovskites.

MIEC-perovskites are also candidate materials as oxidation catalysts [32,33].

2.2 Aim of the present work

Oxygen transport in oxides with mixed conductivity (ionic and electronic) involves two inherently different processes; oxygen exchange between bulk gas and surface and solid state diffusion. To some extent solid state oxygen diffusion is explained for materials with moderate concentration of oxygen vacancies, whereas the kinetics associated with the exchange of oxygen

between the ambient gas and oxide surface is less well comprehended. A large number of properties may in principle affect both bulk diffusion and surface exchange processes. In this work we have chosen to focus on the possible importance of electronic conductivity (n and p) and oxygen vacancies. Thus, we have chosen to examine two different material systems exhibiting high concentration of both vacancies and electronic species and low concentrations of the same species, respectively: The material systems are $La_{1-x}Sr_xCoO_3$ (x = 0, 0.2 and 0.5) which shows metallic conduction corresponding to ~1000 S/cm at 1000 °C and also possess a high oxygen vacancy concentration increasing with Sr content. The "opposite end" of the defect concentrations is represented by the semi conducting material $SrTi_{1-x}Al_xO_3$ (x=0, 0.02, 0.05), showing an electrical conductivity of ~ 0.01 S/cm at 1000 °C and a corresponding low oxygen vacancy concentration increasing with the substitution level of Al. It is worth to notice that the variation in electrical conductivity is five orders of magnitude between the cobaltites and the titanates.

All transport properties (diffusion and surface exchange) have been assessed by electrical conductivity relaxation, and the work also evaluate the pros and cons using this specific method to obtain transport data for the materials in question.

In Paper I the chemical diffusion coefficient, D_{chem}, and the chemical surface exchange coefficient, k_{chem}, are derived from conductivity relaxation in the material system $La_{1-x}Sr_xCoO_3$ (x = 0, 0.2 and 0.5). The main concern has been to establish the behaviour of solid state diffusion at conditions where the concentration of oxygen vacancies are high. In Paper II more fundamental surface kinetic coefficients (k_0) are deduced based on the chemical values from Paper I, aiming at giving a description of the probable rate controlling reactions taking place at the oxide surface

In Paper III Al-substituted $SrTiO_3$ has been investigated in O_2/N_2-atmospheres with main focus on the importance of electrical conductivity and oxygen vacancies with respect to oxygen exchange and transport. In Paper IV we are aiming at giving a description of bulk diffusion and surface exchange at very low partial pressures of oxygen, that is, in mixtures of CO/CO_2.

2.3 The perovskites

Perovskites are a rather large group of compounds with closely related crystal structures, which has taken name from the natural mineral $CaTiO_3$. The general formula of the perovskites is ABX_3, in which A and B is cations, and X is oxygen or fluorine [34]. The oxide perovskites (from now on called the perovskites, omitting the fluorides) have widely varying electrical and magnetic properties, which make them interesting for several applications. Areas of applications where the perovskites are of interest are reformers of natural gas, solid oxide fuel cells (SOFC), oxygen permeable membranes (OPM), oxidation catalysts, oxygen sensors and others.

Many ternary oxides crystallise in the perovskite structure. In the general formula for a perovskite ABO_3, A is a large cation usually an alkali metal, an alkaline earth metal or a rare earth metal while B is a smaller cation, often a transition metal. Several different combinations of oxidation states of the cations are possible, such as $A^{I}B^{V}O_3$, $A^{II}B^{IV}O_3$ and $A^{III}B^{III}O_3$. The ideal perovskite structure can be described as consisting of corner-sharing BO_6 octahedra with the large A cation occupying the body centred, 12 –co-ordinated position. The cubic perovskite structure is illustrated in Fig. 2.

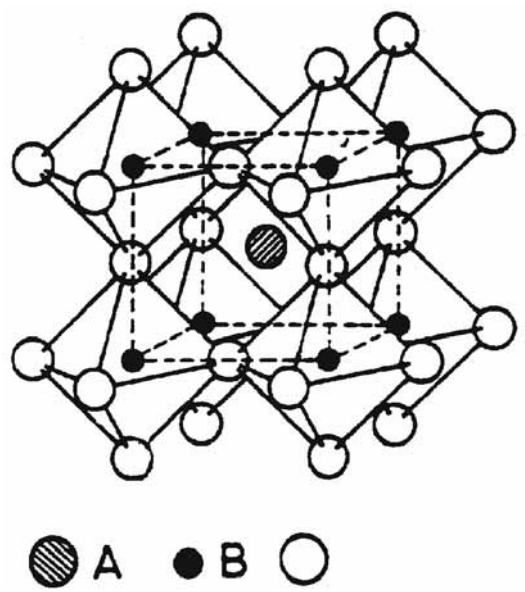

Fig. 2. Schematic drawing of the ideal cubic perovskite structure. Figure from Rao et al. [34]

Rotation or tilting of the BO_6 octahedra, or displacement of the cations, will give a lower symmetry corresponding to e.g. tetragonal, orthorhombic or rhombohedral structures. The unit cell volume will also increase [35]. The possibility for a ternary oxide to crystallise in the perovskite structure can be predicted using the Goldschmidt tolerance factor [36].

$$t = \frac{r_A + r_O}{\sqrt{2}(r_B + r_O)} \quad (1)$$

where r_i denotes the ionic radius of the given ion. Perovskite structures are formed for $0.75 \leq t \leq 1.06$. The ideal cubic perovskite structure has t=1, comprising only a few oxides.

Another important parameter for the crystal symmetry is the nonstoichiometry arising from cation deficiency or oxygen deficiency. The sum of valences of the cations will determine the oxygen stoichiometry, and then again the crystal structure. Vacancies on the anion site are more common than on the cation site, thus, oxygen deficiency in perovskites is more common than vacancies on the cation sublattice. However, metal deficient materials like $LaMnO_{3.16}$ are also known [37]. For perovskites and oxides in general the concentration of vacant oxygen sites can vary several orders of magnitude due to material composition, temperature and oxygen partial pressure, giving rise to many interesting applications of the materials. When B is a transition metal, its valence state will depend on the oxygen partial pressure and temperature. A change in the valence state of the B cation will be compensated by a change in the oxygen stoichiometry. If the oxygen vacancies order so-called superstructures may appear, leading to larger unit cells. The most common in the case of perovskites is the Brownmillerite-structure with the general formula $ABO_{2.5}$ (or $A_2B_2O_5$), where every third oxygen is replaced by a vacancy [38].

2.3.1 Structural properties of Lanthanum coboltite

The lanthanum coboltites ($LaCoO_3$) are materials with a perovskite-related structure. The pure $LaCoO_{3-\delta}$ has a rhombohedral displacement at room temperature [39-43]. With substitution of lanthanum for strontium, the transition from rhombohedral to cubic will be a function of temperature and degree of substitution. When aliovalent cations are introduced, or the temperature is increased, more oxygen vacancies will be formed in the structure, favouring a cubic structure. This transition is given by Petrov et al. [40] and shown in Fig 3.

Mineshige et al. [44] and van Doorn et al. [45] showed that for strontium substituted lanthanum coboltite $La_{1-x}Sr_xCoO_{3-\delta}$, the transition from

rhombohedral to cubic is at x = 0.5, while Kharton et al. [46] showed a transition for x = 0.6. The $SrCoO_{3-\delta}$, (x=1), has been reported to adopt a cubic perovskite structure when $\delta<0.5$ [38], however that requires treatment at very high oxygen partial pressures (P_{O2} > 50 bars). Others have reported coexistence of perovskite and brownmillerite structures, i.e. phase separation above 800 °C [47].

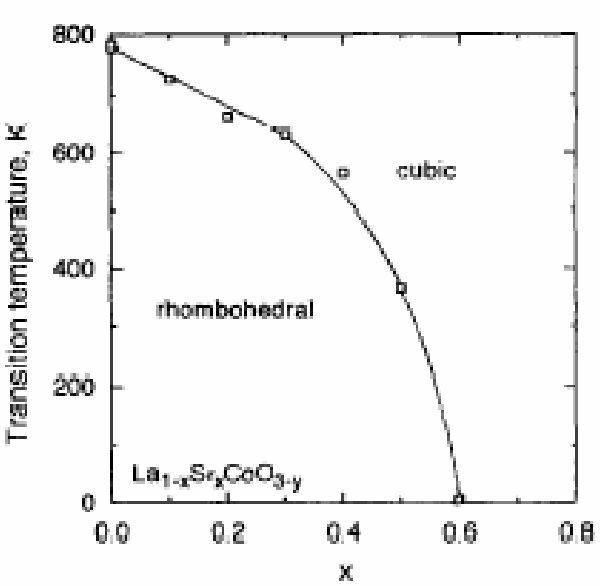

Fig. 3. Transition temperature from rhombohedral to cubic in $La_{1-x}Sr_xCoO_{3-\delta}$ as a function of Sr-content. Figure from Petrov et al. [40]

Säppanen et al. have examined stability [48] and the oxygen nonstoichiometry [49] as a function of oxygen partial pressure in pure $LaCoO_3$, concluding that pure $LaCoO_3$ is stable at $P_{O2}> 10^{-5}$ atm at 1000 °C.

2.3.2 Structural properties of Strontium titanate

The $SrTiO_3$ adopts the cubic perovskite structure above 105 K [50], and is stable in a wide P_{O2} window, ranging from reducing H_2/H_2O mixtures to air-like compositions at 1000 °C. $SrTiO_3$ may also be substituted at both A and B-site to form solid solutions with specific material properties. Lanthanum and barium can be substituted on the A-site, while iron, zirconium and aluminium can be substituted on the B-site [50]. In some cases the substituted solid solutions will deviate from cubic symmetry, at least when the level of substitution exceeds a certain value. Steinsvik et al. [51] investigated the phase compositions in $SrTi_{1-x}Fe_xO_{3-y}$ (x=0-0.8), finding the material to be cubic in the whole range. The structure of aluminium

substituted $SrTiO_3$ is believed to be cubic in almost the same range as for iron substituted since the ionic radiuses of 6 co-ordinated Al^{3+} and Fe^{3+} are similar [52].

2.4 Relation between electron structure and oxygen nonstoichiometry

The defect chemistry of a material can be described in different ways. In a point defect model, the species such as electrons, electron holes, anion and cation vacancies and aliovalent substituted ions, are located at specific lattice sites and thus categorized as localized. In a band model approach, the electrons are donated to a conduction band, and thus no longer localized. It is also possible to describe the defect chemistry as a mixture between the two mentioned models.

2.4.1 Localised electrons and the concept of polarons

In a material with localized electrons, the electronic transport is assumed to consist of charge transfer between localized sites in the structure. This transport is referred to as polaron jumping. In this case, it is possible to describe the defect chemistry by a point defect model. The defect chemistry for the system $La_{1-x}Sr_xFeO_{3-\delta}$ is well described by a point defect model as outlined by Mizusaki et al. [53] and later reviewed and extended by Wærnhus et al [54]. The interaction between oxygen in the atmosphere and in the material can be described by

$$O_O^x + 2Fe_{Fe}^x = V_O^{\bullet\bullet} + 2Fe_{Fe}^{'} + \frac{1}{2}O_2(g) \tag{2}$$

In Eq.(2) Kröger-Vink notation is used [55].

In Eq.(2), it can be seen that the iron changes its valence from 3+ to 2+, thus the extra electrons released are located on iron-sites. Thus, the electrons are located and consequently contribute to the configurational entropy.

In the $LaFeO_3$ system, the electronic defects are located on iron-sites. This can be described by a disproportionation reaction

$$2Fe_{Fe}^x = Fe_{Fe}^{\bullet} + Fe_{Fe}^{'} \tag{3}$$

, describing how two initially three-valent iron cations can exchange an electron giving a two valent and a four valent cation. Introducing the site balance

$$\begin{aligned} [La_{La}^{x}]+[Sr_{La}^{'}] &= 1 \\ [Fe_{Fe}^{x}]+[Fe_{Fe}^{'}]+[Fe_{Fe}^{\bullet}] &= 1 \\ [O_{O}^{x}]+[V_{O}^{\bullet\bullet}] &= 3 \end{aligned} \qquad (4)$$

, and the charge balance (condition for electroneutrality).

$$[Sr_{La}^{'}]+[Fe_{Fe}^{'}]=[Fe_{Fe}^{\bullet}]+2[V_{O}^{\bullet\bullet}] \qquad (5)$$

, where [Sr_{La}'] is the concentration of strontium on the lanthanum site.
By utilizing the reactions and relations given in Eqs (2) to (5) with corresponding equilibrium constants from Eq. (2) and (3), a mathematical basis consistent with a localized model can be derived describing the defect chemistry for the system $La_{1-x}Sr_xFeO_{3-\delta}$.

The defect chemistry for $SrTiO_3$ has been studied by a number of authors [56,57,58,59,60,61,62, 63]. For the case of $SrTiO_3$ the situation is somewhat different than for the $LaFeO_3$ system. The main difference being that the charge disproportionation reaction given in Eq. (3) can not be applied to four valent Ti on the B- site. Thus, applying the charge neutrality condition, the conservation of mass on each site in the structure and the equilibrium constants from each of the reactions, a model may be derived describing the defect chemistry in $SrTiO_3$.

2.4.2 Delocalised electrons and the concept of the band model

For the compound $La_{1-x}Sr_xCoO_{3-\delta}$, a localized electron model can not describe the defect chemistry, as opposed to the $La_{1-x}Sr_xFeO_{3-\delta}$ system. Experimental data for oxygen nonstoichiometry and Seebeck coefficient applied on a charge disproportionation model for the cobalt, Eq. (3), led to inconsistent results [64]. The oxygen nonstoichiometry has been examined by Mizusaki et al. [41] and Petrov et al. [65] with thermogravimetric measurements and coulometric titration, respectively. By utilising the data from Mizusaki et al. [41] and Petrov et al. [65], and data from coulometric titration, Lankhorst et al. [64,66-69] put forward a model for the nonstoichiometry based on itinerant electrons, i.e. not localised electrons, with a rigid electron band. The high electronic conductivities and low Seebeck coefficients [70,71] support this itinerant electron model. The main

difference between the itinerant and localized electron model for nonstoichiometry is that the coboltites do not have any configurational entropy in the Co- sublattice, since the electrons can not be localised on the cobalt cations as for the iron cations cf. Eq. (3)

The substitution of Sr into $LaCoO_3$ can be described by

$$2SrO \xrightarrow{LaCoO_3} 2Sr'_{La} + 2O_O^x + V_O^{\bullet\bullet} \tag{6}$$

Thus more oxygen vacancies are introduced.

The reversible oxidation reaction can be written as

$$O_2(g) + 2V_O^{\bullet\bullet} + 4e^- \rightleftarrows 2O_O^x \tag{7}$$

In Eq. (7), the electrons are delocalised.

By introducing the chemical potential μ_i for each specie i, the equilibrium condition for reaction (7) is

$$\mu_{O_2} + 2\left(\mu_{V_O^{\bullet\bullet}} - \mu_{O_O^x}\right) + 4\mu_{e'} = 0 \tag{8}$$

The oxygen vacancies are assumed to be randomly distributed among equivalent sites and do not interact, while the conduction electrons are delocalised occupying energy levels in a partially filled, rigid electron band. With this assumption we may write the chemical potential for the structure elements, i, viz [68]:

$$\mu_i = \mu_i^0 + RT \ln\left(\left[x_i\right]\right) \tag{9}$$

, where x_i is the mole fraction of specie i , and μ_i^0 is the standard chemical potential for specie i.

The middle term in Eq. (8) includes the chemical potentials for the oxygen structure elements. This can be written as

$$\mu_{V_O^{\bullet\bullet}} - \mu_{O_O^x} = \mu_V = \mu_V^0 + RT \ln\left(\frac{\left[V_O^{\bullet\bullet}\right]}{3 - \left[V_O^{\bullet\bullet}\right]}\right) \tag{10}$$

, where μ_V is an abbreviation for the chemical potentials for oxygen ions and vacancies and $\mu_V^0 = \mu_{V_O^{\bullet\bullet}}^0 - \mu_{O_O^x}^0$ is the standard chemical potential.

Taking the electron band to be rigid, it is possible to relate the chemical potential of the electron specie with the electron occupancy (concentration) [e′] and density of states at the Fermi level, $g(\varepsilon_F)$ [67].

$$\mu_{e'}\left(\left[e'\right]\right) = \mu_{e'}\left(\left[e'\right]=\left[e'\right]^0\right) + \frac{\left(\left[e'\right]-\left[e'\right]^0\right)}{g\left(\varepsilon_F\right)} \tag{11}$$

$[e']^0$ is defined as the electron occupancy at zero vacancy concentration and zero Sr substitution, thus, this is the standard condition. The entropy part for the electrons in Eq. (11) is neglected by assuming that the electron band is broad.

Inserting Eqs (10) and (11) into Eq. (8) and combining with the charge neutrality condition for the system

$$[e']-[e']^0 = 2[V_O^{\bullet\bullet}]-\left[Sr_{La}'\right] = 2[V_O^{\bullet\bullet}]-x \tag{12}$$

where x is the degree of Sr- substitution, one gets the rigid band model as put forward by Lankhorst et al. [66]

$$\mu_{O_2}^{oxide} = \varepsilon_{O_2}^{oxide} - Ts_{O_2}^{oxide} = E_{ox} - \frac{4(2\left[V_O^{\bullet\bullet}\right]-x)}{g(\varepsilon_F)} - TS_{ox} - 2RT\ln\left(\frac{\left[V_O^{\bullet\bullet}\right]}{3-\left[V_O^{\bullet\bullet}\right]}\right) = \mu_{O_2}^{gas} \tag{13}$$

where E_{ox}, S_{ox} are the standard free energy and entropy for oxidation. The values for the parameters E_{ox}, S_{ox} and $g(\varepsilon_F)$ are given in Tab. 1, and μ_{O2}^{gas} is described in App. 2.

Table. 1. Parameters used to calculate the oxygen nonstoichiometry in LSC-02 and LSC-05 taken from Ref [66]. The values for x = 0.5 are obtained by interpolation between x = 0.4 and 0.7.

Parameter	x = 0.2	x =0.4	x = 0.5 Interpolated between x=0.4 and 0.7	x=0.7
E_{ox} (kJ/mol)	-334.1	-301.4	-299	-294.5
S_{ox} (J/mol K)	69.5	69.6	70	70.5
$g(\varepsilon_F)$ $[(kJ/mol)^{-1}]$	0.0159	0.0159	0.0155	0.0152

The oxygen nonstoichiometry can be calculated by using Eq. (13) and the associated parameters.

The model in Eq.(13) fits well with experimental data for the oxygen nonstoichiometry [66], and thus the simplification can be justified.

2.5 Calculations of the transport parameters D_{chem} and k_{chem} from electrical conductivity relaxation experiments.

The experimental setup for the conductivity relaxation experiments are described in Paper I of this thesis [72].

The full mathematical treatment is given in Appendix 1. Only a brief summary will be given here. The parameters D_{chem} and k_{chem} are calculated from the solution of Ficks second law

$$\frac{\partial C(x,t)}{\partial t} = D_{chem} \frac{\partial^2 C(x,t)}{\partial x^2} \tag{14}$$

where C is the concentration of oxygen in the sample, D_{chem} is the chemical diffusion coefficient, x is the dimension and t is the time. The subscript for concentration is omitted, but refers to oxygen species. The boundary conditions give the mathematical definition of the k_{chem} parameter, viz.:

$$J_O(x=\pm l_x) = \mp D_{chem}\frac{\partial C(x=\pm l_x,t)}{\partial x} = k_{chem}\left(C(x=\pm l_x,t) - C_\infty\right) \quad (15)$$

, where J_O denotes the oxygen flux (mono atomic) at the surface and C_∞ is the oxygen concentration at t=∞, i.e. at equilibrium. This is also derived by ten Elshof et al [73] and van der Haar et al. [74].

Suppose the change in oxygen activity/partial pressure is not a discrete step, but follows a continuous change as described in Eq.(16) .

$$P_{O2} = P_{O2,(t=0)} + \Delta P(1 - e^{-\frac{t}{\tau}}) \quad (16)$$

where the τ parameter is called the reactor flushtime. This approach to the oxygen step has been described by den Otter et al [75]. Using the change in oxygen partial pressure described in Eq. (16), the solution of Eq. (14) with the given boundary conditions is

$$\frac{M(t)}{M_\infty} = \frac{M(x,y,z,t) - M_0}{M_\infty - M_0} = 1 - \prod_{j=x,y,z}\sum_{n=1}^{\infty}\frac{2L_j^2}{\Gamma_{n,j}^2\left(\Gamma_{n,j}^2 + L_j^2 + L_j\right)}\left[\frac{e^{-\beta_{n,j}t} - \beta_{n,j}\tau e^{-t/\tau}}{1 - \beta_{n,j}\tau}\right] \quad (17)$$

, where

$$\beta_{n,j} = \frac{\Gamma_{n,j}^2 D_{chem}}{l_j^2} \quad (18)$$

$$\Gamma_{n,x}\tan\Gamma_{n,x} = L_x \quad (19)$$

$$L_x = l_x \cdot \frac{k_{chem}}{D_{chem}} \quad (20)$$

In Eq. (17) the solution with regards to concentration is already integrated with the sample dimension (l_x, l_y, l_z) as limits, to yield the mass change of oxygen in the sample, where M(t) is the mass change after time t, and M_∞ is the total mass change in an experiment. The solution given in Eq (17) is described in Crank [76] and in Appendix 1.

The criteria to use electrical conductivity relaxation data for the calculation of D_{chem} and k_{chem} is that the electrical conductivity changes linearly with the oxygen content of the sample viz. [77]:

$$\frac{\sigma(t)-\sigma_0}{\sigma_\infty-\sigma_0}=\frac{M(t)}{M_\infty} \tag{21}$$

Eq. (21) relates electrical conductivity with D_{chem} and k_{chem} given in Eqs. (17)-(20).

2.6 Solid State Diffusion

The self-diffusion coefficient or the component diffusion coefficient for oxygen, D_O, is represented by random-walk diffusion, i.e. no chemical potential gradients are present. The oxygen transport can also be described by the counter diffusion of oxygen vacancies, hence introducing a (oxygen) vacancy diffusion coefficient, D_V.

A mechanistic approach to the component diffusion coefficient is given by Kingery et al. [78].

$$D_O=\gamma\lambda^2\upsilon e^{-\frac{E_a}{RT}} \tag{22}$$

γ is a geometric factor including the number of closest neighbours of equivalent sites, 8 for the nearest oxygen sites in perovskites, and the probability of the atom to jump back into its original position. λ is the jumping distance, υ is the frequency of lattice vibrations, or attempted ion jumps and E_a is the activation energy for the jump to occur. The mechanistic approach given in Eq. (22) requires a random distribution of the oxygen vacancies. When considering atom movement consisting of atoms jumping into an adjacent vacant site, a term that tells whether the adjacent site is vacant or not must be included. In Eq (22) this is not considered. However, the concentration of oxygen ions and oxygen vacancies, C_O and C_V respectively, can be linked to the average jump frequencies for successful jumps for oxygen ions and vacancies, ν_{ion} and ν_{vac} respectively, and the following expression can be derived [79].

$$\frac{\nu_{vac}}{C_O}=\frac{\nu_{ion}}{C_V} \tag{23}$$

By inserting the relation in Eq. (23) into Eq. (22) one obtains

$$D_O = \gamma\lambda^2 \upsilon_{ion} e^{-\frac{E_a}{RT}} = \gamma\lambda^2 \upsilon_{vac} e^{-\frac{E_a}{RT}} \frac{C_V}{C_O} = D_V \frac{C_V}{C_O} \tag{24}$$

The diffusion coefficient for oxygen vacancies can be identified in Eq. (24) to be equal to

$$D_V = \gamma\lambda^2 \upsilon_{vac} e^{-\frac{E_a}{RT}} \tag{25}$$

The activation energy for the vacancy jump given in Eq (25) is called the enthalpy of migration ΔH_m [80].

At low vacancy concentrations, C_O is almost constant and Eq. (24) can be simplified :

$$D_O = \frac{C_V}{C_O} D_V \approx n_V D_V \tag{26}$$

where n_v is the fraction of oxygen vacancies in the structure.

The "activation energy" for the fraction of vacancies n_v is equal to the enthalpy of formation of vacancies, ΔH_f. This means that the activation energy for oxygen ion migration is equal to $\Delta H_m + \Delta H_f$ [80].

Eq. (26) says that D_O is proportional to the fraction of oxygen vacancies present. This is based on the assumption that a vacancy can jump to all nearest neighbour sites occupied by an atom. From Eq. (26) the oxygen vacancy diffusion coefficient can be regarded as constant, which is stated in Kingery et al. [78] and Kofstad [80] with the same mechanistic approach as given above. However an atom/ion needs a vacant nearest neighbour to jump and thus it is correlated with the vacancy concentration [80]. This means that D_V can be regarded as constant when the concentration of vacancies is so small that vacancy interactions do not occur. When the vacancy concentration becomes sufficiently large, D_V will certainly be influenced. However, the theory on transport in highly defective structures is still not developed. The subject has been discussed [81], however the need for further studies in these fields was emphasised.

The tracer diffusion coefficient D^T denotes diffusion coefficients measured with a tracer technique. (Sometimes D^T is denoted D^* [82]). These measurements can be performed with exchanging the ambient oxygen

surrounding an oxide, primarily made up of ^{16}O, with a gas composition enriched with ^{17}O or ^{18}O [82]. The tracer diffusion coefficient D^T can then be found by measuring the ^{18}O-concentration profile with Secondary Ion Mass spectroscopy (SIMS).

It is also possible to describe the ionic motion with an ionic conductivity, σ_{ion}. This conductivity can be derived from dc ionic conductivity measurements [83], and is the origin for a diffusion coefficient which refers to ionic conductivity, D^σ, which again corresponds to the component diffusion D_O. The ionic conductivity σ_{ion} and D^σ are related via the Nernst-Einstein relationship [80] given in Eq. (27)

$$D^\sigma = \frac{\sigma_{ion} RT}{C_O z_i^2 F^2} \tag{27}$$

The conductivity diffusion coefficient D^σ and the tracer diffusion coefficient D^T are in general not equal, and the correlation between them is referred to as the Haven ratio, H_R [82].

$$\frac{D^T}{D^\sigma} = H_R \tag{28}$$

H_R contains corrections, such as the possibility that different mechanisms contribute to the two different experiments [82,83].

If a gradient in chemical potential or concentration is present, a chemical diffusion coefficient, D_{chem}, is introduced. This is shown by Ficks law, which relates the oxygen flux with the gradient in oxygen concentration.

$$J_O = -D_{chem} \frac{dC_O}{dy} \tag{29}$$

D^T and D_{chem} are linked together [83], as shown in Eq.(30).

$$D_{chem} = \frac{D^T}{H_R RT} \frac{1/2 \partial \mu_{O_2}}{\partial \ln C_O} \tag{30}$$

In the case of oxygen transport in perovskites it is only one mobile species. On this basis, Weppner and Huggins derived the following relation between the oxygen component diffusion coefficient, D_O, and the chemical diffusion coefficient D_{chem} [84].

$$W_O = \frac{t_e}{RT}\frac{\partial \mu_O}{\partial \ln C_O} \simeq \frac{1}{RT}\frac{\partial \mu_O}{\partial \ln C_O} = \frac{D_{chem}}{D_O} \tag{31}$$

t_e is the transport number for the electronic species. This will mostly be equal to unity, since the electronic part of the electrical transport will be dominating for most perovskite materials. μ_O is the chemical potential of atomic oxygen given in Eq. (32).

$$\mu_O = \mu_O^0 + RT \ln \sqrt{P_{O_2}} \tag{32}$$

Thus

$$W_O = \frac{1}{2}\frac{\partial \ln P_{O_2}}{\partial \ln C_O} \tag{33}$$

W_O is referred to as the thermodynamic factor for oxygen ions.

The vacancy diffusion coefficient D_V is related to the component diffusion coefficient given in Eq.(24). Thus

$$\begin{aligned} D_{chem} &= W_O D_O = W_O \frac{C_V}{C_O} D_V \\ &= \frac{1}{2}\frac{\partial \ln P_{O_2}}{\partial \ln C_O}\frac{C_V}{C_O} D_V \\ &= \frac{1}{2}\frac{\partial \ln P_{O_2}}{\partial \ln C_V}\frac{\partial \ln C_V}{\partial \ln C_O}\frac{C_V}{C_O} D_V \\ &= \frac{1}{2}\frac{\partial \ln P_{O_2}}{\partial \ln C_V}\frac{\partial C_V}{\partial C_O}\frac{C_O}{C_V}\frac{C_V}{C_O} D_V \\ &= \frac{1}{2}\frac{\partial \ln P_{O_2}}{\partial \ln C_V}\frac{\partial C_V}{\partial C_O} D_V \\ &= -\frac{1}{2}\frac{\partial \ln P_{O_2}}{\partial \ln C_V} D_V = W_V D_V \end{aligned} \tag{34}$$

The relation $\partial C_V / \partial C_O$ is found by differentiating the mass balance at the oxygen site, Eq. (4), and is equal to –1. Thus,

$$D_{chem} = W_V \cdot D_V = \left(-\frac{1}{2} \cdot \frac{d \ln P_{O2}}{d \ln C_V} \right) \cdot D_V \tag{35}$$

The expression inside the parentheses is the thermodynamic factor for vacancies.

The D_{chem} parameter will in general be different from the component diffusion coefficient, D_O, since they appear in different chemical potential gradients. For a more thorough discussion of diffusion coefficients it is referred to Maier [82].

The thermodynamic factors W_O and W_V will depend on oxygen partial pressure, temperature and composition. By letting the P_{O2} (and composition) be constant it is possible to assign activation energies to the thermodynamic factors. By introducing the activation energies in Eq. (34) and rearranging one obtains.

$$\begin{aligned} D_{chem} &= D^0_{chem} e^{-\frac{E_{a,D_{chem}}}{RT}} \\ &= W_O D_O = W^0_O e^{-\frac{E_{a,W_O}}{RT}} D^0_O e^{-\frac{E_{a,D_O}}{RT}} \\ &= W_V D_V = W^0_V e^{-\frac{E_{a,W_V}}{RT}} D^0_V e^{-\frac{E_{a,D_V}}{RT}} \end{aligned} \tag{36}$$

Where $D^0_{chem}, D^0_o, D^0_V, W^0_o$ and W^0_V all are pre-exponential coefficients. From Eq (36) it can be seen that

$$\begin{aligned} E_{a,D_{chem}} &= E_{a,W_o} + E_{a,D_o} = E_{a,W_o} + \Delta H_m + \Delta H_V \\ &= E_{a,W_V} + E_{a,D_V} = E_{a,W_V} + \Delta H_m \end{aligned} \tag{37}$$

This means that

$$\begin{aligned} \Delta H_V &= E_{a,W_V} - E_{a,W_o} \\ &= E_{a,D_o} - E_{a,D_V} \end{aligned} \tag{38}$$

Thus, the apparent vacancy formation enthalpy can be calculated directly from the thermodynamic factors.

2.6.1 Solid State Diffusion of oxygen in perovskites

In Fig. 4 the vacancy diffusion coefficient for oxygen vacancies are given for materials in the series $La_{1-x}Sr_xCoO_{3-\delta}$, $La_{1-x}Sr_xFeO_{3-\delta}$ together with $(La,Ca)AlO_3$ and $BaBiO_3$ [85].

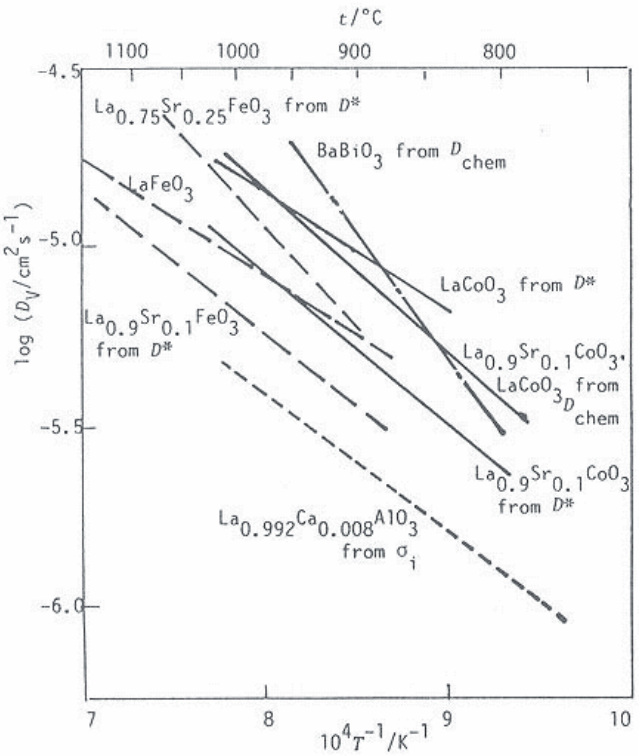

Fig. 4. Oxygen vacancy diffusion coefficients for perovskite oxides plotted against temperature. Included in figure is also the source for the calculated D_V's. Figure from Mizusaki [85].

In the figure it can be seen that the D_V coefficients are all within the same order of magnitude. The values for the coboltites and ferrites in Fig. 4 originate basically from Ishigaki et al. [86,87] at oxygen partial pressures around ~5 kPa (0.05 bar). Fig 4 shows that D_V for the ferrites is stacked in an unexpected order; with the 10 % Sr substituted ferrite having a smaller D_V than the pure $LaFeO_3$, again smaller than the 25 % Sr substituted one. This is also seen among the coboltites; 10 % Sr substituted is smaller than the pure $LaCoO_3$. The reason for this unexpected order is not known, but probably it is due to experimental uncertainty. Wang et al. [88] have investigated the vacancy diffusion coefficient in $La_{1-x}Sr_xCoO_{3-\delta}$ from many authors and found that D_V increases with increasing Sr-content. Measurements with AC impedance spectroscopy show the same trend [89].

Carter et al. [17] studied the oxygen component diffusion, D_O, in $(La,Sr)(Mn,Co)O_{3-\delta}$ solid solutions by tracer experiments, giving values for the oxygen tracer diffusion coefficient, D*. They found that for increasing amounts of cobalt, the values for the diffusion coefficient increased, while the corresponding activation energy decreased. This was due to the higher nonstoichiometry of oxygen in the samples, consistent with Eq. (26). Ramos and Atkinson [91] have studied the oxygen tracer diffusion in $(La,Sr)(Fe,Cr)O_{3-\delta}$ in wet and dry atmospheres. The values for the D^*-coefficient were of the same order of magnitude as for the values obtained by Carter et al. [17], and an increase of D_O^* with the introduction of more oxygen vacancies was seen.

The flux of oxygen in the system $La_{1-x}Sr_xCo_{1-y}Fe_yO_{3-\delta}$ has been reported by many authors [90,92,93,93,94,95,96,97,98]. These are performed at different oxygen partial pressure gradients, temperatures and compositions, thus a comparison of the oxygen fluxes with respect to the composition in the different works is difficult. Lein et al. [95] reports an increasing flux of oxygen with increasing amount of cobalt in the specimen when oxygen potential gradient and temperature (1147 °C) are kept at the same level. That is, pointing out the importance of oxygen vacancies which will increase with increasing cobalt content [90]. Also flux data can be used to calculate the chemical diffusion coefficient of oxygen in the specimens, and from them more fundamental transport coefficients such as component or vacancy diffusion coefficients, but unfortunately only a few authors have done this. This makes the comparison between the different materials more complicated if possible at all.

Many works reports the chemical diffusion coefficient, D_{chem} obtained by different experimental techniques. For instance the D_{chem} have been obtained by electrical conductivity relaxation [73,74,88], oxygen coulometric titration [64] and permeation/ electrochemical cell [99]. ten Elshof et al. [73] have investigated $La_{1-x}Sr_xFeO_3$ finding a D_{chem} value in x= 0.1 to be only dependent on the temperature. Wærnhus [54] have later re-examined this composition finding a small P_{O2} dependency with increasing D_{chem} with decreasing P_{O2} and thus increasing oxygen nonstoichiometry. This is not the case for $La_{0.5}Sr_{0.5}CoO_{3-\delta}$ where a decreasing D_{chem} is reported with decreasing P_{O2} obtained from reduction experiments ($P_{O2,end} < P_{O2,start}$) [74,88]. van der Haar et al. [74] explains this decreasing D_{chem} with the possible ordering of oxygen vacancies. However, van der Haar et al. [74] have only presented values for D_{chem} from reduction runs. Wang et al. [88], on the other hand, reports increasing D_{chem} with decreasing P_{O2} for oxidation runs. This is further discussed in Paper 2 in this thesis [72].

In general for the system (La,Sr)(Fe,Co)$O_{3-\delta}$ the component diffusion coefficients, D_O, increase with increasing amount of Sr and Co, which can be explained with the increasing population of oxygen vacancies.

For the material system $SrTiO_3$ with substitution both on A-site and B-site, Ishigaki et al. [87] have compiled a collection of D_V calculated from D_{chem} and thermodynamic factors for both $SrTiO_3$ and related material systems. The results are given in Fig 5.

It can be seen that D_V for pure $SrTiO_3$ deviates by several orders of magnitude, as well as a significant variation in activation energies. In the figure the line marked with $SrTiO_3$ (2) originates from Paladino et al. [100] while $SrTiO_3$ (3) originates from Walters and Grace [101]. The main difference between these is that Paladino [100] have performed mass relaxations in O_2/N_2 mixtures, while Walters and Grace [101] have measured in far more reducing atmospheres of H_2/H_2O mixtures using electrical conductivity relaxation. In principle both methods should give

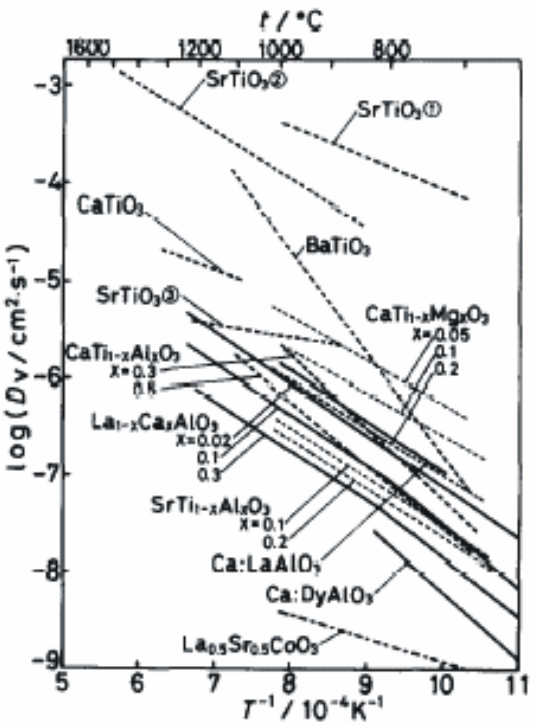

Fig. 5. Data for D_V in $SrTiO_3$ and structural related systems. From Ishigaki [87].

similar values, independent of method. A possible explanation for this difference is not offered by Ishigaki [87], but it could be due to experimental

difficulties. Later, Schwarz and Anderson [102] ($SrTiO_3$ (1)) derived values for D_V based on a capacitance manometric method, reporting values in good agreement with Paladino [100].

Another interesting aspect seen from Fig 5 is that the introduction of Al on the Ti-site causes a decrease in the D_V parameter for both $CaTiO_3$ and $SrTiO_3$. This is surprising since with a small change in the oxygen vacancy concentration the D_V should be unaffected.

Claus et al. [103] have studied the tracer diffusion of oxygen in $SrTiO_3$ with SIMS, finding values for the chemical diffusion coefficients which are comparable to the ones obtained from electrical conductivity relaxation [104]. The calculated values for D_V [103] is in good agreement with Refs [100,101]. Claus et al. also found that the tracer diffusion coefficients increased with increasing level of iron impurities, corresponding to the increased level of oxygen vacancies in the sample.

The chemical diffusion coefficient in $SrTiO_3$ at various levels of iron impurities have been investigated in the temperature interval 450-1000 K with a variety of techniques; optical adsorption [105,106,107], chemical polarization experiments [62], conductivity experiments [108] and permeation experiments [109], all giving similar D_{chem} values.

2.7 Surface exchange

The exchange of oxygen between the atmosphere and a material can be described by the equilibrium reaction in Eq. (39).

$$O_2(g) + 2V_O^{\bullet\bullet} = 2O_O^x + 4h^{\bullet} \tag{39}$$

The charge transfer is here represented with electron holes.

Reaction (39) can be shifted to the right (oxidation) and left (reduction) depending on the ambient chemical potential. In both cases it can be divided into several elementary reactions. These elementary reactions involve adsorption, dissociation/association of the oxygen molecule, charge transfer(s), incorporation/excorporation of oxygen ions in/out of the vacancies. Some examples of different elementary reactions are given by Merkle and Maier [110] for the material system Fe-doped $SrTiO_3$ and ten Elshof et al. [73] and Wærnhus [54] for the material system $La_{1-x}Sr_xFeO_3$.

2.7.1 Irreversible thermodynamics

The oxidation and reduction reaction can be described as a flux of oxygen in or out of the material. If a material is in equilibrium with the oxygen pressure in the surroundings at any given temperature, these fluxes are equal. If the oxygen activity in the ambient is changed by a small amount, oxygen will flow in or out of the sample as described in Eq. (40) [111].

$$j_{O_2} \equiv j_{ox} - j_{red} = j_{ex}^{0} \frac{\Delta\mu_{O_2}}{RT} \tag{40}$$

The step in chemical potential can be described by the change in free energy for the oxidation reaction (or reduction reaction). In Eq. (40) the transport is based on the flux of molecular oxygen, O_2. The relationship between flux of atomic and molecular oxygen is $j_O = 2 \cdot j_{O2}$. The parameter j^0_{ex} describes the surface exchange rate (flux) of molecular oxygen at equilibrium, meaning that the amount of molecular oxygen entering the sample (j_{ox}) equals the amount leaving (j_{red}). This means

$$j_{ox} = j_{red} = j_{ex}^{0} \tag{41}$$

The statement given in Eq. (41) is visualised i Fig 6 a).

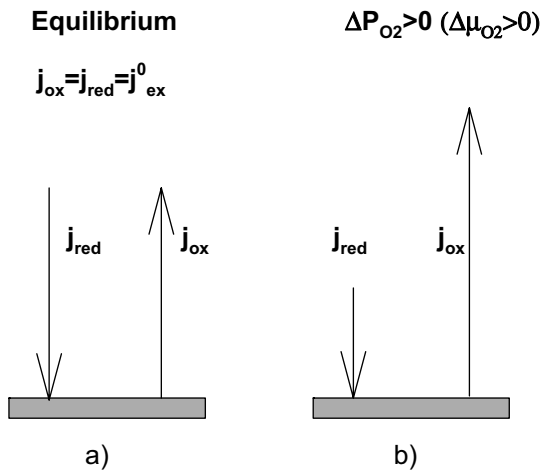

Fig. 6. Schematic presentation of the oxidation and reduction fluxes in the situations of a) equilibrium $j_{ox}= j_{red} =j^0_{ex}$ and b) after a small increase in P_{O2} is applied $\Delta P_{O2}>0$ ($\Delta\mu_{O2}>0$).

In Fig 6 b) a small perturbation in the oxygen chemical potential is applied, and in this case it represents an oxidation. The oxidation flux j_{ox} will increase and the reduction flux j_{red} will decrease.

The expression given in Eq (40) can be derived by considering irreversible thermodynamics. The affinity A of any chemical reaction at temperature T is given by [112].

$$A = -\sum_i \nu_i \mu_i(T) \tag{42}$$

, where ν_i is the stoichiometric coefficient and μ_i is the chemical potential for specie i , which can be written as

$$\mu_i(T) = \mu_i^0(T) + RT \ln a_i \tag{43}$$

, where a_i is the activity of specie i. For a chemical reaction in equilibrium the affinity A is equal to zero. Inserting Eq.(43) into Eq. (42) gives

$$\begin{aligned} A = 0 &= \sum_i \nu_i \mu_i^0 + \sum_i RT\nu_i \ln a_i \\ &= \sum_i \nu_i \mu_i^0 + RT \sum_i \ln a_i^{\nu_i} \\ &= \sum_i \nu_i \mu_i^0 + RT \ln K(T) \end{aligned} \tag{44}$$

In Eq. (44) the equilibrium constant K(T) is introduced. By substituting Eq. (44) in to Eq. (42) the affinity becomes

$$\begin{aligned} A &= -\sum_i \nu_i \mu_i^0(T) - RT \sum_i \nu_i \ln a_i \\ &= RT \ln \frac{K(T)}{\prod_i a_i^{\nu_i}} \end{aligned} \tag{45}$$

By considering the simple oxidation reaction of a metal M

$$M + O_2 = MO_2 \tag{46}$$

The usual kinetic expression for Eq. (46) is given as

$$r = r_{ox} - r_{red} = k_{ox} a_M P_{O_2} - k_{red} a_{MO_2}$$
$$= k_{ox} a_M P_{O_2} \left(1 - \frac{k_{red}}{k_{ox}} \frac{a_{MO_2}}{a_M P_{O_2}} \right) \quad (47)$$

k_{ox} and k_{red} are the rate constants for the oxidation and reduction process respectively. It is well known that the ratio k_{ox}/k_{red} is equal to the equilibrium constant K(T). Using this fact and the relationship given in Eq. (45), Eq. (47) can be written

$$r = k_{ox} a_M P_{O_2} \left(1 - \frac{k_{red}}{k_{ox}} \frac{a_{MO_2}}{a_M P_{O_2}} \right)$$
$$= r_{ox} \left(1 - \frac{K(T)^{-1}}{a_M P_{O_2} a_{MO}^{-1}} \right) \quad (48)$$
$$= r_{ox} \left(1 - \exp\left(-\frac{A}{RT} \right) \right)$$

When small perturbations to the equilibrium is applied i.e.

$$\left| \frac{A}{RT} \right| \ll 1 \quad (49)$$

Eq. (48) will be reduced to

$$r = r_{ox} \frac{A}{RT} \quad (50)$$

The r_{ox} is equal to the equilibrium rate of reaction (46).

It is possible to "translate" the reaction rate given in Eq. (50) to a flux of oxygen as the one given in Eq. (40). By taking into consideration that the reaction rate of a redox reaction as the one given in Eq. (46), involves only one gaseous specie to enter and leave the structure. This means that the reaction rate, r, and the oxygen flux j_{O2} are proportional with an area factor as the only difference between them, thus Eq. (50) can be written

$$j_{O_2} = j_{ox} \frac{A}{RT} \quad (51)$$

The affinity will be equal to zero for reaction (39) when it is in equilibrium, and this situation is described in Fig 6a).

$$A = \mu_{O_2} + 2\mu_{V_O^{\bullet\bullet}} - 2\mu_{O_O^x} - 4\mu_{h^\bullet} = 0 \tag{52}$$

The situation a short time after the change in oxygen activity (partial pressure) is applied is described in Fig 6b). The chemical potential of gaseous oxygen will change with the oxygen partial pressure. However, a gradient in the chemical potential will be set up. By assigning a virtual oxygen chemical potential to the defect chemical potentials, the affinity can be written

$$\begin{aligned} A &= \mu_{O_2}^{at\ surface} + 2\mu_{V_O^{\bullet\bullet}}^{in\ surface} - 2\mu_{O_O^x}^{in\ surface} - 4\mu_{h^\bullet}^{in\ surface} \\ &= \mu_{O_2}^{at\ surface} - \mu_{O_2}^{in\ surface} = \Delta\mu_{O_2} \end{aligned} \tag{53}$$

Thus Eq. (51) can be written

$$j_{O_2} = j_{ox}\frac{A}{RT} \approx j_{ex}^0\frac{\Delta\mu_{O_2}}{RT} \tag{54}$$

Eq. (54) is equal to Eq. (40)

2.7.2 Relation between various surface exchange coefficients

In Eq. (40) it is the difference in chemical potential of molecular oxygen that is the driving force for the reaction. However, it is possible to express the driving force in several different ways, either by the difference in the chemical potential of atomic oxygen through the surface, or the difference in the concentration of atomic oxygen. The latter gives $\Delta C_O = C_{actual} - C_{new\ eq}$, i.e. the difference between the actual and the new equilibrium concentration.

The difference in the chemical potentials for atomic and molecular oxygen, $\Delta\mu_O$ and $\Delta\mu_{O2}$ respectively, are related and the evaluation of this is given in Fig. 7

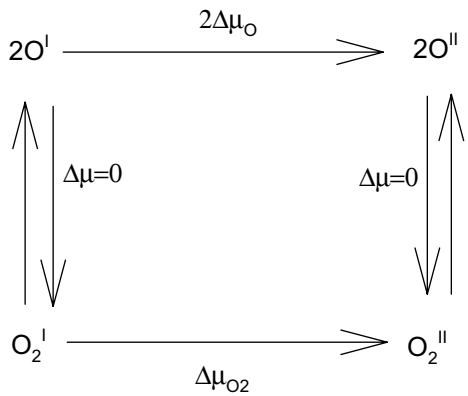

Fig. 7. Diagram showing the relation between $\Delta\mu_{O2}$ and $\Delta\mu_{O}$.

The difference in oxygen chemical potential can be described by the following reaction (55)

$$O_2^{at\ surface} \rightleftarrows O_2^{in\ surface} \quad , \qquad \Delta\mu = \Delta\mu_{O_2} \tag{55}$$

Each of these species is in equilibrium with monatomic oxygen by reaction (56)(superscripts let out).

$$O_2 = 2O \quad , \qquad \Delta\mu = 0 \tag{56}$$

And thus the reaction

$$O^{at\ surface} \rightleftarrows O^{in\ surface} , \qquad \Delta\mu = \Delta\mu_O \tag{57}$$

From the diagram in Fig 2 and Eq. (55)-(57) the relation $\Delta\mu_{O2} = 2\Delta\mu_O$ can be deduced.

Using the relations $2j_{O2} = j_O$, and $\Delta\mu_{O2} = 2\Delta\mu_O$, the flux given in Eq.(54) can be derived from difference in chemical potential as driving force to difference in concentration.

$$
\begin{aligned}
j_O &= 2 j_{O_2} = 2 j_{ex}^0 \frac{\Delta \mu_{O_2}}{RT} = 4 j_{ex}^0 \frac{\Delta \mu_O}{RT} \\
&= 4 j_{ex}^0 \frac{\Delta \mu_O}{RT} \frac{1}{\Delta \ln C_O} \Delta \ln C_O \\
&= 4 j_{ex}^0 W_O \Delta \ln C_O \\
&= \frac{4 j_{ex}^0 W_O}{C_O} \Delta C_O
\end{aligned}
\tag{58}
$$

The Δ is in this context the difference in chemical potential or concentration for the involved species across the surface. The thermodynamic factor W_O is recognised from Eq.(31).

In Eq. (58) the flux is related to the oxygen concentration with a proportionality factor. This factor is called the chemical surface exchange coefficient k_{chem}, since it relates the flux with a concentration difference. This can be compared with the definition of the D_{chem} parameter given in Eq. (29). By equating terms it can be seen that

$$
\frac{4 j_{ex}^0 W_O}{C_O} = k_{chem} \tag{59}
$$

The relation between surface exchange flux, concentration and k_{chem} is described in more detail in Fig 8. Given a sample with thickness L at equilibrium with ambient P_{O2}. The difference in oxygen concentration across the surface is zero and thus there is no net transport of oxygen through the surface. This is described in Fig 8a). At a given time **t=0** a change of oxygen partial pressure in the ambient is applied. The oxygen concentration at the surface will change corresponding with the new oxygen partial pressure, but the oxygen concentration in the surface will remain with the same value as before the change in oxygen partial pressure was applied. Thus a flux of oxygen into the sample will occur, and the flux will have its maximum value at the starting time **t=0.** This is described in Fig. 8b. At a time t>0 there will be a net flux of oxygen into the sample, and a concentration profile is established. This is described in Fig. 8c. When the oxygen concentration at and in the surface is equal, the net flux of oxygen will be zero again. This is described in Fig 8d.

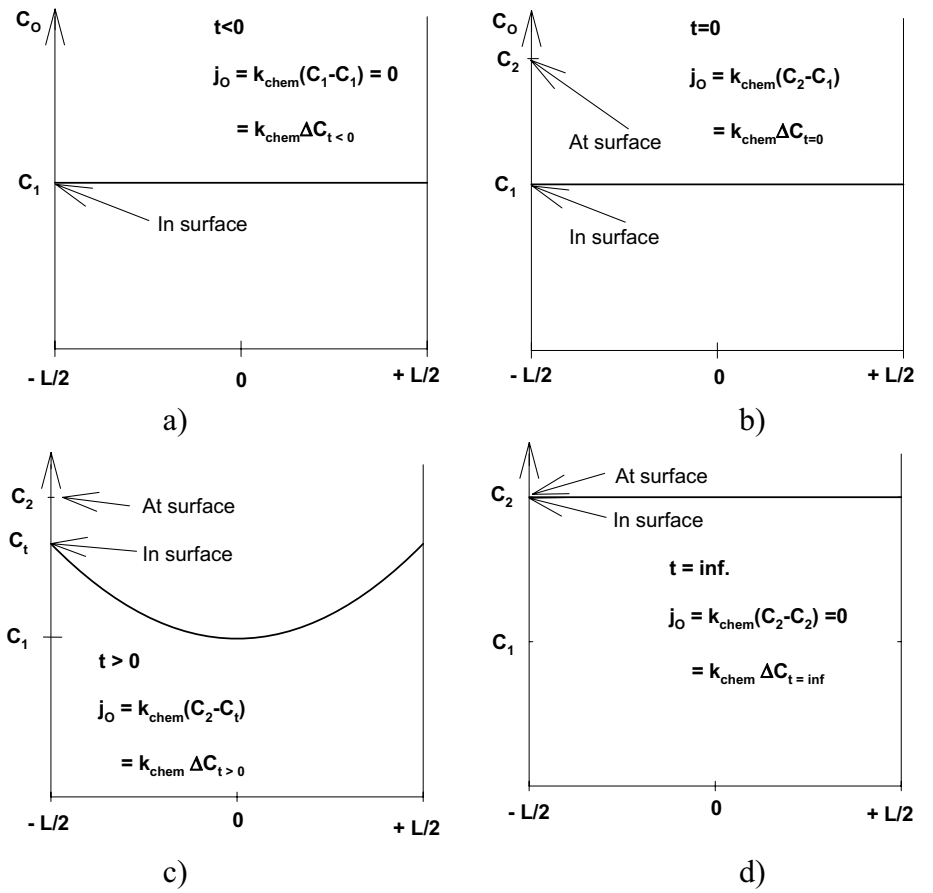

Fig. 8. The oxygen concentration across the surface and through the sample is described as a function of position and at different times. a) Before a change in the oxygen partial pressure, t<0. b) At the time the change is applied, t=0. c) After a given time t. d) When the new equilibrium is established, t=∞.

In Eq. (58) the thermodynamic factor is recognised from Eq. (31). By equating terms it can be seen that

$$k_{chem} = \frac{4 j_{ex}^{\cdot 0} W_O}{C_O} = k_0 W_O \tag{60}$$

Thus k_{chem} and k_0 is related equally as D_O and D_{chem} cf. Eq. (31).

k_0 is the surface exchange coefficient when no gradient in oxygen chemical potential is applied, and can be determined from experiments performed in

thermodynamic equilibrium e.g. $^{18}O/^{16}O$ isotopic exchange [73]. The k_0 is sometimes referred to as a tracer surface exchange coefficient k^* [113,114]. Thus, the relation between the different rate coefficients may be summarised by:

$$j_{ex}^0 = \frac{1}{4} C_O k_0 = \frac{1}{4} \frac{C_O}{W_O} k_{chem} \tag{61}$$

With Eq. (60) and (61) the different surface exchange parameters are related to each other, using the thermodynamic factor W_O and the concentration of the oxygen species.

2.7.3 Surface exchange of oxygen in perovskites

Maier have employed a phenomenological approach to the surface exchange coefficient [113,114] deriving equations relating surface exchange coefficients obtained from inherently different experimental techniques. This approach is useful when comparing data for oxygen surface exchange.

In the literature the oxygen surface exchange has been examined by a variety of techniques, most of them result in data both for bulk diffusion and surface exchange. In the following surface exchange for a number of relevant compounds obtained by different techniques will be presented and discussed.

Electrical conductivity relaxation have been performed on $La_{1-x}Sr_xCoO_{3-\delta}$ [74,88], $La_{1-x}Sr_xFeO_3$ [73] and on the mixed system $La_{1-x}Sr_x(Fe,Co)O_3$ [115] at temperatures between 600 and 950 °C. All of these works report a proportionality with P_{O2}^n for the k_{chem} values where n varies between 0.65 and 0.85 for the ferrites [73], and between 0.30 and 0.44 for some of the coboltites [74,88], with the mixed system more close to the ferrite system [115]. The variation in P_{O2} dependencies with increasing Sr-content has been reported by van der Haar et al [74] where the coboltite changes its dependency from ~0.80 with Sr-content corresponding to x =0.7 to ~0.70 for x=0.2. The uncertainties in these P_{O2} dependencies are rather high, so the effect of the Sr-content with respect to the P_{O2} dependency is not unambiguous. For the ferrites the P_{O2} dependency is rather constant with increasing Sr-content [73]. A typical value for the surface exchange parameter k_{chem} from Refs [73,74,88,115] is in the interval $10^{-2.9}$-$10^{-3.2}$ at P_{O2} corresponding to air, and at ~800 °C and independent of the material.

k_{chem} activation energies for the ferrites are reported by ten Elshof et al. [73] to be about 125 kJ/mol, while in the mixed system of cobaltites and ferrites the activation energy is between 60 and 70 kJ/mol [115]. For the coboltites it varies between 216 kJ/mol for the composition where x=0.2 to about 110 kJ/mol where x=0.7 [74], thus decreasing activation energy with increasing Sr-content. However, generally the activation energies vary with oxygen partial pressure, with a slight tendency to increase with decreasing oxygen partial pressure.

The study by Wang et al. [88] also shows an interesting behaviour with respect to the effect of P_{O2}-variation. In their conductivity relaxation experiments on $La_{0.5}Sr_{0.5}CoO_{3-\delta}$, they systematically changed the start partial pressure of oxygen and the end partial pressure, with variable step sizes. They found that k_{chem} were more or less constant when keeping $P_{O2,end}$ constant at 1 atm, while when varying the $P_{O2,end}$ the k_{chem} was found to have a proportionality with the $P_{O2,end}$. This shows that k_{chem} is dependent on the oxygen partial pressure. The same experimental trend as Wang et al. [88] has later been reproduced by Chen et al. [116], studying epitaxial thin films of the same material. From these two works, it can be seen that k_{chem} is influenced by the partial pressure surrounding the sample.

The chemical surface exchange coefficients have also been studied by Diethelm and van Herle [99] with an electrochemical cell (Belzner cell) for the material $La_{0.6}Sr_{0.4}Fe_{0.8}Co_{0.2}O_{3-\delta}$. They found values significantly lower than values obtained from tracer experiments, explaining the difference that the state of the surface (i.e. grain size, orientation or the possible presence of impurities) will have great influence on the surface exchange process, and not just the material itself. An example of the effect of surface treatment is reported by ten Elshof et al. [115], they showed an increase in k_{chem} by half an order of magnitude by treating the surface by etching with nitric acid. The main effect of the etching was probably an enhanced effective surface area.

Eq. (60) relates three important quantities related to surface exchange kinetics. k_0 is usually associated with the so-called tracer surface exchange coefficient, k*, and is related to conditions at equilibrium. From Eq. (60) we can derive k_0 from k_{chem} if the thermodynamic factor, W_O, is known and enable us to compare surface exchange data obtained from tracer- and relaxation experiments, respectively.

The k_0 for $(La,Sr)FeO_3$ have been given by ten Elshof et al. [73] and values for the P_{O2} dependency and activation energies were almost as for k_{chem} from the same work. The absolute value for k_0 is on the other hand several

orders of magnitude lower than k_{chem} due to a rather large thermodynamic factor.

Ishigaki et al. [86,87,117] studied the tracer diffusion coefficient for $LaCoO_3$, $LaFeO_3$ and also for some Sr-substituted coboltites and ferrites. They provided also data for k^*, however only at two specific partial pressures, one for each B-site cation. For the Sr-substituted ferrites the k^* increased with increasing amount of Sr-content [87]. For the coboltites they were not able to obtain k* values since the coefficients did not converge in the iterations for the least square fitting procedure between model and experimental.

De Souza and Kilner [118] have studied the $(La,Sr)(Mn,Co)O_{3-\delta}$ system with tracer diffusion demonstrating a strong correlation between D^* and k^* corresponding to an almost constant ratio (D^* / k^*). They reasoned that the behaviour was due to the major role the oxygen vacancies were playing in the surface reaction in these materials.

In general there are a lot of works dealing with the surface exchange of oxygen in perovskites like $(La,Sr)(Co,Fe,Mn)O_{3-\delta}$ in addition to those mentioned earlier in this literature review [17,89,91,92,93,97,98,99,119,120,121,122]. In all these works measurements are in general performed in different ranges with respect to temperature, oxygen partial pressure and composition, thus, often unabling us to compare data in a direct manner and be more conclusive. However, for the system $(La,Sr)(Fe,Co)O_{3-\delta}$; the following general marks can be put forward: The surface exchange coefficients (both k_{chem} and k_0) increase with the increase of oxygen vacancies (by i.e. substitution of Sr and/or Co into the structure), which is illustrated in Fig 9. At constant temperatures the coefficients all show a P_{O2} dependency described by $k_0 \quad P_{O2}^n$, where $n>0$.

In Fig 9 k_0 and k^* for the $La_{1-x}Sr_xCoO_{3-\delta}$ and $La_{1-x}Sr_xFeO_{3-\delta}$ from literature references are plotted vs. temperature. The oxygen partial pressures for the values in the figures are not at the same level, but vary between 0.05-0.20 atm. The P_{O2} dependency at each temperature is thus not taken into consideration.

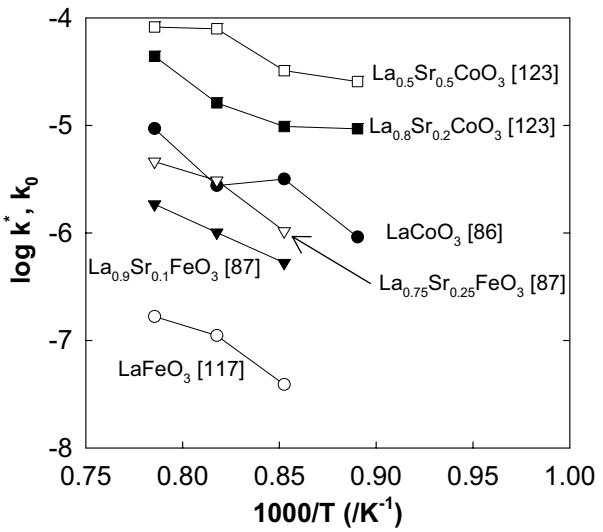

Fig. 9. Values for k_0 and k^* taken from literature plotted vs. temperature. P_{O2} in the different plots is 0.05-0.20 atm. Lines serve as guides to the eye.

In Fig 9 the materials $La_{1-x}Sr_xCoO_3$ has a typical electrical conductivity of ~1000 S/cm [70], while the materials $La_{1-x}Sr_xFeO_3$ has ~0.01 S/cm [30], that is a difference of 4-5 orders of magnitude. This difference in electrical conductivity is not reflected by Fig 9, and indicates that the surface exchange rate is not controlled by the electronic conductivity.

For the compositions given in Fig 9 the oxygen vacancy concentration increases with the Sr content and is also generally higher for the coboltites than the ferrites. The P_{O2} in each of the measurements in Fig 9 is between 0.05-0.20 atm, which for simplicity can be regarded as the same. As outlined by Merkle and Maier [110] the rate-determining step must contain the oxygen partial pressure and the concentration of oxygen vacancies and electrons, viz.:

$$rate = const \cdot P_{O2}^{m} \cdot \left[V_O^{\bullet\bullet} \right]^n \cdot \left[e^{'} \right]^p \tag{62}$$

, where m, n and p are coefficients. The rate can be related to j^0_{ex} given in Eq. (61), and thus to the k_0 parameter. Fig. 9 thus emphasise the importance of vacancies on the k_0 coefficient.
In Fig 10 Eq. (61) has been used to calculate the equilibrium flux j^0_{ex} for $La_{0.8}Sr_{0.2}CoO_{3-\delta}$ and $La_{0.5}Sr_{0.5}CoO_{3-\delta}$ [123] and for $La_{0.9}Sr_{0.1}FeO_3$ [54].

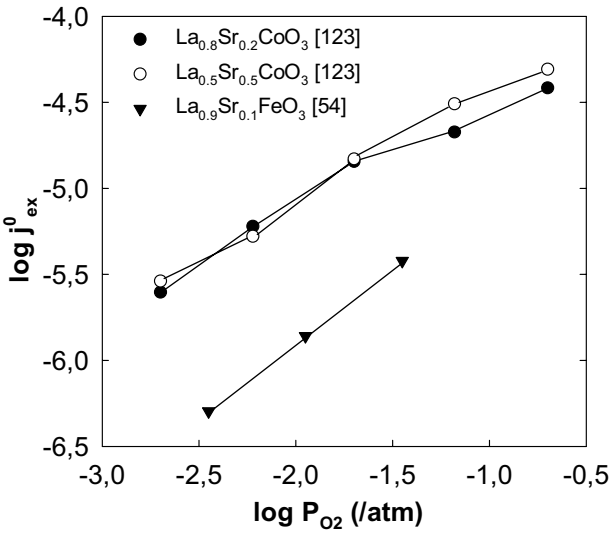

Fig. 10. Calculated equilibrium flux j^0_{ex} for $La_{0.8}Sr_{0.2}CoO_{3-\delta}$ and $La_{0.5}Sr_{0.5}CoO_{3-\delta}$ [123] and for $La_{0.9}Sr_{0.1}FeO_3$ [54]. Lines are guide to the eye.

From Fig 10 it can be seen that materials with the highest oxygen vacancy concentration show the highest equilibrium flux j^0_{ex}. Thus, the highest flux of oxygen is expected in materials with the largest amounts of oxygen vacancies.

For the case of $SrTiO_3$ the amount of work on the surface exchange is more limited. However, $SrTiO_3$ has been used as a model material to explore the transport of oxygen in oxides [50].

Leonhardt et al. [124] have examined the surface exchange reaction in Fe doped $SrTiO_3$ by performing relaxation experiments monitored with a modified optical technique [125], and tracer experiments analysed by SIMS. They report an increasing surface exchange coefficient from tracer experiments, k^*, with increasing content of iron impurities, as well as an increasing surface exchange coefficient from relaxation experiments, k_{chem}, with increasing oxygen partial pressure. The effect of adding thin metal or metal oxide films on the surface of the $SrTiO_3$ materials were also studied, in order to find the effect on the surface exchange. This caused a lowering of the activation energy for k_{chem} and an increase in the coefficient itself, thus, evidently speeding up the surface kinetics and approaching equilibrium conditions at the surface due to the metal coatings.

Schlüter et al [108] have studied the chemical surface exchange coefficient with permeation, and concluded that the values from the work fall well into trends of values obtained by other methods, e.g. Bieger et al [106], which studied the surface exchange with an optical method.

Although a great amount of work has been done to explore the surface exchange kinetics, there are only a few works which have approached the phenomena from a reaction mechanism point of view, suggesting various possible reaction pathways for the exchange of oxygen. As mentioned earlier, the surface exchange reaction (Eq.(39)) can be divided into several elementary reactions. These elementary reactions involve adsorption, dissociation/association of the oxygen molecule, charge transfer(s), incorporation/excorporation of oxygen ions in/out of the vacancies. In the search for a reaction mechanism that describes the surface exchange reaction, many different reaction pathways have been proposed [54,73,126,127] on the actual material systems. However, the identification of possible rate-determining steps relies on firm experimental data. There is also a possibility that there exist more than one reaction pathway at the same time with different elementary reactions, meaning that the total rate is a result of more than one rate determining step. The most detailed considerations have been given by Merkle and Maier [110] elucidating different possible reaction pathways. The P_{O2} dependency of the rate was predicted from the defect chemistry. Two major conclusions were made in this work; the rate-determining step (RDS) contains an O_2^{n-} (n=0, 1 or 2) molecular oxygen specie, and that an electron participates before or in the RDS.

3 REFERENCES

1. Balachandran U., Dusek J.T., Mieville R.L., Poeppel R.B., Kleefisch M.S., Pei S., Kobylinski T.P., Udovich C.A.and Bose A.C., "Dense ceramic membranes for partial oxidation of methane to syngas ", Appl. Cat. A, 133, (1995),19-29.
2. Singhal, S.C., " Solid oxide fuel cells for stationary, mobile and military applications", Solid State Ionics 152-153, (2002), 405-410.
3. Bossel, U.G., "First European Solid Oxide Fuel Cell Forum: A Platform for Science, Engineering and Technology, 3-7 October 1994, Lucerne, Switzerland", J.Power Sources 57 [1-2], (1995), 141-143.
4. Minh, N.Q., "Ceramic Fuel Cells", J.Am.Ceram.Soc. 76, No.3, (1993), 563-588.
5. Singhal, S.C., "Science and technology for solid-oxide fuel cells", MRS Bull., 25, (2000), 16-21.
6. Brandon, N.P., Skinner, S. and Steele, B.C.H., "Recent advances in materials for fuel cells", Annu.Rev.Mater.Res. 33, (2003), 183-213.
7. Ishihara, T., Matsuda, H. and Takita, Y., "Doped $LaGaO_3$ perovskite type oxide as a new oxide ionic conductor", J.Am.Ceram.Soc. 116, (1994), 3801-3803.
8. Stevens, R., " An introduction to Zirconia", Magnesium Elektron, London, UK, (1986).
9. Etsell, T.H. and Flengas, S.N., "Electrical properties of solid oxide electrolytes", Chem.Rev. 70, (1970), 339.
10. Subbarao, E.C. and Maiti, H.S., "Solid electrolytes with oxygen ion conduction", Solid State Ionics 11, (1984), 317-338.
11. Takahashi, T., Iwahara, H. and Suzuki, K., *Proceedings of the Third Int.Symp. on fuel cells*, Brusells, Belgium, (1969), p 113.
12. Ohno, Y., Nagata, S., and Sato, H., "Effect of electrode materials on the properties of high temperature solid electrolyte fuel cells", Solid State Ionics, 3/4 , (1981), 439.
13. Tedmon, C.S., Spacil, H.S. and Mitoff, S.P., "Cathode materials and performance in high-temperature zirconia electrolyte fuel cells", J.Electrochem.Soc. 116, (1969),1170.
14. Hammou, A. and Guindet, J. "Solid oxide fuel cells", in "The CRC Handbook of solid state electrochemistry", Eds Gelligns, P.J. and Bouwmeester, H.J.M., CRC Press (1997).
15. Bouwmeester, H.J.M. and Burgraaf, A.J., "Fundamentals of inorganic membrane science and technology", Elsevier, Amsterdam, (1996), p. 435-526.
16. Mazanec, T.J., " Prospects for ceramic electrochemical reactors in industry", Solid State Ionics 70, (1994), 11-19.

17. Carter, S., Selcuk, A., Chater, R.J., Kajda, J., Kilner, J.A. and Steele, B.C.H., "Oxygen transport in selected nonstoichiometric perovskite-structure oxides", Solid State Ionics 53-56, (1992), 597-605.
18. Kharton, V.V., Naumovich, E.N. and Nikolaev, "Materials of high-temperature electrochemical oxygen membranes", J. Membr.Sci. 111, (1996), 149-157.
19. Qiu, L., Lee, T.H., Yang, Y.L, Jacobson, A.J. and Liu, L.-M., "Oxygen permeation studies of $SrCo_{0.8}Fe_{0.2}O_{3-\delta}$", Solid State Ionics, 76, (1995), 321-329
20. Kharton, V.V., Nikolaev, A.V., Naumovich, E.N., Samokhval, V.V., "Electronic and oxygen conductivity of $SrCo(Fe,Cu)O_{3-\delta}$ solid solutions", Inorg. Mater. 30 (4),(1994), 492-495.
21. Kharton, V.V., Tikhonovich, V.N., Li, S.B., Naumovich, E.N., Kovalevsky, A.V., Viskup, A.P., Bashmakov, I.A., Yaremchenko, A.A., "Ceramic microstructure and oxygen permeability of $SrCo(Fe,M)O_{3-\delta}$ (M= Cu or Cr) perovskite membranes", J. Electrochem.Soc. 145, No.4, (1998), 1363-1373.
22. Kovalevsky, A.V., Kharton, V.V., Tikhonovich, V.N., Naumovich, E.N., Tonoyan, A.:, Reut, O.P. and Boginsky, L.S., "Oxygen permeation through $Sr(Ln)CoO_{3-\delta}$ (Ln=La, Nd, Sm, Gd) ceramic membranes ", Mater.Sci.Eng.B., 52, (1998), 105-116.
23. Kharton, V.V., Shuangbao, L., Kovalevsky, A.V., Viskup, A.P., Naumovich, E.N. and Tonoyan, A.A., "Oxygen permeability and thermal expansion of $SrCo(Ti)O_{3-\delta}$ perovskites", Mater Chem Phys.53, (1998), 6-12.
24. Teraoka, Y., Nobunaga, T., Okamoto, K., Miura, N. and Yamazoe, N., "Influence of constituent metal-cations in substituted $LaCoO_3$ on mixed conductivity and oxygen permeability", Solid State Ionics 48 [3-4], (1991), 207-212.
25. Teraoka, Y., Zhang, H.M., Okamoto, K. and Yamazoe, N., "Mixed ionic-electronic conductivity of $La_{1-x}Sr_xCo_{1-y}Fe_yO_{3-\delta}$ perovskite type oxides", Mat. Res.Bull. 23, (1988), 51-58.
26. Teraoka, Y., Zhang, H.M., Furukawa, S. and Yamazoe, N., "Oxygen permeation through perovskite type oxides", Chem.Lett. 11, (1985), 1743-1746.
27. Tsai, C.Y., Dixon A.G., Ma, Y.H., Moser, W.R. and Pascucci, M.R., "Dense perovskite, $La_{1-x}A'_xFe_{1-y}Co_yO_{3-\delta}$ (A' = Ba, Sr, Ca), membrane synthesis, applications and characterization", J.Am.Ceram.Soc. 81, No.6, (1998), 1437-1444.
28. Stewenson, J.W., Armstrong, T.R., Pederson, L.R. and Weber, W.J., "The First Int Symp. on ceramic membranes" Eds. Anderson, H.U, Khandkar, A.C. and Liu, M., (1995), p. 94.

29. Mizusaki, J., Sasamoto, T., Cannon, W.R. and Bowen, H.K., "Electronic conductivity, Seebeck coefficient and defect structure of $LaFeO_3$", J.Am.Ceram.Soc. 65, (1982), 363.
30. Mizusaki, J., Sasamoto, T., Cannon, W.R. and Bowen, H.K., "Electronic conductivity, Seebeck coefficient and defect structure of $La_{1-x}Sr_xFeO_3$ (x=0.1 and 0.25)", J.Am.Ceram.Soc. 66, (1983), 247.
31. Fouletier, J., Mantel, E. and Kleitz, M., "Performance-characteristics of conventional oxygen gauges", Solid State Ionics 6, (1982), 1.
32. Gellings, P.J. and Bouwmeester, H.J.M., "Ion and mixed conducting oxides as catalysts", Cat.Today. 12, (1992), 1-105.
33. Voorhoeve, R.J.H. *in* "Advanced Materials in Catalysis" (J.J. Burton and R.L. Garten, Eds.), 1977.
34. Rao, C.N.R. and Gopalakrishnan, J., "New Directions in Solid State Chemistry", 2nd ed., Cambridge University Press (1997), pp. 28-29.
35. Glazer, A.M., "Simple ways of determining perovskite structures", Acta Cryst, A31, (1975), 756-762.
36. Goldschmidt,V.M., Skr.Nor.Vidensk.-Akad. [K1] 1: Mat.-Naturvidensk. K1 No. 2, (1926).
37. Van Roosmalen, J.A.M., Cordfunke, E.H.P., Helmholdt, R.B. and Zandbergen, H.W., "The defect chemistry of $LaMnO_{3\pm\delta}$; 2: structural aspects of $LaMnO_{3\pm\delta}$", J.Solid State Chem. 110, (1994), 100-105.
38. Rao, C.N.R., Gopalakrishnan, J., Vidyasagar, K., "Superstructures, Ordered defects and nonstoichiometry in metal oxides of perovskite and related structures", Ind. J.Chem. 23A, (1984), 265-284.
39. Jonker, G.H. and van Zandten, J.H., "Magnetic compunds with perovskite structure. III. Ferromagnetic compounds of cobalt", Physica 19, (1953), 120.
40. Petrov, A.N., Kononchuk, O.F., Andreev, A.V. and Cherepanov, V.A., " Crystal structure, electrical amd magnetic properties of $La_{1-x}Sr_xCoO_{3-y}$", Solid State Ionics, 80, (1995), 189-199.
41. Mizusaki, J., Mima, Y., Yamauchi, S, Fueki, K., and Tagawa, H., "Nonstoichiometry of the Perovskite-type oxides $La_{1-x}Sr_xCoO_{3-\delta}$", J.Solid State Chem. 80, (1989), 102-111.
42. Mineshige, A., Kobune, M., Fujii, S., Ogumi, Z., Inaba, M., Yao, T. and Kikuchi, K., "Metal-Insulator transition and crystal structure of $La_{1-x}Sr_xCoO_3$ as functions of Sr-content, temperature and oxygen partial pressure", J.Solid State Chem. 142, (1999), 374.
43. Wold, A., Post, B. and Banks, E., "Lanthanum rhodium and lanthanum cobalt oxides", J.Am.Ceram.Soc. 79, (1957), 6365.
44. Mineshige, A., Inaba, M., Yao, T., and Ogumi, Z., "Crystal structure and metal-Insulator transition of $La_{1-x}Sr_xCoO_3$", J. Solid State Chem., 121, (1996), 423

45. Van Doorn, R.H.E. and Burggraaf, A.J., "Structural aspects of the ionic conductivity of $La_{1-x}Sr_xCoO_{3-\delta}$", Solid State Ionics 128, (2000), 65.
46. Kharton, V.V.. Naumovich, E.N., Vecher, A.A. and Nikolaev, A.V., "Oxide ion conduction in solid solutions $Ln_{1-x}Sr_xCoO_{3-\delta}$ (Ln =La, Pr, Nd)", J. Solid State Chem. 120, (1995), 128.
47. Takeda, Y., Kanno, R., Takada, T., Yamamoto, O., Takano, M. and Bando, Y., "Phase relation and oxygen nonstoichiometry of perovskite-like compound $SrCoO_x$ ($2.29<x<2.80$)", Z.Anorg.allg.Chem. 540/541, (1986), 259-270.
48. Seppännen , M., Kytö, M., and Taskinen, P., "Stability of the Ternary phases in the La-Co-O System", Scand.J.Metallurgy 8, (1979), 199-204
49. Seppännen , M., Kytö, M., and Taskinen, P., "Defect structure and nonstoichiometry of $LaCoO_3$", Scand.J.Metallurgy 9, (1980), 3-11.
50. De Souza, R.A., Fleig, J., Merkle, R. and Maier, J., "$SrTiO_3$: a model electroceramic", Z.Metallkd. 94, No.3, (2003), 218-225
51. Steinsvik, S., Bugge, R., Gjønnes, J, Taftø, J. and Norby, T., "The defect structure of $SrTi_{1-x}Fe_xO_{3-y}$ (x=0-0.8), investigated by electrical conductivity measurements and electron energy loss spectroscopy (EELS)", J.Phys.Chem.Solids 58 (6), (1997), 969-976.
52. Shannon, R.D., "Revised effective ionic radii and systematic studies of interatomicdistances in halides and chalcogenides", Acta Chrystallogr. A32, (1976), 751-767.
53. Mizusaki, J., Yoshihiro, M., Yamauchi, S. and Fueki, K., "Nonstoichiometry and defect structure of the perovskite-type oxides oxides $La_{1-x}Sr_xFeO_{3-\delta}$", J.Solid State Chem. 58, (1985), 257-266.
54. Wærnhus, I.," Defect Chemistry, Conductivity and mass transport properties of $La_{1-x}Sr_xFeO_{3-\delta}$ (x=0 and 0.1)" , Thesis, Norwegian University of Science and Technology, (2003). b) Paper 4 in that thesis
55. Kröger, F.A., "The chemistry of inperfect crystals Vol. 2.", North-Holland Pub. (1974).
56. Walters, L.C. and Grace, R.E., "Formation of point defects in Strontium titanate", J.Phys.Chem.Solids 28, (1967), 239-244.
57. Chan, N.-H., Sharma, R.K. and Smyth, D.M., "Nonstoichiometry in $SrTiO_3$", J.Electrochem Soc 128, No. 8, (1981), 1762-1769.
58. Eror, N.G. and Balachandran, U., "High-Temperature defect structure of acceptor doped strontium titanate", J.Am.Ceram.Soc. 65, No. 9, (1982), 426-431.
59. Waser, R., "Bulk conductivity and defect chemistry of acceptor doped strontium titanate in the quenched state", J.Am.Ceram.Soc. 74, No. 8, (1991), 1934-1940.

60. Choi, G.M. and Tuller, H., Defect structure and electrical properties of Single crystal $Ba_{0.03}Sr_{0.97}TiO_3$, J.Am.Ceram.Soc. 71, No. 4, (1988), 201-205.
61. Moos, R. and Härdtl, K.H., "Defect chemistry of donor doped and undoped Strontium titanate ceramics between 1000° and 1400 °C, J.Am.Ceram.Soc., 80, No. 10, (1997), 2549-62.
62. Denk, I., Münch, W. and Maier, J., "Partial conductivities in $SrTiO_3$: Bulk Polarization experiments, oxygen concentration cell measurements, and defect-chemical modelling", J.Am.Ceram.Soc. 78, No. 12, (1995), 3265-3272.
63. Maier J., Scwitzgebel, G. and Hagemann, H.-J., "Electrochemical investigations of conductivity and chemical diffusion in pure and doped cubic $SrTiO_3$ and $BaTiO_3$", J.Solid State Chem 58, (1985), 1-13.
64. Lankhorst, M.H.R. and Bouwmeester, H.J.M., "Determination of oxygen nonstoichiomtery and diffusivity in mixed conducting oxides by oxygen coulometric titration, I. Chemical diffusion in $La_{0.8}Sr_{0.2}CoO_{3-\delta}$", J.Electrochem Soc. 144, No.4, (1997), 1261-1267.
65. Petrov, A.N., Cherepanov, V.A., Kononchuk, O.F. and Gavrilova, L.Ya., "Oxygen nonstoichiometry of $La_{1-x}Sr_xCoO_{3-\delta}$ ($0< x \leq 0.6$)", J.Solid State Chem. 87, (1990), 69-76.
66. Lankhorst, M.H.R., Bouwmeester, H.J.M. and Verweij, H., "High-temperature coulometric titration of $La_{1-x}Sr_xCoO_{3-\delta}$: Evidence for the effect of electronic band structure on nonstoichiometric behaviour", J.Solid State Chem 133, (1997), 555-567.
67. Lankhorst, M.H.R. and Bouwmeester, H.J.M., "Determination of oxygen nonstoichiomtery and diffusivity in mixed conducting oxides by oxygen coulometric titration, II. Oxygen nonstoichiometry and defect model for $La_{0.8}Sr_{0.2}CoO_{3-\delta}$", J.Electrochem Soc. 144, No.4, (1997), 1268-1273.
68. Lankhorst, M.H.R, Bouwmeester, H.J.M. and Verweij, H., "Thermodynamics and transport of Ionic and electronic defects in crystalline oxides", J.Am.Ceram.Soc. 80 [9], (1997), 2175-2198.
69. Lankhorst, M.H.R, Bouwmeester, H.J.M. and Verweij, H., "Use of the rigid band formalism to interpret the relationship between O chemical potential and electron concentration of $La_{1-x}Sr_xCoO_{3-\delta}$", Phys.Rev.Lett. 77, No.14. (1996), 2989-2992.
70. Mizusaki, J.,Tabuchi, J.,Matsuura, T., Yamauchi, S. and Fueki, K., "Electrical conductivity and Seebeck coefficient of nonstoichiometric $La_{1-x}Sr_xCoO_{3-\delta}$", J. Eletrochem. Soc. 144, No.7, (1989), 2082-2088.
71. Tai,L.-W., Nasrallah, M.M., Naderson, H.U., Sparlin, D.M. and Sehlin, S.R., " Structure and electrical properties of $La_{1-x}Sr_xCo_{1-}$

$_yFe_yO_3$. Part 1. The system $La_{1-x}Sr_xCo_{1-y}Fe_yO_3$", Solid State Ionics 76, (1995), 259-271.

72. Watterud, G., Wiik, K. and Julsrud, S., "Oxygen Transport in $La_{1-x}Sr_xCoO_{3-\delta}$ (x=0, 0.2 and 0.5) assessed with electrical conductivity relaxation. Part I: Bulk Diffusion and k_{chem}." Part I of this thesis
73. ten Elshof, J.E., Lankhorst, M.H.R. and Bouwmeester, H.J.M, " Oxygen exchange and diffusion coefficients of strontium doped lanthanum ferrites by electrical conductivity relaxation", J.Electrochem.Soc. 144, No. 3, (1997), 1060-1067.
74. van der Haar, L.M., den Otter, M.W., Morskate, M., Bouwmeester, H.J.M. and Verweij, H., Chemical diffusion and oxygen surface transfer of $La_{1-x}Sr_xCoO_{3-\delta}$ studied with electrical conductivity relaxation", J.Electrochem.Soc. 149, No.3, (2002),J41-J46.
75. den Otter, M.W., Bouwmeester, H.J.M, Boukamp, B.A. and Verweij, H., "Reactor flush time correction in relaxation experiments", J.Electrochem.Soc. 148, (2001), J1.
76. Crank, J., "The Mathematics of Diffusion", 2nd Ed. , Oxford Science Publications, (1975).
77. Yasuda, I and Hikita, T. , "Precise determination of the chemical diffusion coefficient of calcium doped lanthanum chromite by means of electrical conductivity relaxation", J.Electrochem.Soc. 141, No. 5, (1994), 1268-1273.
78. Kingery, W.D, Bowen, H.K and Uhlmann, D.R., "Introduction to ceramics", Wiley-Interscience, (1976).
79. Schmalzried, H. , "Solid State reactions", Academic Press Inc., (1974).
80. Kofstad, P., "Nonstoichiometry, Diffusion and electrical conductivity in binary metal oxides", John Wiley and Sons (1972).
81. 2nd International Conference on Transport in Nonstoichiometric Compounds, Round Table Discussion, Kofstad, P. (leader), Solid State Ionics 12 (1984), 171.
82. Maier, J, "Physical chemistry of ionic materials: Ions and electrons in solids", John Wiley & Sons (2004).
83. Bouwmeester, H.J.M. and Burggraaf, A.J. in "Dense Ceramic Membranes for oxygen separation" in "The CRC Handbook of the Solid State Electrochemistry", P.J. Gellings and H.J.M. Bouwmeester Eds., CRC Press Inc., (1997).
84. Weppner, W. and Huggins, R.A., "Determination of the kinetic parameters of mixed conducting electrodes and application to the system Li_3Sb", J. Electrochem.Soc. 124, No. 10, (1977), 1569-1578.
85. Mizusaki, J., "Nonstoichiometry, diffusion and electrical properties of perovskite-type oxide electrode materials", Solid State Ionics 52, (1992), 79-91.

86. Ishigaki, T., Yamauchi, S., Mizusaki, J., Fueki, K. and Tamura, H., "Tracer diffusion coefficient of oxide ions in $LaCoO_3$ Single crystal", J.Solid State Chem., 54**,** (1984), 100-107.
87. Ishigaki, T., Yamauchi, S., Kishio, K., Mizusaki, J., and Fueki, K., "Diffusion of oxide ion vacancies in perovskite-type oxides", J.Solid State Chem., 73**,** (1988), 179-187.
88. Wang, S., Verma, A., Yang, Y.L., Jacobsson, A.J. and Abeles, B., "The effect of the magnitude of the oxygen partial pressure change in electrical conductivity relaxation measurements: oxygen transport kinetics in $La_{0.5}Sr_{0.5}CoO_{3-\delta}$", Solid State Ionics 140, (2001), 125-133.
89. Adler, S.B., "Mechanism and kinetics of oxygen reduction on porous $La_{1-x}Sr_xCoO_{3-\delta}$ electrodes", Solid State Ionics 111, (1998), 125-134.
90. van Hassel, B.A., Kawada, T., Sakai, N., Yokokawa, H., Dokiya, M. and Bouwmeester, H.J.M., "Oxygen permeation modelling of perovskites", Solid State Ionics 66, (1993), 295-.305
91. Ramos, T., and Atkinson, A., "Oxygen diffusion and surface exchange in $La_{1-x}Sr_xFe_{0.8}Cr_{0.2}O_{3-\delta}$ (x=0.2, 0.4 and 0.6)", Solid State Ionics 170, (2004), 275-286.
92. ten Elshof, J.E, Bouwmeester, H.J.M., Verweij, H., "Oxygen transport through $La_{1-x}Sr_xFeO_3$ membranes. I: Permeation in air/He gradients", Solid State Ionics 81, (1995), 97-105.
93. ten Elshof, J.E, Bouwmeester, H.J.M., Verweij, H., "Oxygen transport through $La_{1-x}Sr_xFeO_3$ membranes. II: Permeation in CO/CO_2 gradients", Solid State Ionics 89, (1996), 81-92.
94. Chen, C.H., Bouwmeester, H.J.M., van Doorn, R.H.E., Kruidhof, H. and Burggraaf, A.J., "Oxygen permeation of $La_{0.3}Sr_{0.7}CoO_{3-\delta}$", Solid State Ionics 98, (1997), 7-13.
95. Lein, H.L, Wiik, K. and Grande, T., Oxygen permeation and cation demixing of $La_{0.5}Sr_{0.5}Fe_{1-x}Co_xO_{3-\delta}$ ($0\leq x\leq 1$)", (2005), to be published
96. ten Elshof, J.E, Bouwmeester, H.J.M., Verweij, H., "Oxidative coupling of methane in a mixed-conducting perovskite membrane reactor". Appl.Catal. A. , 130, (1995), 195-212
97. Lane, J.A., Benson, S.J., Waller, D. and Kilner, J.A., "Oxygen transport in $La_{0.6}Sr_{0.4}Co_{0.2}Fe_{0.8}O_{3-\delta}$", Solid State Ionics 121, (1999), 201-208.
98. Huang, K. and Goodenough, J.B., "Oxygen permeation through cobalt-containing perovskites, surface oxygen exchange vs. lattice oxygen diffusion", J.electrochem.Soc 148, No. 5, (2001), E203-E214.
99. Diethelm, S. and van Herle, J., "Oxygen transport through dense $La_{0.6}Sr_{0.4}Fe_{0.8}Co_{0.2}O_{3-\delta}$ perovskite-type permeation membranes", J.Eur.Ceram.Soc. 24, (2004), 1319-1323.
100. Paladino, A.E., "Oxidation kinetics of single-crystal $SrTiO_3$", J.Am.Ceram.Soc 48, No. 9, (1965), 476-478.

101. Walters, L.C. and Grace, R.E., "Formation of point defects in Strontium titanate", J.Phys.Chem.Solids 28, (1967), 239-244.
102. Schwarz, D.B. and Anderson, H.U., "Determination of oxygen chemical diffusion coefficients in single crystal $SrTiO_3$ by capacitance manometry", J.Electrochem.Soc 122, No. 5, (1975), 707-710.
103. Claus, J., Leonhardt, M. and Maier, J., "Tracer diffusion and chemical diffusion in acceptor doped $SrTiO_3$", J.Phys.Chem.Solids 61, (2000), 1199-1207.
104. Müller, A. and Härdtl, K.H., "Ambipolar diffusion phenomenain $BaTiO_3$ and $SrTiO_3$", Apll.Phys. A, 49, (1989), 75-82.
105. Noll, F., Münch, W., Denk, I. and Maier, J., " $SrTiO_3$ as a prototype of a mixed conductor: Conductivities, oxygen diffusion and boundary effects", Solid State Ionics 86-88, (1996), 711-717.
106. Bieger, T., Maier, J. and Waser, R., "Optical investigation of oxygen incorporation in $SrTiO_3$", Solid State Ionics 53-56, (1992), 578-582.
107. Bieger, T., Maier, J. and Waser, R., "Kinetics of oxygen incorporation in $SrTiO_3$: An optical investigation", Sens.Act. B, 7, (1992), 763-768.
108. Tragut, Ch., Härdtl, K.H., "Kinetic behaviour of resistive oxygen sensors", Sens.Act. B, 4, (1991), 425-429.
109. Schlüter, H.-J., Barsoum, M. and Maier, J., "Kinetic studies of oxygen incorporation in $SrTiO_3$ by permation experiments, Solid State Ionics 101-103, (1997), 509-515.
110. Merkle, R. and Maier, J., "Oxygen incorporation into Fe-doped $SrTiO_3$: Mechanistic interpretation of the surface reaction", Phys.Chem.Chem.Phys 4, (2002), 4140-4148.
111. Bouwmeester, H.J.M., Kruidhof, H. and Burggraaf, A.J., "Importance of the surface exchange kinetics as rate limiting step in oxygen permeation through mixed-conducting oxides", Solid State Ionics 72, (1994), 185-194.
112. Prigogine, I., "Thermodynamics of irreversible processes", 2nd Ed., John Wiley & Sons, (1961).
113. Maier, J., "On the correlation of macroscopic and microscopic rate constants in solid state chemistry", Solid State Ionics 112 (1998), 197-228.
114. Maier, J., "Interaction of oxygen with oxides: How to interpret measured effective rate constants?", Solid State Ionics 135 (2000), 575-588.
115. ten Elshof, J.E., Lankhorst, M.H.R. and Bouwmeester, H.J.M., " Chemical diffusion and surface exchange of $La_{0.6}Sr_{0.4}Co_{0.6}Fe_{0.4}O_{3-\delta}$", Solid State Ionics 99, (1997), 15-22.
116. Chen, X., Wang, S., Yang, Y.L., Smith, L., Wu, N.J., Kim, B.-I., Perry, S.S., Jacobson, A.J. and Ignatiev, A., "Electrical conductivity

relaxation studies of an epitaxial $La_{0.5}Sr_{0.5}CoO_{3-\delta}$ thin film", Solid State Ionics 146, (2002), 405-413.

117. Ishigaki, T., Yamauchi, S., Mizusaki, J., Fueki, K. and Tamura, H., "Diffusion of oxide ions in $LaFeO_3$ single crystal", J.Solid State Chem., 55**,** (1984), 50-53.
118. De Souza, R.A. and Kilner, J.A., "Oxygen transport in $La_{1-x}Sr_xMn_{1-y}Co_yO_{3\pm\delta}$ perovskites. Part II: Oxygen surface exchange.", Solid State Ionics 126, (1999), 153-161.
119. Kim, S., Wang, S., Yang, Y.L., Wu, N., Ignatiev, A., Jacobson, A.J. and Abeles, B., "Oxygen surface exchange in mixed ionic electronic conductors: Applications to $La_{0.5}Sr_{0.5}Fe_{0.8}Ga_{0.2}O_{3-\delta}$", J Electrochem Soc., No. 6, 147, (2000), 2398-2406.
120. Kilner, J.A., De Souza, R.A., Fullarton, I.C., "Surface exchange of oxygen in mixed conducting perovskite oxides", Solid State Ionics 86-88, (1996), 703-709.
121. Ezin, A.N., Kurumchin, E.Kh., Muryugin, I.V., Tsidilkovski, V.I. and Vdovkin, G.K., "The types of surface exchange and diffusion of oxygen in $La_{0.7}Sr_{0.3}CoO_{3-\delta}$", Solid state ionics 112, (1998), 117-122.
122. Van Doorn, R.H.E., Fullarton, I.C., de Souza, R.A., Kilner, J.A., Bouwmeester, H.J.M., and Burggraaf, A.J., "Surface oxygen exchange of $La_{0.3}Sr_{0.7}CoO_{3-\delta}$", Solid State Ionics 96, (1997), 1-7
123. Watterud, G., Wiik, K. and Julsrud, S., "Oxygen Transport in $La_{1-x}Sr_xCoO_{3-\delta}$ (x=0, 0.2 and 0.5) assessed with electrical conductivity relaxation. Part II: The mechanisms of oxygen surface exchange." Part II of this thesis
124. Leonhardt, M., De Souza, R.A., Claus, J. and Maier, J., "Surface kinetics of oxygen incorporation into $SrTiO_3$", J. Electrochem Soc. 146, No.2, (2002), J19-J26.
125. Denk, I., Noll, F. and Maier, J., "*In situ* profiles of oxygen diffusion in $SrTiO_3$: Bulk behaviour and boundary effects", J.Am.Ceram.Soc 80, No. 2, (1997), 279-285.
126. Ishihara, T., Kilner, J.A., Honda, M., Sakai, N., Yokokawa, H. and Takita, Y., "Oxygen surface exchange and diffusion in $LaGaO_3$ based perovskite type oxides", Solid State Ionics 113-115, (1998), 593-600.
127. Steele, B.C.H, "Interfacial reactions associated with ceramic ion transport membranes", Solid State Ionics 75, (1995), 157-165.

OXYGEN DIFFUSION AND SURFACE EXCHANGE IN $La_{1-x}Sr_xCoO_{3-\delta}$ (x=0, 0.2 and 0.5) ASSESSED BY ELECTRICAL CONDUCTIVITY RELAXATION. Part I: Bulk Diffusion and k_{chem}.

Geir Watterud[a], Stein Julsrud[b] and K. Wiik[*a],
[a] Department of Materials Science and Engineering
Norwegian University of Science and Technology
N-7491 Trondheim, Norway.
[b] Scanwafer AS, N-3907 Porsgrunn, Norway

ABSTRACT

Oxygen transport in $LaCoO_3$ (LC), $La_{0.8}Sr_{0.2}CoO_{3-\delta}$ (LSC-02) and $La_{0.5}Sr_{0.5}CoO_{3-\delta}$ (LSC-05) have been measured with electrical conductivity relaxation in the temperature interval 850 to 1000 °C, and for oxygen partial pressures between 0.2 and 0.002 atm.

Activation energies for the oxygen component diffusion coefficient, D_O, and the oxygen vacancy diffusion coefficient, D_V, were determined. The activation energies for D_O varies from 279 kJ/mol for LC to 174-222 kJ/mol for LSC-02 and 90-105 kJ/mol for LSC-05, decreasing with increasing Sr-content. The activation energies for the vacancy diffusion coefficient, D_V, are lower than for the component diffusion coefficients and typical values are 77 kJ/mol for LC, 85 kJ/mol for LSC-02 and 75 kJ/mol for LSC-05, that is, almost independent of Sr-content.

The enthalpies of vacancy formation decreases with increasing Sr content. The values are 206 kJ/mol for LC, 75 kJ/mol for LSC-02 and 15 kJ/mol for LSC-05 which agrees well with values reported in the literature.

For low vacancy concentrations in LC and LSC-02, D_V is virtually constant. However, at some high vacancy concentration, corresponding with every eleventh or tenth oxygen site being vacant, there appears to be a pronounced increase in D_V with increasing nonstoichiometry. The behaviour is not

---

Corresponding author: Kjell Wiik, Department of Materials Technology, Norwegian University of Science and Technology, N-7491 Trondheim, Norway, e-mail: kjell.wiik@material.ntnu.no, Telephone no.: +47 73 59 40 82, fax no:+47 73 59 08 60

easily explained, but may be related to a decreasing activation energy for vacancy diffusion with increasing nonstoichiometry.

The component diffusion coefficient, D_O, shows a linear increase with increasing oxygen vacancy concentration regardless of which composition studied. At high vacancy concentrations, an increase in the slope is observed consistent with the correlation between D_O and D_V.

Keywords:
$La_{1-x}Sr_xCoO_{3-\delta,}$ Electrical conductivity relaxation, Chemical surface exchange coefficient, Chemical diffusion coefficient, Activation energies, Component diffusion coefficient, Vacancy Diffusion coefficient, Enthalpy of vacancy formation.

INTRODUCTION

Lanthanum coboltites, pure and substituted with strontium, are characterised by their ability to accept relatively high concentrations of oxygen vacancies at elevated temperatures. This fact combined with the relative high mobility of the vacancies causes this material to exhibit a high oxygen ionic conductivity. In combination with a high metallic like electronic conductivity [1], these materials are truly mixed conductors and attractive candidates for oxygen separation membranes [2], oxidation catalysts [3,4] and electrodes in solid oxide fuel cells and oxygen sensors [5].

The different material properties for pure and strontium doped lanthanum coboltites have been investigated extensively. Säppanen et al. have examined stability [6] and the oxygen nonstoichiometry [7] in pure $LaCoO_3$. They concluded that pure $LaCoO_3$ is stable at oxygen partial pressures above approx. 10^{-5} atm at 1000 °C. When Sr is substituted into the matrix, more oxygen vacancies are introduced. This causes an increase in the lower oxygen partial pressure stability limit of the compound; thus the interval of stability will be narrower.

The oxygen transport in oxide based mixed conductors may be divided in two inherently different processes comprising surface exchange processes and solid-state oxygen ion diffusion in the bulk phase.

The transport properties of $La_{1-x}Sr_xCoO_{3-\delta}$ have been investigated by many authors [8,10,11,12]. van der Haar et al. [8] have studied the oxygen diffusion and oxygen surface exchange in $La_{1-x}Sr_xCoO_{3-\delta}$ (x=0.2, 0.5 and 0.7) in the temperature range 600-850 °C with electrical conductivity relaxation. It was found that the chemical diffusion coefficient, D_{chem}, and the chemical surface exchange coefficient, k_{chem}, both decreased with decreasing P_{O2} for all compositions. They concluded that the somewhat counter-intuitive behaviour of D_{chem} might be due to ordering of the oxygen vacancies taking place at low P_{O2}´s. However, according to Nowotny and Rekas [9] the defect chemistry in undoped and Sr doped $LaCoO_{3-\delta}$ is best described by a random model, i.e. no oxygen vacancy ordering.

Ishigaki et al. studied the oxygen diffusion in single crystal $LaCoO_3$ [10] by means of tracer diffusion in the temperature interval 700-1000 °C. The activation energy for migration of oxygen vacancies (D_V) were estimated to 18 kcal/mol (75 kJ/mol) and for oxygen ions (D_O^*) to 75 kcal/mol (315 kJ/mol). For the composition $La_{0.9}Sr_{0.1}CoO_{3-\delta}$ the value for vacancy diffusion (D_V) was 79 kJ/mol and for oxygen ions (D_O^*) 270 kJ/mol [11].

Lankhorst et al. [12] have studied chemical diffusion in $La_{0.8}Sr_{0.2}CoO_{3-\delta}$ at temperatures between 700 and 1000 °C, by the method of oxygen coulometric titration. They reported an activation energy for D_{chem} to be 135 kJ/mol. The reported D_{chem} values showed only a weak P_{O2} dependency, changing from an increasing dependency at low temperatures to a decreasing at higher temperatures. No explanation for the observed P_{O2} dependency is offered.

In this work we investigate the processes of oxygen bulk diffusion and oxygen surface exchange by means of electrical conductivity relaxation measurements. Numerical values for D_{chem} and k_{chem} are presented as well as derived coefficients such as oxygen component diffusion- (D_O) and oxygen vacancy diffusion coefficients (D_V). Diffusion behaviour is discussed in relation to temperature, P_{O2} and composition (x). In Part II of this paper the surface exchange processes will be further investigated based on reported k_{chem} values. Possible surface exchange mechanisms, both for oxidation and reduction, will be put forward and discussed.

THEORY

Delocalised electrons and the significance of oxygen nonstoichiometry

In contrast to the $La_{1-x}Sr_xFeO_{3-\delta}$-system [14,15] we are unable to describe the defect chemistry for the $La_{1-x}Sr_xCoO_{3-\delta}$-system by a localised electron model. Experimental data for oxygen nonstoichiometry and Seebeck coefficient fitted to a charge disproportionation model for the cobalt ion led to inconsistent results [12]. The oxygen nonstoichiometry have been examined by Mizusaki et al. [16] and Petrov et al. [17] by means of thermogravimetry and coulometric titration, respectively. Based on these data Lankhorst et al. [12,18,19,20,21] have put forward a model for the nonstoichiometry based on itinerant electrons, i.e. delocalised electrons. The model is supported by the high electronic conductivities and low Seebeck coefficients [1,22].

In Kröger -Vink notation [23] the reversible oxidation reaction can be written, viz.

$$O_2(g) + 2V_O^{\bullet\bullet} + 4e^- \rightleftarrows 2O_O^x \qquad (1)$$

In Eq. (1), the electrons are assumed to be delocalised.

Applying chemical potentials for the different defect species, a relation between oxygen nonstoichiometry and oxygen chemical potential can be formulated. The rigid band model, as employed by Lankhorst et al. [18], assume that the conduction band energies do not change while changing the number of electrons in the band. The relation is given by Eq. (2).

$$\mu_{O_2}^{oxide} = \varepsilon_{O_2}^{oxide} - Ts_{O_2}^{oxide} = E_{ox} - \frac{4(2\left[V_O^{\cdot\cdot}\right] - x)}{g(\varepsilon_F)} - TS_{ox} - 2RT\ln\left(\frac{\left[V_O^{\cdot\cdot}\right]}{3-\left[V_O^{\cdot\cdot}\right]}\right) = \mu_{O_2}^{gas} \tag{2}$$

where E_{ox}, S_{ox} are the standard free energy and entropy of oxidation of the oxide, while the x denotes the fraction of Sr substitution. Numeric values are given in Tab. 1, and μ_{O2}^{gas} is described in App. 1.

Table 1. Parameters used to calculate the oxygen nonstoichiometry in LSC-02 and LSC-05 taken from Ref [18]. The values for x = 0.5 are obtained by interpolation between x = 0.4 and 0.7.

Parameter	x = 0.2	x =0.4	x = 0.5 Interpolated between x=0.4 and 0.7	x=0.7
E_{ox} (kJ/mol)	-334.1	-301.4	-299	-294.5
S_{ox} (J/mol K)	69.5	69.6	70	70.5
$g(\varepsilon_F)$ $[(kJ/mol)^{-1}]$	0.0159	0.0159	0.0155	0.0152

The variation in oxygen nonstoichiometry with composition (x), P_{O2} and temperature is adequately described by Eq. (2). A significant distinction between a localised and a delocalised model is the absence of configurational entropy on the B-sublattice in the delocalised case, consequently Co is not assigned any configurational entropy in $LaCoO_3$.

Solid State Diffusion

The self-diffusion coefficient or the component diffusion coefficient for oxygen, D_O, is described by random-walk diffusion, i.e. no chemical potential gradients are present. The oxygen transport can also be described as counter diffusion of oxygen vacancies, thus introducing a vacancy diffusion coefficient, D_V. A mechanistic approach to the component diffusion and vacancy diffusion coefficients is given by Kingery et al. [24] and Kofstad [25].

The D_O and D_V coefficients are related through [26]

$$C_O D_O = C_V D_V \tag{3}$$

, where C_O and C_V are the concentration of oxygen ions and vacancies, respectively. At sufficiently low concentrations of oxygen vacancies each vacant oxygen site is surrounded by occupied oxygen sites only, and the corresponding oxygen vacancy diffusion coefficient, D_V, is independent of the population of oxygen vacancies [25]. In the same regime $\frac{C_V}{C_O} \approx n_V$, thus Eq. (3) may be rewritten accordingly:

$$D_O = \frac{C_V}{C_O} D_V \approx n_V D_V \tag{4}$$

where n_V is the fraction of vacancies.

Given the presence of a gradient in chemical potential or concentration, the transport is adequately described by "Fickian" diffusion (Fick´s 1st. law), which relates the oxygen flux to a chemical diffusion coefficient, D_{chem}, and the gradient in oxygen concentration.

$$J_O = -D_{chem} \frac{dC_O}{dy} \tag{5}$$

where y is the direction of diffusion. In the case of oxygen transport in perovskites oxygen ions are the only mobile species. On this basis, Weppner and Huggins derived the following relation between the oxygen component diffusion coefficient, D_O, and the chemical diffusion coefficient D_{chem} [27]:

$$W_O = \frac{1}{RT}\frac{\partial \mu_O}{\partial \ln C_O} = \frac{D_{chem}}{D_O} \tag{6}$$

where μ_O is the chemical potential of atomic oxygen given in Eq. (7).

$$\mu_O = \mu_O^0 + RT \ln \sqrt{P_{O_2}} \tag{7}$$

Thus

$$W_O = \frac{1}{2}\frac{\partial \ln P_{O_2}}{\partial \ln C_O} \tag{8}$$

where W_O (in honour of Wagner) is referred to as a thermodynamic factor (or enhancement factor) related to oxygen ions.

The vacancy diffusion coefficient D_V is related to the component diffusion coefficient, D_O, given in Eq.(3), hence, a thermodynamic factor for vacancies can also be introduced.

$$D_{chem} = W_V D_V = \left(-\frac{1}{2} \cdot \frac{d \ln P_{O2}}{d \ln C_V} \right) \cdot D_V \tag{9}$$

Transport coefficients as well as thermodynamic factors will all be temperature dependent, thus allowing us to associate activation energies, apparent or real, to all the variables. Kofstad [25] states that the activation energy for the vacancy diffusion is equal to the enthalpy of oxygen ion migration, ΔH_m, since the vacancy can move to any occupied neighbour oxygen site in the structure. Since the oxygen component diffusion coefficient, D_O, is the product between the concentration of oxygen vacancies, n_V, and vacancy diffusion coefficient, D_V, (Eq. 4), the corresponding activation energy for oxygen diffusion should be equal to the sum between the enthalpy of oxygen vacancy formation, ΔH_V, and oxygen migration, ΔH_m, viz.

$$E_{a,D_o} = \Delta H_V + \Delta H_m \tag{10}$$

The thermodynamic factors, W_O and W_V, will also depend on oxygen partial pressure and composition. However, at constant partial pressures and composition apparent activation energies, E_{a,W_o} and E_{a,W_V}, may also be assigned to the thermodynamic factors. By letting the P_{O2} (and composition)

be constant it is possible to assign activation energies to the thermodynamic factors. By introducing the activation energies in Eq. (6) and (9) and rearranging one obtains

$$\begin{aligned} D_{chem} &= D^0_{chem} e^{-\frac{E_{a,D_{chem}}}{RT}} \\ &= W_O D_O = W^0_O e^{-\frac{E_{a,W_O}}{RT}} D^0_O e^{-\frac{E_{a,D_O}}{RT}} \\ &= W_V D_V = W^0_V e^{-\frac{E_{a,W_V}}{RT}} D^0_V e^{-\frac{E_{a,D_V}}{RT}} \end{aligned} \tag{11}$$

where $D^0_{chem}, D^0_o, D^0_V, W^0_o$ and W^0_V are pre-exponential coefficients. Combining Eq. (10) and Eq (11) gives:

$$\begin{aligned} E_{a,D_{chem}} &= E_{a,W_o} + E_{a,D_o} = E_{a,W_o} + \Delta H_m + \Delta H_V \\ &= E_{a,W_V} + E_{a,D_V} = E_{a,W_V} + \Delta H_m \end{aligned} \tag{12}$$

This means that

$$\begin{aligned} \Delta H_V &= E_{a,W_V} - E_{a,W_o} \\ &= E_{a,D_o} - E_{a,D_V} \end{aligned} \tag{13}$$

Thus, the apparent vacancy formation enthalpy can either be derived from the thermodynamic factors, or from the activation energies for oxygen ion and vacancy diffusion coefficients.

For a more thorough discussion of phenomenological diffusion coefficients it is referred to Maier [28].

The chemical surface exchange coefficient

In analogy with chemical diffusion coefficients we may also define a chemical surface exchange coefficient, k_{chem}, where the oxygen exchange flux, J_o, is proportional with the "distance" from equilibrium expressed in terms of concentration [8,29], viz.

$$J_O = k_{chem}\left(C_t - C_\infty\right) \tag{14}$$

where C_t is the actual concentration of oxygen at the surface at any given time t and C_∞ is the equilibrium concentration of oxygen at the surface. The assessment of D_{chem} and k_{chem} are described and discussed in a later section. A more thorough discussion of k_{chem} is given in [13].

EXPERIMENTAL

Synthesis

Polycrystalline samples with composition $LaCoO_{3-\delta}$ (LC), $La_{0.8}Sr_{0.2}CoO_{3-\delta}$ (LSC-02) and $La_{0.5}Sr_{0.5}CoO_{3-\delta}$ (LSC-05) were synthesised by spray drying. Aqueous solutions of stoichiometric amount of cation nitrates (Merck or Fluka, p.a.) were made, and glycine (Merck, p.a.) was added as a complexing agent in a glycine/nitrate mole ratio of 5/9. In order to obtain a high compositional accuracy all reagents were calibrated thermogravimetrically with three parallels for each metal nitrate. Based on data from the calibration procedure the resulting uncertainty with respect to cation stoichiometry was found to be approx. ± 0.2 %, hence implicating the following compositional uncertainties: $La_{1.000\pm0.002}Co_{1.000\pm0.002}O_{3-\delta}$, $La_{0.800\pm0.0016}Sr_{0.200\pm0.0004}Co_{1.000\pm0.002}O_{3-\delta}$ and $La_{0.500\pm0.001}Sr_{0.500\pm0.001}Co_{1.000\pm0.002}O_{3-\delta}$.The total concentration of cations in the solution was approximately 0.8 M and the solutions were dried in a Büchi Mini Spray Dryer B-191 with hot air (150 °C) as the drying medium. The resulting solid precursors were ignited for decomposition to oxide by allowing it to fall through a vertical alumina tube preheated to 800-900 °C. The resulting oxide powders were ball milled (Si_3N_4-balls) overnight in 100% ethanol or isopropanol. The milled powders were further calcined at 900 – 1000 °C for 24 hours in air. The powders were then ball milled (Si_3N_4-balls) for 24 hours and heat-treated at 600 °C for 24 hours. The calcined powders were analysed by X-ray powder diffraction (XRD) (Cu Kα, Phillips PW1730/10) and it was shown that all samples were single phase (with a rhombohedral perovskite structure). The powders were uniaxially pressed to bars with approximate dimensions 50 x 10x 3.5 mm and subsequently isostatically pressed at 200 MPa and 20 °C. The bars were sintered at 1200 °C for 6 h (LC), 1150 °C for 2 h (LSC-02) based on Ref. [30] and 1150 °C for 12 h (LSC-05) based on Ref. [31]. The heating rate for all samples was 200 °C/h, while the cooling rate was 200 °C/h for LC and LSC-02, and 50 °C/h down to 750 °C and then 6 °C/h down to 450 °C for LSC-05. Bulk densities of the sintered bars were measured by the Archimedean method using isopropanol, and all samples were sintered to densities higher than 97 % of crystallographic densities ([30,31]). Densities of the samples studied are given in Tab 2.

Table 2. Measured densities, crystallographic densities and percentage densities of the samples in this study. Values taken from [30,31].

Sample	Crystallographic density [g/cm^3]	Measured density [g/cm^3]	Percentage density
$LaCoO_3$	7.26 [30]	7.06	97.2 %
$La_{0.8}Sr_{0.2}CoO_3$	6.91 [30]	6.83	98.8 %
$La_{0.5}Sr_{0.5}CoO_3$	6.42 [31]	6.38	99.3 %

XRD analysis of the sintered samples showed single-phase material. Prior to the measurements the samples were cut and polished with polycrystalline diamonds with 3 μm particle size. Typical sample dimensions for conductivity relaxation experiments were 3 mm x 3 mm x 23 mm.

Microstructure

In Fig 1 the microstructure in all the samples both before and after the experiments are given.

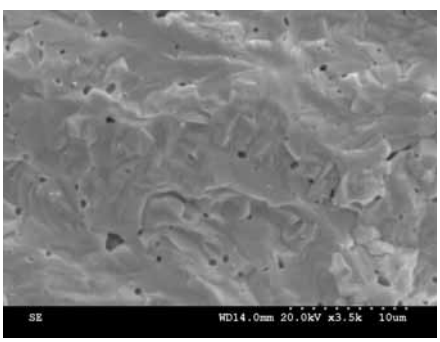

a)

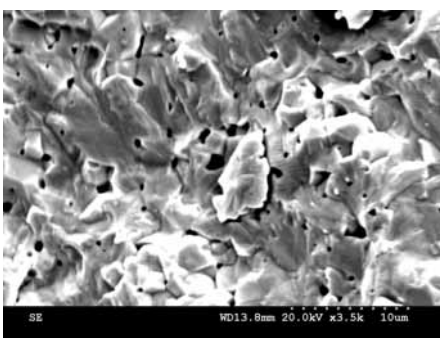

b)

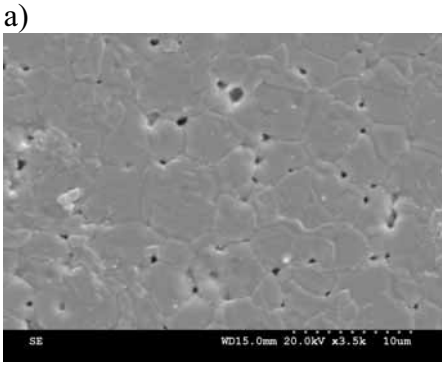

c)

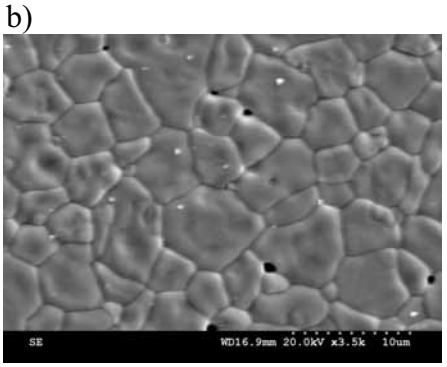

d)

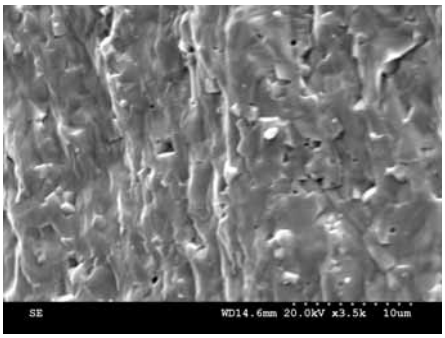
SE
WD14.6mm 20.0kV x3.5k 10um

e)

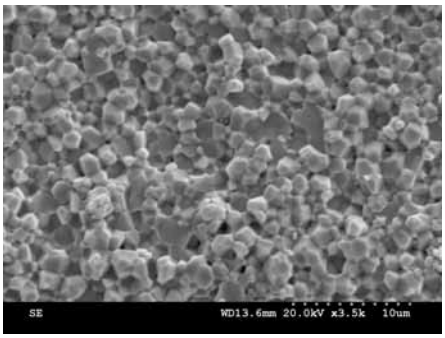
SE
WD13.6mm 20.0kV x3.5k 10um

f)

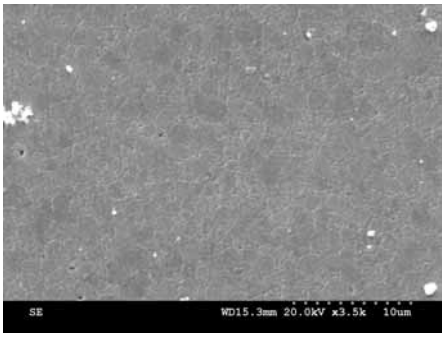
SE
WD15.3mm 20.0kV x3.5k 10um

g)

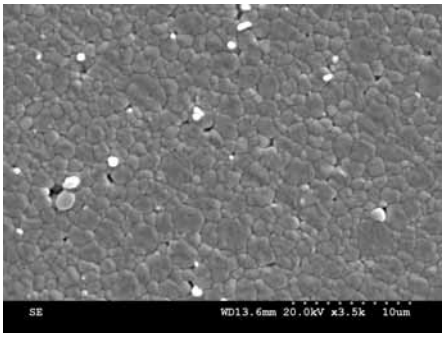
SE
WD13.6mm 20.0kV x3.5k 10um

h)

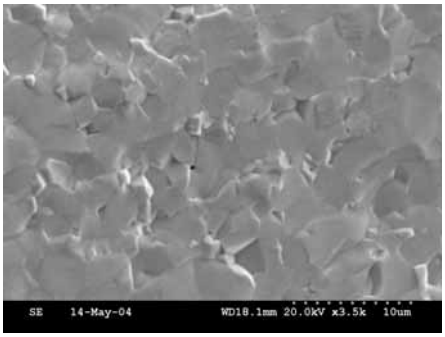
SE 14-May-04
WD18.1mm 20.0kV x3.5k 10um

i)

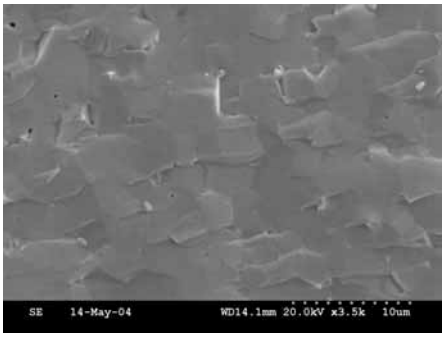
SE 14-May-04
WD14.1mm 20.0kV x3.5k 10um

j)

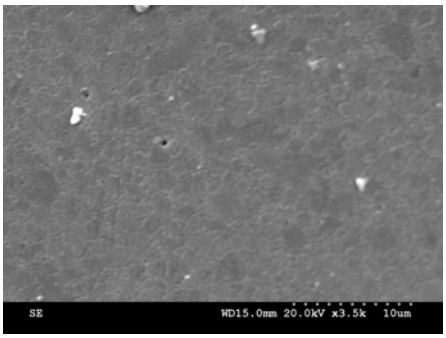

k)

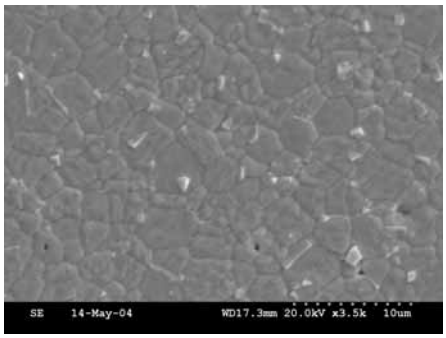

l)

Fig. 1. a) Fracture of LC b.e., b) Fracture of LC a.e., c) Surface of LC b.e., d) Surface of LC a.e., e) Fracture of LSC-02 b.e., f) Fracture of LSC-02 a.e., g) Surface of LSC-02 b.e., h) Surface of LSC-02 a.e., i) Fracture of LSC-05 b.e., j) Fracture of LSC-05 a.e., k) Surface of LSC-05 b.e., l) Surface of LSC-05 a.e. (b.e.= before experiments, a.e. =after experiments)

In Fig 1 a) –d) the bulk- and surface microstructure for LC are given, both prior to and after the experiment. From Fig 1 c) and d) it can be seen that, apart from thermally etched grain boundaries, no significant grain growth at the surface has taken place during the experiment. The conservation of bulk microstructure during the experiment is also evident from Fig. 1 a) and b). Total time at elevated temperatures is between 3 and 4 weeks.
In Fig 1 e) – h) the microstructure for LSC-02 is given. It is interesting to notice that the mode of fracture change from intra granular before the experiment (Fig. 1 e)) to inter granular after prolonged heating at elevated temperatures (Fig. 1 f)). Due to the change in fracture mode, it is not possible to conclude whether the bulk microstructure is preserved during the experiment. However, since the surface microstructure seems to be unaltered (Fig. 1 g) and h)) and in accordance with the bulk microstructure given in Fig. 1 h), it is likely to assume that the microstructure of LSC-02 also is preserved during the experiment.
For LSC-05 a minute grain growth seems to have taken place at the surface (Fig. 1 k) and l)) while a change in bulk microstructure is not evident. It can be concluded that a change in microstructure, if any, is very small even for LSC-05.

Conductivity relaxation

Oxygen surface exchange and diffusion were measured by the electrical conductivity relaxation technique. This technique involves measuring the time variation of the electrical conductivity after a well-defined step in the oxygen activity in the ambient atmosphere. The experimental set-up is the same as the one given by Wærnhus et al. [14] and is given in Fig 2.

The measurements were performed in the temperature interval between 850-1000 °C (900-1000°C for LC), and an oxygen partial pressure ranging from 0.2 to 0.002 atm in oxygen/nitrogen gas mixtures. The samples have been held at experimental temperatures for time periods of about four to six weeks. The change in oxygen partial pressure has been one (LC) or half an order (LSC-02 and LSC-05) of magnitude ($|\Delta \log P_{O2}| = 1.0$ or 0.5), respectively. The different oxygen partial pressures were produced by adjusting the flow ratios between oxygen and nitrogen in the total gas flow. The total flow in all experiments was either 250 or 500 ml/min at 25 °C. The oxygen partial pressure was changed in a stepwise manner by switching a four-way valve (Fig 2b). The time constant, τ, for the change in oxygen partial pressure in the vicinity of the sample depends on the total gas flow rate and vary typically between 0.9 and 0.4 seconds. A more thorough presentation of τ is given in the next section.

The electrical conductivity was measured with a standard four-point method. The positions of the voltage and current probes are given in Fig 2c. According to Hansen et al. [32] the distance between the voltage probe and the current probe should be greater than 3 times the smallest dimension. Fulfilling this requirement will result in a uniform electrical field between the voltage probes. This requirement was met in all experiments

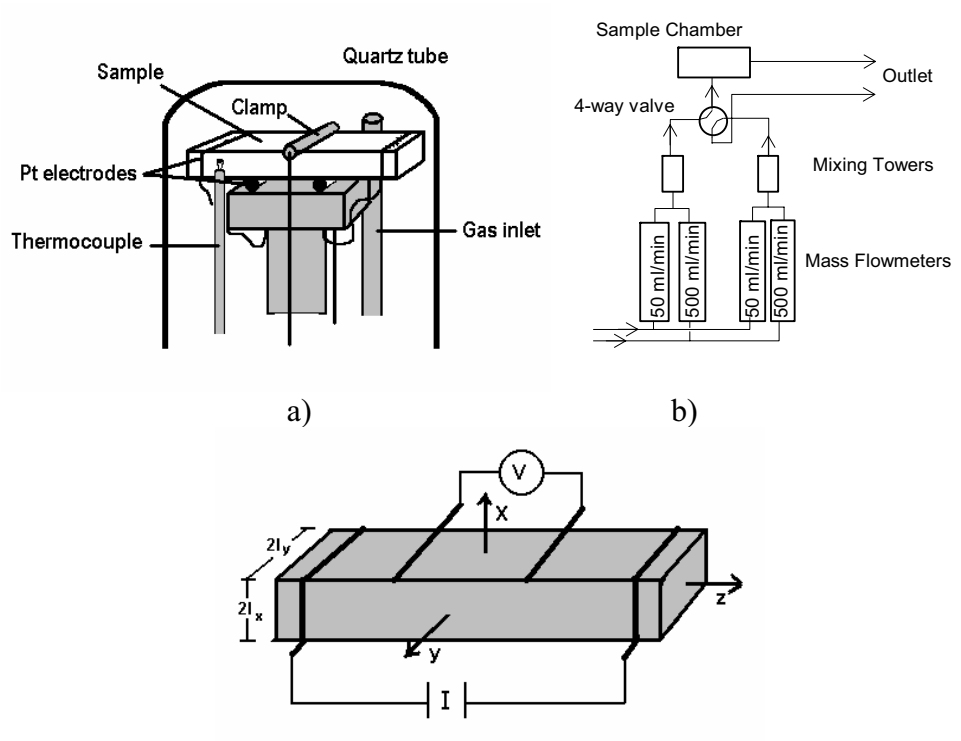

Fig. 2. a) The experimental set-up for the high temperature conductivity measurements, b) Schematic drawing of the equipment for gas mixing, c) The orientation of the sample and a visual guide to where the electrodes are attached. Figures taken from Wærnhus et al. [14]

Calculation of the transport parameters D_{chem} and k_{chem}.

The time dependent oxygen transport (non steady state) can be described by Fick´s second law

$$\frac{\partial C(x,t)}{\partial t} = D_{chem}\frac{\partial^2 C(x,t)}{\partial x^2} \tag{15}$$

, where C is the concentration of oxygen in the sample, D_{chem} is the chemical diffusion coefficient, x is the distance and t is the time. By introducing initial and boundary conditions as outlined by ten Elshof et al

[29] and van der Haar et al. [8], the mathematical definition of the k_{chem} parameter is given by:

$$J_O(x=\pm l_x) = \mp D_{chem}\frac{\partial C(x=\pm l_x,t)}{\partial x} = k_{chem}\left(C(x=\pm l_x,t) - C_\infty\right) \tag{16}$$

, where J_O denotes the oxygen flux (mono atomic) at the surface and C_∞ is the oxygen concentration at t=∞, i.e. equilibrium is established.

Suppose the change in oxygen activity/partial pressure is not stepwise, but follows a continuos change as described in Eq.(17) .

$$P_{O2} = P_{O2}(t=0) + \Delta P(1 - e^{-\frac{t}{\tau}}) \tag{17}$$

where the τ parameter is defined as the reactor flushtime. This approach to the oxygen step has been described by den Otter et al [33]. Introducing the change in oxygen partial pressure as described in Eq. (17), the solution to Eq. (15) becomes:

$$\frac{M(t)}{M_\infty} = \frac{M(x,y,z,t) - M_0}{M_\infty - M_0} = 1 - \prod_{j=x,y,z}\sum_{n=1}^{\infty}\frac{2L_j^2}{\Gamma_{n,j}^2\left(\Gamma_{n,j}^2 + L_j^2 + L_j\right)}\left[\frac{e^{-\beta_{n,j}t} - \beta_{n,j}\tau e^{-t/\tau}}{1 - \beta_{n,j}\tau}\right] \tag{18}$$

, where

$$\beta_{n,j} = \frac{\Gamma_{n,j}^2 D_{chem}}{l_j^2} \tag{19}$$

$$\Gamma_{n,x}\tan\Gamma_{n,x} = L_x \tag{20}$$

$$L_x = l_x \cdot \frac{k_{chem}}{D_{chem}} \tag{21}$$

and sample dimensions, l_x and l_y, are defined in in Fig. 2, whereas M is the mass of oxygen in the sample. Eq. (19) is the so called “trancendental equation” and the accuracy of the calculations partly depends on the magnitude of n. For all calculations in this work the number has been fixed and set to n=15, giving a high accuracy fit between the modelled and measured relaxations. Eq (18) is described in Crank [34].

The total gas flow used in the experiments was either 250 or 500 ml/min, depending on the requested partial pressure of oxygen, giving reactor flush times of 0.88 s and 0.44 s (τ) at 1000 °C, respectively. Flush time corrections are based on experimental data, replacing the sample with a thin film mixed conductor, and is described in more detail by Wærnhus et al.[14].

In order to apply conductivity relaxation as a method for the assessment of transport coefficients in mixed conductors, the conductivity, σ, must be linear proportional with the oxygen stoichiometry, (= 3-δ). The relation between electrical conductivity, σ, and total mass of oxygen (or oxygen stoichiometry) in a sample, M is derived by Yasuda and Hikita [35] and given in Eq. (22).

$$\frac{\sigma(t)-\sigma_0}{\sigma_\infty-\sigma_0}=\frac{M(t)}{M_\infty} \tag{22}$$

Eq. (22) relates electrical conductivity with D_{chem} and k_{chem} given in Eqs. (18)-(21).

In Fig 3 the conductivity from the experiments with LC, LSC-02 and LSC-05 is plotted versus the oxygen stoichiometry, whereas the oxygen stoichiometry vs. oxygen partial pressure is given in Fig. 10.

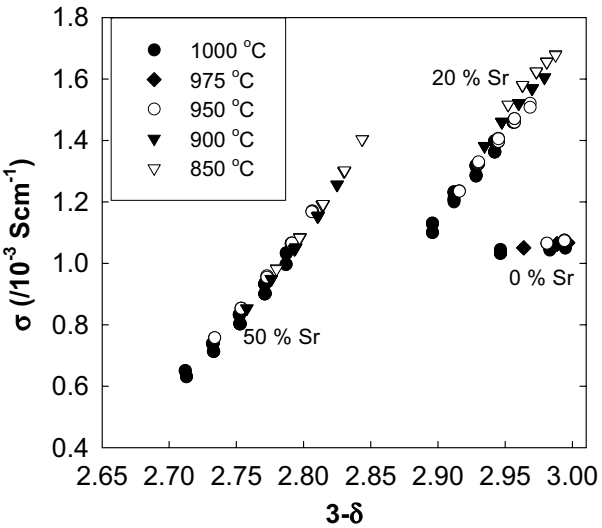

Fig. 3. Conductivity versus oxygen stoichiometry for all compositions.

It can be seen from Fig 3 that the linearity requirement is reasonably well fulfilled for small changes in oxygen stoichiometry for all compositions. Another interesting aspect of Fig 3, is how the conductivity changes with nonstoichiometry. For the unsubstituted $LaCoO_3$ there is a less pronounced conductivity dependency with (3-δ) compared with the two Sr-substituted compositions. This reflects the difference in changing the cobalt valence from 2-valent to 3-valent ($LaCoO_3$) and from 3-valent to 4-valent (LSC-02 and LSC-05), respectively. It is also obvious that whereas the Sr-content has a pronounced effect on the conductivity, the temperature only have a small effect showing a decreasing tendency with temperature (metallic behaviour) as reported by Mizusaki et al. [1].

Due to the high conductivities in the lanthanum coboltite samples, the current density used in all the experiments was 1/6 A/mm^2, corresponding to a total current of about 2 A through the sample. These high current densities were necessary to minimise the noise to signal ratio and obtain sufficient accuracy.

Calculations of D_{chem} and k_{chem} from the experimental runs have been performed with MATLAB [36]. A least square fitting procedure has been used to obtain the best fit between model (calculated) and experimental data.

Treatment of the data obtained from conductivity relaxation

A schematic presentation of a typical step in oxygen partial pressure and the resulting time dependent conductivity is given in Fig. 4a. For LC the step in oxygen partial pressure was one order of magnitude while for LSC-02 and LSC-05 the step was always 0.5 order of magnitude, $\log P_{O2}^{II} - \log P_{O2}^{I} = -(\log P_{O2}^{I} - \log P_{O2}^{II})=0.5$.

Normally, the calculation of k_{chem} and D_{chem} is based on the whole relaxation, that is from one equilibrium state to another. However, given that the relaxation behaviour is both determined by surface exchange and bulk diffusion, it is reasonable to assume that the initial part of the relaxation is dominated by surface exchange (k_{chem}) while the remaining part is dominated by bulk diffusion (D_{chem}). Based on these arguments the k_{chem} coefficient was calculated on different fractions of the total relaxation, e.g. 30 %, 50 % and 70 % of the total conductivity change. For the present system it was found that k_{chem} calculations based on 50% of the total relaxation, gave the best fit between model (Eq. (17)) and experimental

data. D_{chem} were calculated based on the total relaxation, and gave a close fit between model and experimental data.

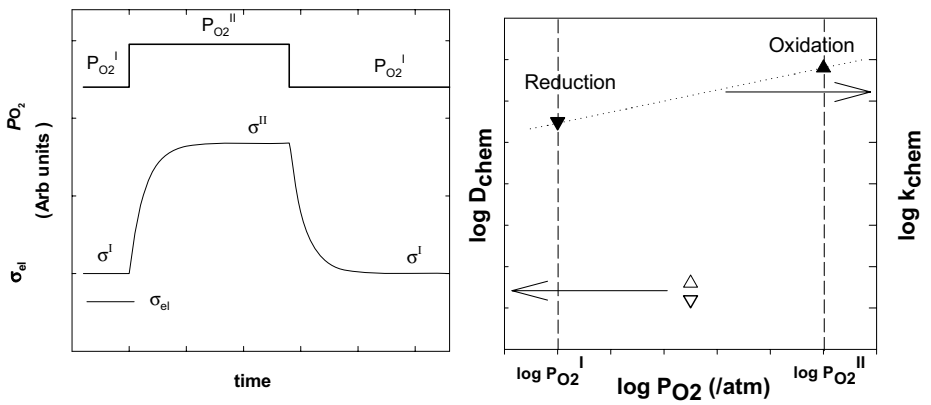

a) b)

Fig. 4. a) Schematic representation of the time variation of the electrical conductivity, with both an oxidation and a reduction drawn. b) Schematic representation of how the different D_{chem} and k_{chem} are related to the actual partial pressure of oxygen. For both figures $\log P_{O2}^{II} - \log P_{O2}^{I} = \pm 0.5$

The variation in D_{chem} and k_{chem} may be described as a function of oxygen partial pressure. The question is, however, which partial pressure should be assigned to which coefficient. The choice is described in Fig. 4b: Oxygen diffusion coefficients normally depend on the population of oxygen vacancies and accordingly also depend on P_{O2}. In that respect, we have chosen the logarithmic mean of the P_{O2}´s, as the representative oxygen partial pressure for the D_{chem} in question (Cf. Fig. 4b). For k_{chem} the situation is different; it is reasonable to assume that the surface will "see" the "new" P_{O2} shortly after a change in gas composition. Thus, the final P_{O2} is taken as the representative pressure for the k_{chem} in question (again, cf. Fig. 4b).

RESULTS AND DISCUSSION

Chemical transport- and exchange coefficients, D_{chem} and k_{chem}

$LaCoO_3$

The chemical diffusion coefficient D_{chem} and the chemical surface exchange coefficient, k_{chem}, for LC at temperatures between 950 and 1000 °C are given in Fig. 5. The coefficients are based on one order of magnitude change in P_{O2}, that is, between $2.0 \cdot 10^{-2}$ and $2.0 \cdot 10^{-3}$ atm.

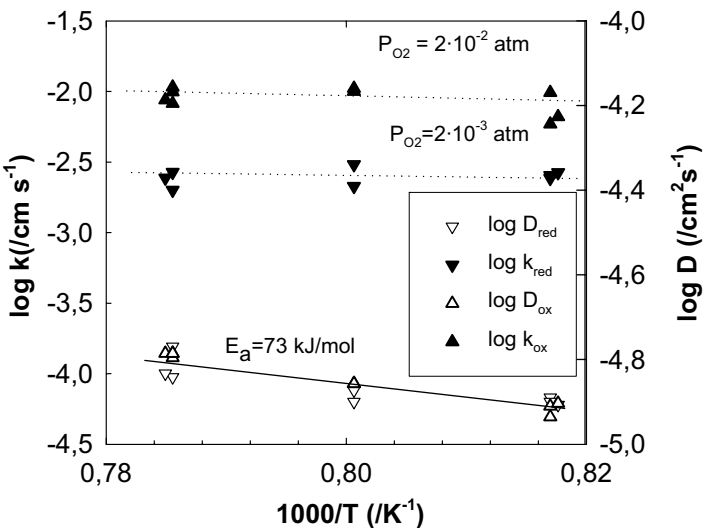

Fig. 5. D_{chem} and k_{chem} for $LaCoO_3$ in the temperature range between 950 and 1000 °C. Oxygen partial pressures are between $2 \cdot 10^{-2}$ and $2 \cdot 10^{-3}$ atm, i.e. one order of magnitude.

It can be seen that the plot of log D_{chem} versus 1000/T is linear, corresponding to an apparent activation energy of 73 ± 35 kJ/mol. Whereas k_{chem} is virtually temperature independent both for oxidation and reduction. Apparently, the k_{chem} associated with reduction is 0.5 orders of magnitude lower compared to the exchange coefficient associated with oxidation. However, due to small changes in conductivity, even with a one order of magnitude change in P_{O2}, the noise to signal ratio was high resulting in a high experimental uncertainty. In conclusion, only a few data with a high inaccuracy could be obtained, pointing out the inadequacy of conductivity relaxation as a method for measuring transport- and exchange coefficients in undoped lanthanum cobaltite (LC).

$La_{1-x}Sr_xO_3$ (x=0.2 and 0.5)

The diffusion coefficient, D_{chem} , and surface exchange coefficient, k_{chem} , resulting from both oxidation and reduction, are plotted versus P_{O2} for LSC-02 and LSC-05 at 1000 °C in Figs. 6 and 7, respectively.

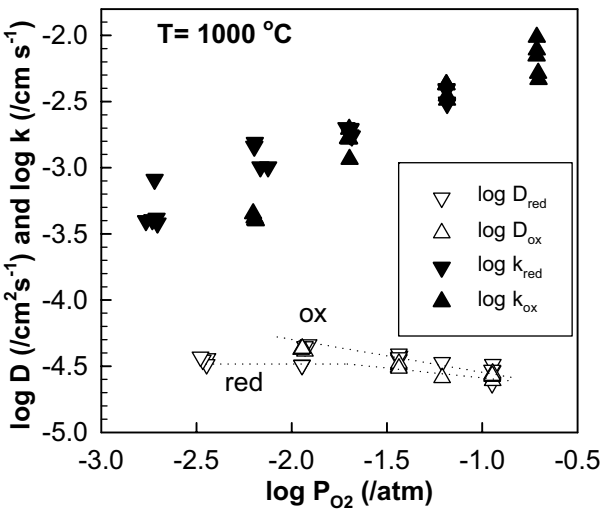

Fig. 6. D_{chem} and k_{chem} for LSC –02 at 1000 °C and between oxygen partial pressures $2 \cdot 10^{-1}$ and $2 \cdot 10^{-3}$ atm, each step half an order of magnitude. The dotted lines are guide to the eye.

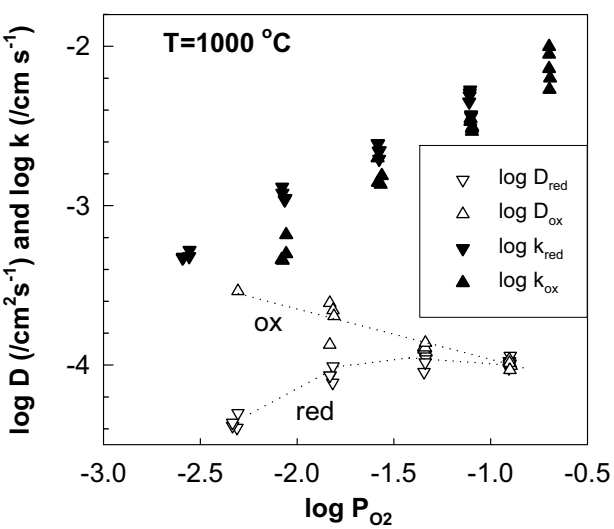

Fig. 7. D_{chem} and k_{chem} for LSC –05 at 1000 °C and between oxygen partial pressures $2 \cdot 10^{-1}$ and $2 \cdot 10^{-3}$ atm, each step half an order of magnitude. The dotted lines are guide to the eye.

The transport- and exchange coefficients given in Figs. 6 and 7 are calculated as previously described. Both k_{chem} and D_{chem} show a pronounced P_{O2} dependency. However, whereas D_{chem} associated with reduction and oxidation virtually coincide at high oxygen partial pressures, the values separate at low P_{O2} with an apparent decrease in D_{chem} obtained from reduction runs and a corresponding increase in oxidation values. In principle, the obtained D_{chem} values should be independent of whether an oxidation or reduction process takes place. Furthermore, at moderate concentrations of oxygen vacancies, the vacancy diffusion coefficient, D_V, should be independent of the vacancies. Thus, with reference to Eq. (9), we should expect the chemical diffusion coefficient to increase with decreasing

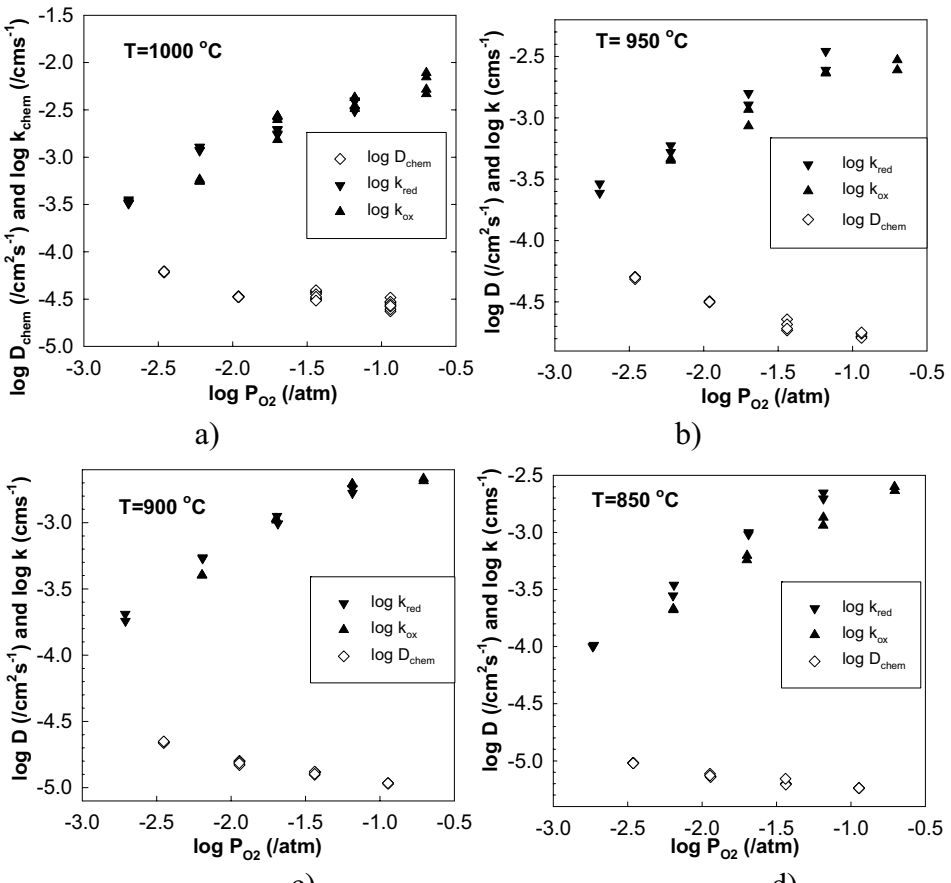

Fig. 8. D_{chem} and k_{chem} for LSC–02 at a) 1000 °C , b) 950 °C, c) 900 °C, d) 850 °C and between oxygen partial pressures $2 \cdot 10^{-1}$ and $2 \cdot 10^{-3}$ atm, after described treatment.

P_{O2} since the W_V increase with decreasing P_{O2} for both Sr substituted cobaltites (Cf. Fig. 13 d) and 13 f)). From Fig. 6 and 7, apparently only the D_{chem} obtained from oxidation behaves consistent and is thus taken as the representative bulk diffusion coefficient. Since D_{chem} obtained from reduction don not behave consistent, these values are discarded and k_{chem} for reduction experiments are recalculated using the D_{chem} from the oxidation experiments, and the results are given in Figs. 8 and 9. It is reasoned that this procedure should increase the credibility of the surface exchange coefficients, k_{chem}, obtained from reduction experiments. However, this procedure will inevitably give more reliable oxidation data than reduction data.

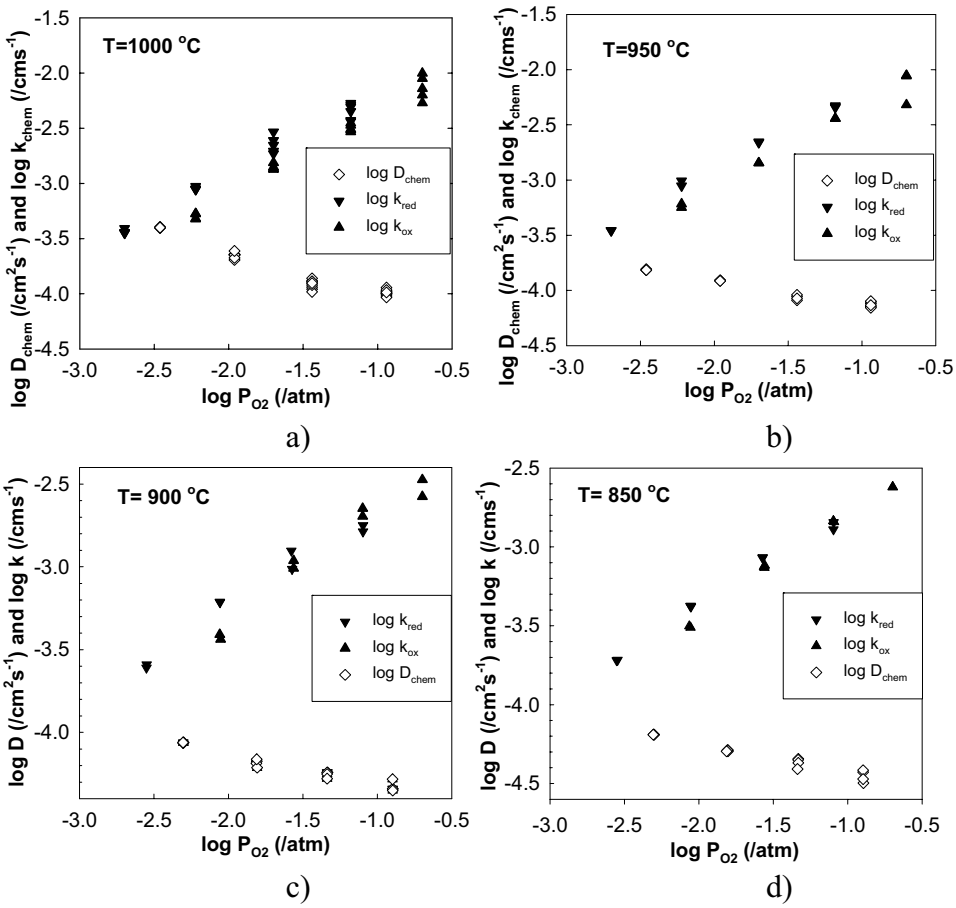

Fig. 9. D_{chem} and k_{chem} for LSC –05 at a) 1000 °C , b) 950 °C, c) 900 °C, d) 850 °C and between oxygen partial pressures $2 \cdot 10^{-1}$ and $2 \cdot 10^{-3}$ atm, after described treatment.

The question remains, why the D_{chem} values from reduction seemingly show an inconsistent behaviour, that is a declining value with decreasing P_{O2}.

A possibility is that during reduction experiments, the surface supplied oxygen from the sample is not transported effectively away. This will result in a lower oxygen flux and a correspondingly low chemical diffusion coefficient. However, the experiments are performed at high temperatures and at quite high total gas flows (500 ml/min), thus gas diffusion as a rate controlling step is highly unlikely.

Van der Haar [8] reported values for the oxygen transport parameters originating only from reduction experiments, showing decreasing values for D_{chem} with decreasing P_{O2} in $La_{1-x}Sr_xCoO_{3-\delta}$ (x = 0.2, 0.5 and 0.7) in the temperature interval 600 – 850 °C. The authors stated that a probable explanation for this behaviour was ordering of oxygen vacancies. In the present work oxygen transport properties at temperatures between 850 – 1000 °C have been investigated. The decreasing D_{chem} values only appear in the reduction runs and if ordering of vacancies takes place at low P_{O2} this should also affect the D_{chem} resulting from oxidation relaxations. Thus, for the experimental conditions in the present investigation we believe that ordering of vacancies is not the reason for the observed declining D_{chem} from reduction relaxations.

Finally, the discrepancy between oxidation and reduction experiments may originate from the numerical procedure calculating values for D_{chem} and k_{chem} from the experiments. E.g. den Otter et al. [37] showed that reliable results for D_{chem} and k_{chem} could be obtained when

$$0.03 \leq \frac{k_{chem} l_j}{D_{chem}} \leq 30 \qquad (23)$$

, where l_j is the length in the x-, y- or z- direction. This requirement is fulfilled for all values reported in Figs 8 and 9, supporting the validity of the calculations. Still, based on the present investigation we cannot rule out the "mathematical procedure" as a potential reason for the observed behaviour. This would require a more thorough analysis of the equations describing D_{chem} and k_{chem}. The diverging results with respect to oxidation and reduction relaxations at low P_{O2}´s are still basically left unexplained.

While the remaining part of this paper will focus on oxygen diffusion coefficients in the given material system, the surface exchange properties will be more thoroughly discussed in a succeeding paper [13].

Possible restrictions due to insufficient oxygen supply

In order to assess fundamental transport coefficients by conductivity relaxation, it is of vital importance that the rate of oxygen supply from the gas flow is well in excess of the amount actually consumed by the sample. If not, the resulting transport coefficients will only be due to the rate of oxygen supply in the gas flow rather than reflecting the transport properties of the sample. Van der Haar et al. [8] and ten Elshof et al. [29] discarded transport data obtained by oxidation relaxations claiming insufficient supply of oxygen in their experiments.

Whether this is an issue in the present work will be discussed in the following. The oxygen nonstoichiometry for all three compositions are given in Fig 10. Data for LC are taken from [7,16], while for LSC-02 and LSC-05 the nonstoichiometry are calculated using Eq. (2) with parameters given in Tab. 1. In Fig 10 d) the nonstoichiometry at 1000 °C for all three compounds are compared.

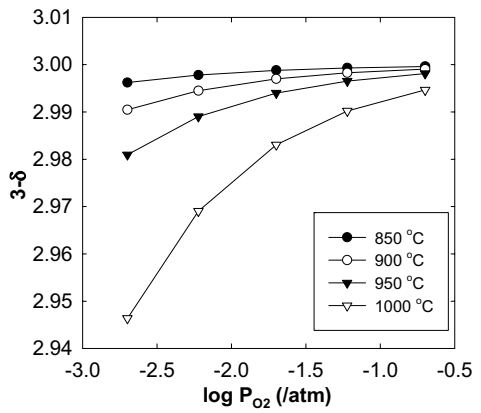

a)

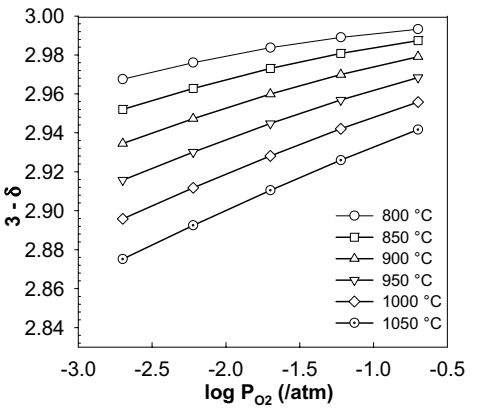

b)

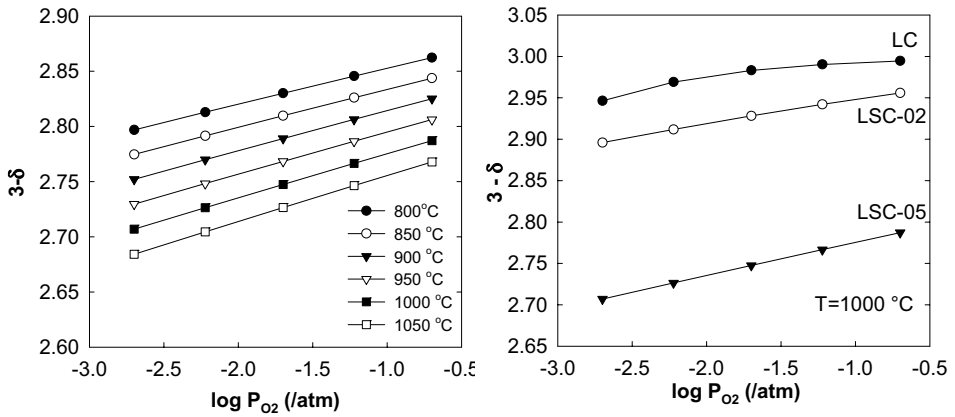

Fig. 10. Oxygen nonstoichiometry in the compositions a) LC, b) LSC-02 and c) LSC-05 at various P_{O2} and temperatures. In d) all three compositions are plotted at 1000 °C. Data for LC are taken from [7,15], The others are calculated using Eq. (2) and values given in Tab. (1).

The worst case will be considered. From Fig. 10 c) it is seen that for a given change in P_{O2} LSC-05 will exchange the largest amount of oxygen. Thus, consider an oxidation relaxation at 1000°C corresponding to a 0.5 order of magnitude change in oxygen partial pressure from $2 \cdot 10^{-3}$ to $6 \cdot 10^{-3}$ atm, given in Fig. 11a.

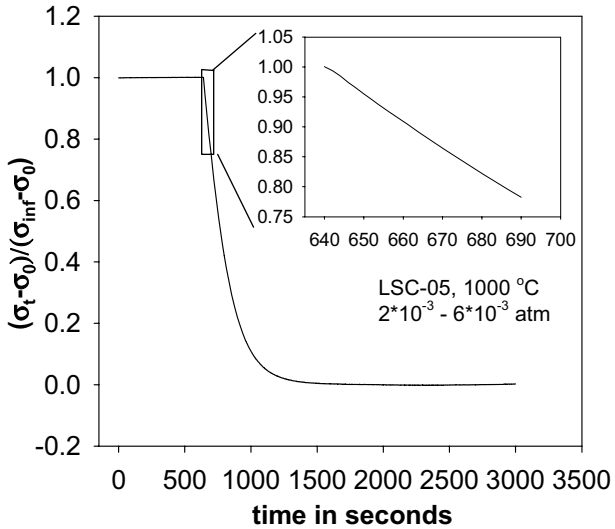

Fig. 11. Plot of a conductivity relaxation in LSC-05 at 1000 °C, corresponding to a step in oxygen partial pressure of $2 \cdot 10^{-3}$ - $6 \cdot 10^{-3}$ atm.

With reference to the oxidation relaxation given in Fig 11, the oxygen content in LSC-05 will increase with an amount of oxygen corresponding to the change in oxygen stoichiometry from δ=0.316 to δ=0.296, calculated from Eq. (2) and visualised in Fig. 10 c) and d). Since a linear relation is present, according to Eq. (22), a change in 10 % in conductivity correspond to 10 % change in the total mass of oxygen in the sample. Accordingly, the total amount of oxygen corresponding to a 10% change in conductivity can be calculated, and is given in Eq. (24)

$$mols\ of\ O_2\ needed = \frac{1}{2} mols\ of\ O\ needed = \frac{1}{2} \cdot total\ \#\ of\ cells \cdot \frac{(\delta_1 - \delta_2)}{N_a}$$

$$\frac{0.3 \cdot 0.3 \cdot 2.3\ (cm^3)}{2 \cdot (3.91755 \cdot 10^{-8})^3 (cm^3) \cdot 6.022 \cdot 10^{23}\ mol^{-1}} (0.3158 - 0.3138) = 5.76 \cdot 10^{-6}\ mol\ O_2 \tag{24}$$

The cell parameter for LSC-05 is 3.91755 Å in a cubic primitive unit cell [31], and the calculation is for a sample with dimensions 3x3x23 mm^3.

According to Fig 11, the time needed for a 10 % change is around 20 s, equivalent to an oxygen flux of approx. $2.88 \cdot 10^{-7}$ mol O_2/s. The oxygen supply as a function of gas flow and oxygen partial pressure in this particular apparatus is given in Fig 12.

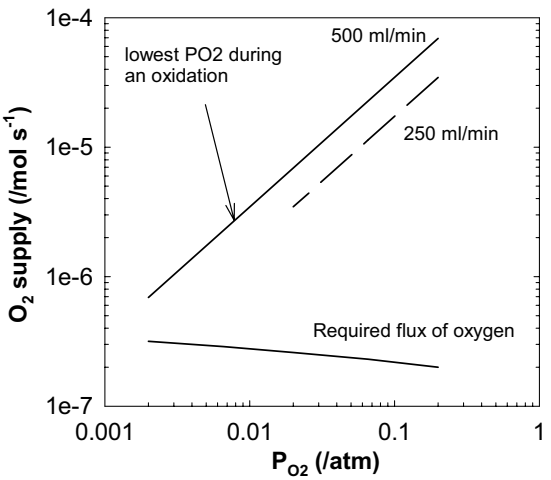

Fig. 12. Available oxygen supply from the apparatus used in the experiments. Values in mol/s as a function of oxygen partial pressure. The line of required flux is calculated from oxygen non-stoichiometric data and sample dimensions.

From Fig 12, the oxygen flow directed to the sample at $P_{O2}= 6\cdot10^{-3}$ atm and a total gas flow of 500 ml/min will correspond to $3\cdot10^{-6}$ mol O_2/ s. That is, the total supply of oxygen in the first 20 seconds will be approximately 10 times higher than the consumed amount of oxygen, i.e. the sample will consume about 10 % of the total oxygen flow. Thus, mass flow limitations should not be present in any of the experiments.

Derived transport coefficients for bulk diffusion; D_O and D_V.

By introducing the thermodynamic factors, W_O and W_V, one can derive the oxygen component diffusion coefficient, D_O, and vacancy diffusion coefficient, D_V, from the relations established in Eq. (6) and (9).

The thermodynamic factors for oxygen ions, W_O, and oxygen vacancies, W_V, are calculated for all compositions based on the oxygen nonstoichiometry data from Fig. 10 and given in Fig 13.

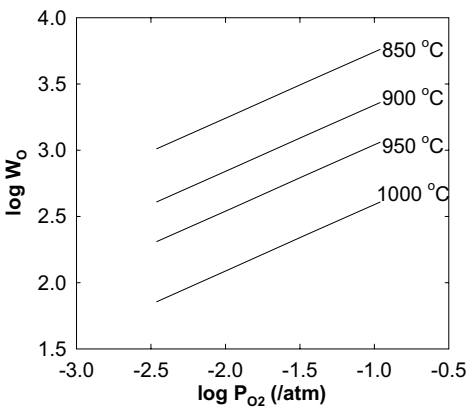

a)

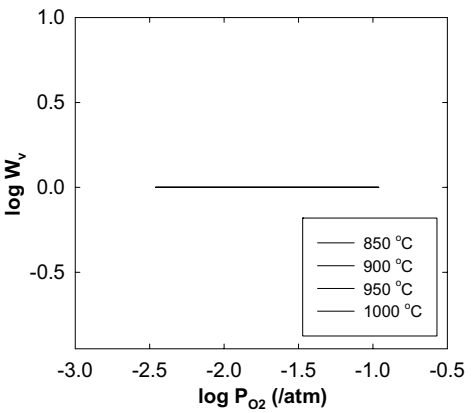

b)

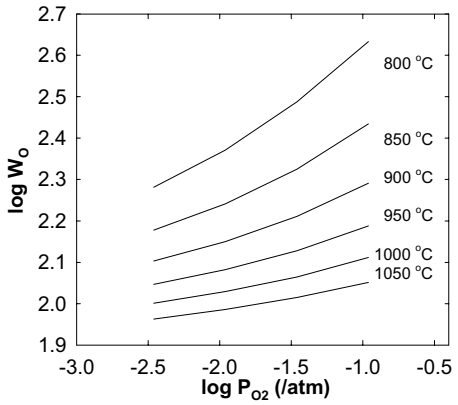
log W_O
log P_{O2} (/atm)
800 °C
850 °C
900 °C
950 °C
1000 °C
1050 °C

c)

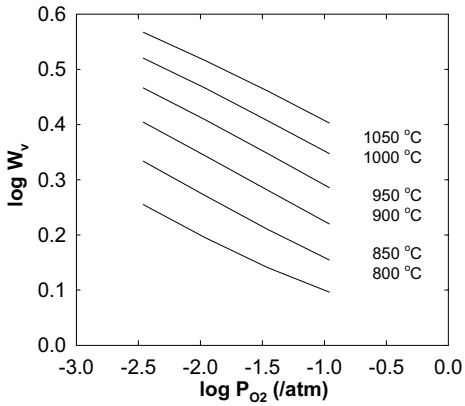
log W_v
log P_{O2} (/atm)
1050 °C
1000 °C
950 °C
900 °C
850 °C
800 °C

d)

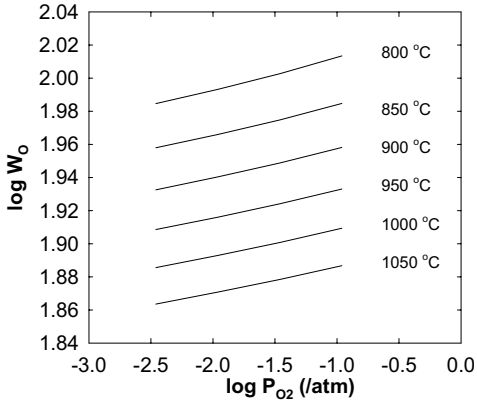
log W_O
log P_{O2} (/atm)
800 °C
850 °C
900 °C
950 °C
1000 °C
1050 °C

e)

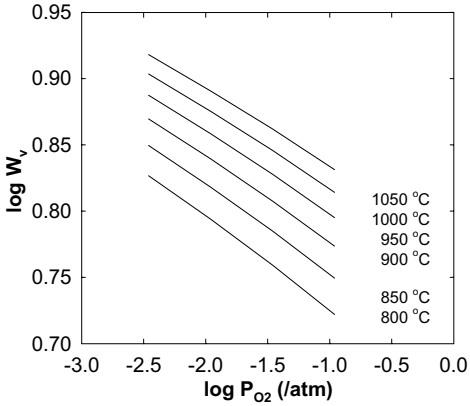
log W_v
log P_{O2} (/atm)
1050 °C
1000 °C
950 °C
900 °C
850 °C
800 °C

f)

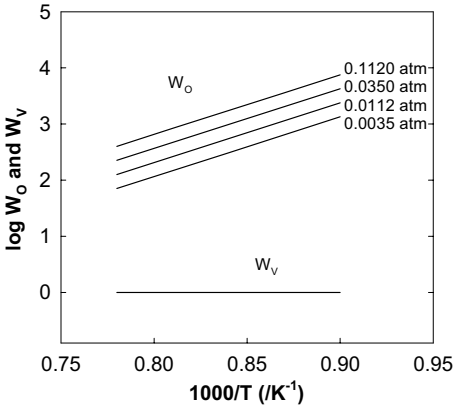
log W_O and W_v
1000/T (/K^{-1})
W_O
W_v
0.1120 atm
0.0350 atm
0.0112 atm
0.0035 atm

g)

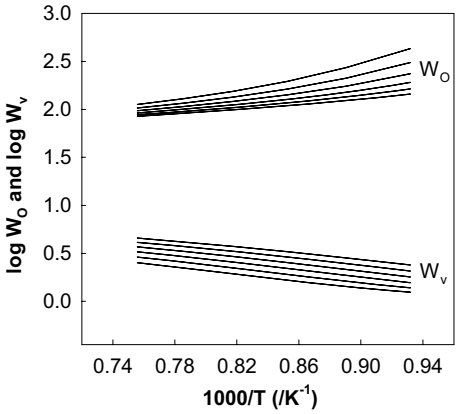
log W_O and log W_v
1000/T (/K^{-1})
W_O
W_v

h)

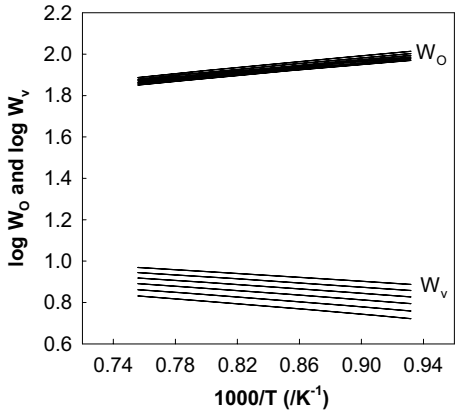

i)

Fig. 13. Thermodynamic factors vs. P_{O2} for oxygen (W_O) and vacancies (W_v) for LC: a) W_O , b) W_v ; LSC-02: c) W_O , d) W_v ; LSC-05: e) W_O , f) W_v . In Figs g), h) and i) the Thermodynamic factors W_O and W_v are plotted versus inverse temperature for LC, LSC-02 and LSC-05 respectively.

The influence of temperature and P_{O2} on D_{chem}, D_O and D_V.

$LaCoO_3$

In Fig 5, where D_{chem} and k_{chem} for LC were given, the activation energy for chemical diffusion is calculated to 73 ± 35 kJ/mol as an average between the oxidation and reduction values. The uncertainty is rather large due to a narrow temperature range in the measurements. Taking into consideration that the thermodynamic factor for vacancies in LC is equal to unity at all temperatures and partial pressures (see Fig 13b), one can conclude that D_{chem} equals D_V, via Eq.(9). Utilising a tracer diffusion technique on single crystal $LaCoO_3$, Ishigaki et al. [10] reported the activation energy for vacancy diffusion to be 77 ± 25 kJ/mol, quite close to own values.

It may be deduced from Fig 13 g) that the thermodynamic factor for oxygen in LC gives a contribution to the chemical diffusion coefficient D_{chem} of – 206 ± 15 kJ/mol. This means that the activation energy for the component diffusion coefficient, D_O, in LC is equal to 279 ± 35 kJ/mol according to Eq (12). Ishigaki et al. [10] reported the activation energy for the tracer diffusion coefficient for oxygen vacancies D_O^* in $LaCoO_{3-\delta}$ to be 315 ± 21 kJ/mol, which is only slightly higher than those obtained in this study.

By using the approach from Eq. (13) one obtains the apparent enthalpy of vacancy formation to be equal to 206 ± 15 kJ/mol. The value from Ishigaki

et al [10] is 215 kJ/mol, corresponding well with values obtained in this study.

Ishigaki et al. [10] measured the oxygen diffusion in a single crystal $LaCoO_3$ with SIMS, while the samples in this work was polycrystalline and measured with electrical conductivity relaxation. The difference in crystallinity may affect the activation energies. Kharton et al. [38] studied the effect of preparation methods on oxygen transport in $LaCoO_{3-\delta}$ finding that the ionic conductivity was influenced by the grain size.

According to Eq. (13) the apparent enthalpy of vacancy formation in LC calculated from contribution from the thermodynamic factor is equal to 206 kJ/mol. Based on the measurements of activation energies for D_O and D_V in Ishigaki et al [10], the ΔH_V was calculated to 235 kJ/mol, again in good agreement with the calculated value from this work, taking the uncertainties into account.

$La_{0.8}Sr_{0.2}CoO_3$

The average of the coefficients D_O and D_V are plotted for LSC-02 against 1000/T in Fig 14 at different partial pressures of oxygen (a and b) and against P_{O2} at different temperatures (c and d). In Fig 14 e) values for D_{chem} in LSC-02 are plotted versus 1000/T. Variation with P_{O2} for D_{chem} are given in Fig 8

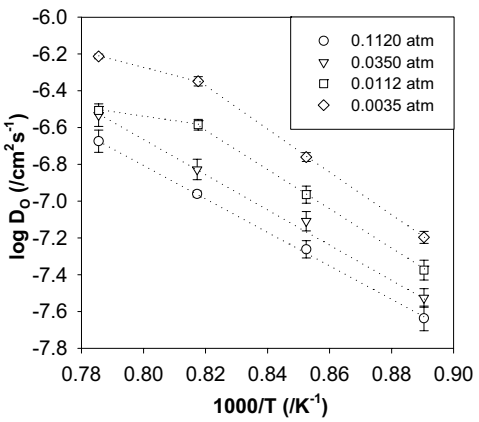

a)

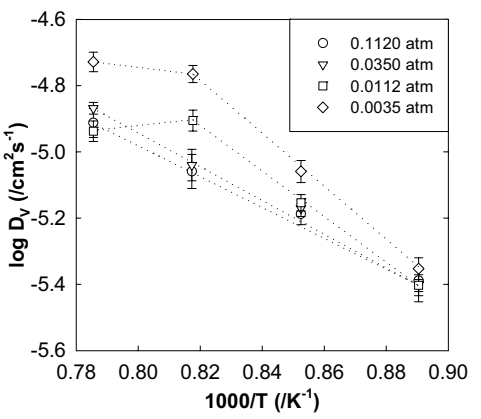

b)

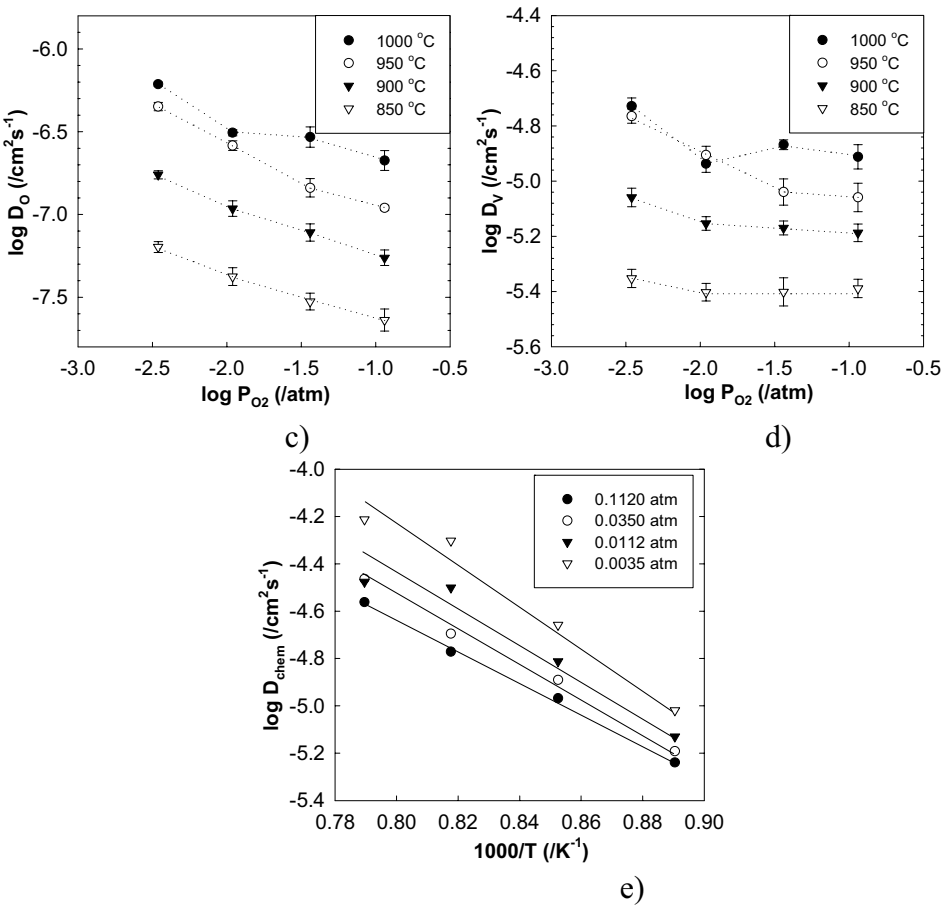

Fig. 14. a) D_0 versus 1000/T, b) D_V versus 1000/T c) D_0 versus P_{O2}, d) D_V versus P_{O2}, e) D_{chem} versus 1000/T for LSC-02. Legend in the temperature plots describes the oxygen partial pressure calculated from log P_{mid} = (log P_{start} + log P_{end})/ 2, where P_{start} and P_{end} is start and end partial pressure of each relaxation experiment respectively. Dotted lines serve as guide to the eye.

It is seen from Fig. 14 a) and b) that both D_O and D_V show a linear dependency with 1/T at temperatures below 1000 °C at all partial pressures, while a linear dependency is fulfilled at all temperatures for the two highest partial pressures. Only taking into account the linear regions, the activation energies for D_O are in the interval from 174 to 222 ± 20 kJ/mol, with an increasing activation energy with decreasing P_{O2}. For the D_V the activation energies are in the interval 85 – 153 ± 20 kJ/mol, also increasing with decreasing P_{O2}.

Van der Haar et al. [8] measured the activation energy for D_{chem} in the temperature interval 600-850 °C to be in the interval 108 –154 kJ/mol, with increasing activation energy with decreasing P_{O2}. By using the treatment

given in Eq (12) it is possible to calculate the activation energy for D_O based on D_{chem} given in [8]. In Fig 13 h) the thermodynamic factors for oxygen, W_O, and oxygen vacancies, W_V, for LSC-02, are plotted against reciprocal temperature. From this figure it is possible to extract a contribution to the activation energy of – 43 ± 15 kJ/mol from W_O and 32 ± 4 kJ/mol from W_V. According to Eq (12), the activation energies for D_O from van der Haar et al. [8] are in the interval 151-197 kJ/mol, in satisfactory agreement with values reported in the present work, taking into consideration that the values are obtained at different temperatures.

Lankhorst et al. [12] reported the activation energy for D_{chem}, in LSC-02 to be 135 kJ/mol and almost independent of P_{O2}. The latter value was obtained with coulometric titration. This means, according to Eq (12), that the activation energy for D_O from this work is 178 kJ/mol, again in good agreement with values obtained from this study.

Ishigaki et al [11] found the activation energy for D_O^* in $La_{0.9}Sr_{0.1}CoO_{3-\delta}$ to be 270 ± 38 kJ/mol measured with tracer diffusion measurements, at P_{O2} equal to 0.045 atm. Assuming a linear development in activation energies with Sr content (x), Ishigaki´s values [10,11] may be extrapolated from x = 0 (310 kJ/mol) and x = 0.1 (270 kJ/mol) to x = 0.2. This gives an activation energy of 230 kJ/mol at P_{O2}= 0.05 atm, again within the same range as reported in this work.

However, Carter et al. [39] found an activation energy for the oxygen self-diffusion coefficient D_O^* in LSC-02 corresponding to 60 ± 20 kJ/mol, measured with a tracer technique at P_{O2}=0.75 atm. This value is significantly lower than values reported in the present study. The reason for the discrepancy is not known.

The activation energies for D_{chem} reported by van der Haar et al. [8] and Lankhorst et al. [12] can be used to calculate the activation energies for D_V by means of Eq (12) (activation energy for W_V). Activation energies for D_V ranging from 76-122 kJ/mol and 103 kJ/mol, respectively, were found. All values agrees well with the values from this study.

Extrapolating the activation energies for D_V given by Ishigaki et al. [10,11] (x=0 (77 ±21 kJ/mol) and x=0.1 (79 ±25 kJ/mol)) one obtains for x=0.2 an activation energy equal to 81 ± 25 kJ/mol at P_{O2}=0.05, which agrees well with values from this work.

According to Eq (13) the difference in activation energies for D_O and D_V should in principle give an apparent enthalpy of vacancy formation. Based

on values obtained in this work calculation give values in the range from 75 to 90 ± 20 kJ/mol, increasing with P_{O2}.

Ishigaki et al [10,11] gives values for the apparent enthalpy of vacancy formation equal to 215 kJ/mol for $LaCoO_3$ and 184 kJ/mol for $La_{0.9}Sr_{0.1}CoO_3$. With an extrapolation one obtains for the LSC-02 composition 153 kJ/mol, which differs with approximately a factor of 2 from the values reported in this study.

Petrov et al. [17] have used thermogravimetric analysis to give values for the apparent vacancy formation enthalpies for the compositions $La_{0.9}Sr_{0.1}CoO_{3-\delta}$ and $La_{0.7}Sr_{0.3}CoO_{3-\delta}$ at a constant oxygen partial pressure and constant oxygen nonstoichiometries. From Fig 10b) it is seen that the oxygen nonstoichiometry in LSC-02 varies from $\delta = 0.02$, at 850 °C and $P_{O2} = 0.2$ atm to $\delta = 0.11$, at 1000 °C and $P_{O2} = 0.002$ atm, which corresponds to the temperature and partial pressure "window" in which this work is performed. For x=0.3 Petrov et al. [17] give values for ΔH_V between 36 and 68 kJ/mol depending on P_{O2}, while x = 0.1 gives values for ΔH_V ranging between 54 and 95 kJ/mol. Extrapolating to composition x=0.2 give values in a similar range as obtained in the present work.

In Fig 14 c) and d) the coefficients D_O and D_V for LSC-02 are plotted versus oxygen partial pressure. It can be seen that D_O increases with decreasing P_{O2}, consistent with Eq. (4) since the vacancy concentration increases with decreasing P_{O2}. However, some deviation is seen at low P_{O2}´s at 1000°C. The behaviour of D_V in terms of P_{O2} and temperature is given in Fig. 14 d). For dilute solutions the diffusion coefficient of the vacancies, D_V, should not depend on the concentration of vacancies (Kingery et al. [24] and Kofstad [25]). That is, D_V should be virtually independent of P_{O2} and for a given compound a function of temperature only. From Fig. 14 d) it is seen that the P_{O2} (or vacancy concentration) independence is reasonably well fulfilled at all temperatures at high P_{O2}´s. However, at high temperatures and low P_{O2}´s a tendency of increasing D_V with decreasing P_{O2} is seen. No such behaviour has previously been reported in the literature. On the contrary, a decreasing D_V has been reported for $La_{0.6}Sr_{0.4}Co_{0.8}Fe_{0.2}O_{3-\delta}$ at oxygen partial pressures below 0.01 atm. [40]. The authors suggest that the decrease is due to an association of the defects at high concentrations of oxygen vacancies.

The reason for the observed increase in the D_V coefficient is unclear, but it seems that D_V is virtually constant until a threshold value of oxygen vacancies is reached. Beyond the threshold value D_V apparently starts to

increase. This will be further discussed in the next section related to data obtained for $La_{0.5}Sr_{0.5}CoO_3$.

$\underline{La_{0.5}Sr_{0.5}CoO_3}$

The D_O and D_V coefficients are plotted for LSC-05 against 1000/T in Fig 15 at different partial pressures of oxygen (a,b), and against P_{O2} at different temperatures in (c,d), respectively. In Fig 15 e) values for D_{chem} in LSC-05 are plotted versus 1000/T. Variation with P_{O2} for D_{chem} are given in Fig 9.

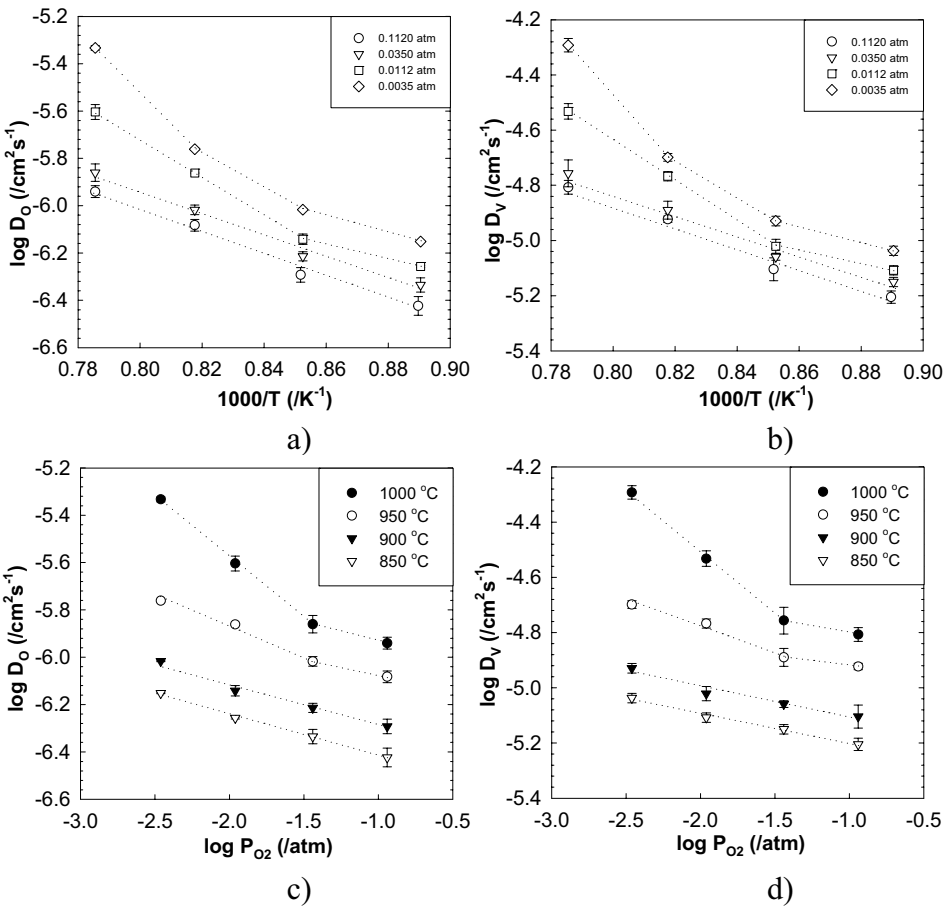

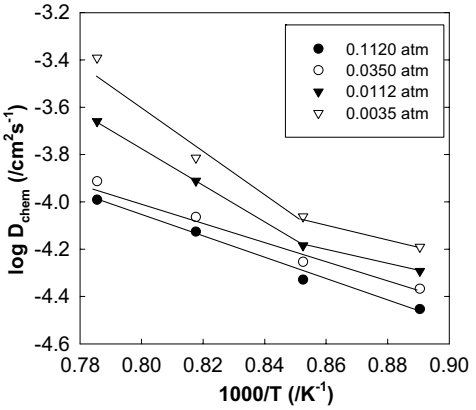

e)

Fig. 15. a) D_0 versus 1000/T, b) D_V versus 1000/T, c) D_0 versus P_{O2}, d) D_V versus P_{O2}, e) D_{chem} versus 1000/T for LSC-05. Legend in the temperature plots describes the oxygen partial pressure calculated from log P_{mid} = (log P_{start} + log P_{end})/ 2, where P_{start} and P_{end} is start and end partial pressure of each relaxation experiment respectively. Dotted lines serve as guide to the eye.

It can be seen from Fig. 15 a) and b) that a rather strict linear relationship exists for both D_O and D_V in terms of 1/T at the two highest P_{O2}´s. Deviation from linearity is observed at high temperatures and low P_{O2}´s. Disregarding the two lowest P_{O2}´s at 1000°C the activation energy for D_O is between 90 and 102 ± 22 kJ/mol, while the activation energy for D_V is between 75 and 88 ± 18 kJ/mol. The activation energy increases with decreasing P_{O2} as seen for the LSC-02 composition. This is also observed by van der Haar et al. [8], who reported an increase in the activation energies for D_{chem}, in the $La_{1-x}Sr_xCoO_{3-\delta}$ system, with decreasing oxygen partial pressure, at temperatures in the interval 600 – 800 °C, i.e. below the temperatures employed in this work.

The values for activation energies for D_{chem} from van der Haar et al. [8] are in the interval 106 – 136 kJ/mol. From Fig 13 i) it can be deduced that the contribution to the activation energy from W_O in LSC-05 is equal to -13 ± 5 kJ/mol, whilst for W_V it is equal to 8-12 ± 5 kJ/mol. From Eq. (12) this means that activation energies for D_O from [8] are in the interval 119 – 149 kJ/mol, somewhat higher than values originating from the present study.

The difference in the activation energies for D_O and D_V is equal to the apparent energy of vacancy formation ΔH_V in LSC-05, and is calculated to be 15 ±14 kJ/mol. Petrov et al. [17] reported an enthalpy of vacancy formation for $La_{0.4}Sr_{0.6}CoO_{3-\delta}$ to be in the interval between 10 and 20

kJ/mol, at almost the same oxygen stoichiometries and P_{O2}´s as in the present work. This is in excellent agreement to the results from this work.

The D_O coefficients for LSC-05 given in Fig 15 c) show a linear increase with decreasing P_{O2}. This is consistent with Eq.(4), given that the oxygen vacancy concentration increases with decreasing P_{O2}. However, the vacancy diffusion coefficients, D_V, given in Fig 15 d), are seen to increase steadily with decreasing P_{O2} at all oxygen partial pressures. A seemingly pronounced dependency between D_V and the population of vacancies is apparent. This will be discussed in more detail in a later section

Apparent activation energies and the effect of the dopant level of Sr.

The average activation energies and enthalpies for all compositions, LC, LSC-02 and LSC-05, are given in Fig. 16.

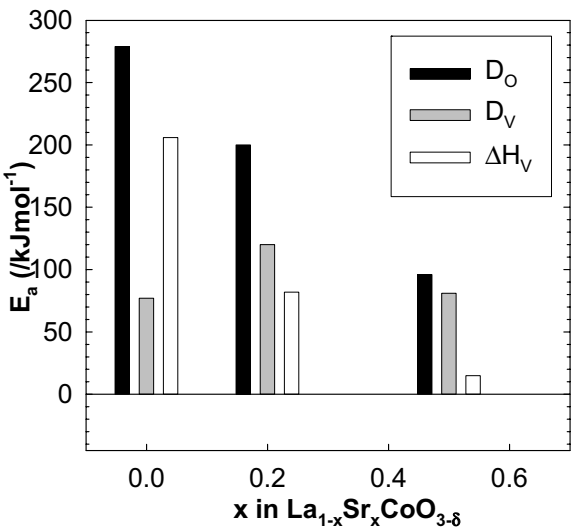

Fig. 16. Diagram showing the development in activation energies with increasing degree of strontium substitution in $La_{1-x}Sr_xCoO_{3-\delta}$ for the oxygen component diffusion coefficient, D_O, the oxygen vacancy diffusion coefficient, D_V and the apparent enthalpy of vacancy formation ΔH_V.

For the vacancy diffusion coefficient, the absolute values for the activation energies are in the range 77 kJ/mol for LC, 85-154 kJ/mol for LSC-02 and 75-88 kJ/mol for LSC-05, that is, fairly independent of the level of Sr substitution. This observation do suggest that the migration path as well as path properties for vacancy jumps (oxygen jumps) are fairly independent of Sr level in the given compositional interval. However, as previously pointed out, observed activation energies at high temperatures and low pressures are even higher than reported in Fig. 16 and could point towards a change in migration mechanism/path.

The calculated values for the apparent enthalpies of vacancy formation decreases with increasing Sr substitution: 206 kJ/mol for LC, 75-90 kJ/mol for LSC-02 and 15 kJ/mol for LSC-05. The same behaviour with increasing strontium substitution is also reported in the literature [11], and do suggest that the strength of the oxygen bonds decrease with increasing Sr level, thus facilitating the formation of vacancies.

Finally, the activation energies for D_O are by far highest for the LC composition (279 kJ/mol) and decreases when strontium is introduced. (174-222 kJ/mol for LSC-02 and 90 - 102 kJ/mol for LSC-05). The observed trend in activation energy with Sr content is consistent with Eq. (4): Given a virtually constant activation energy for D_V the variation in activation energy for D_O should be given by the variation in the apparent enthalpy for vacancy formation.

D_O, D_V and the significance of oxygen vacancies.

In Fig 17 average logarithmic D_O and D_V coefficients are plotted at 850 °C for all three compositions and 950 °C for LSC-02 and LSC-05 against the ratio between the oxygen vacancy concentration and the oxygen ion concentration (Eq. (3)).

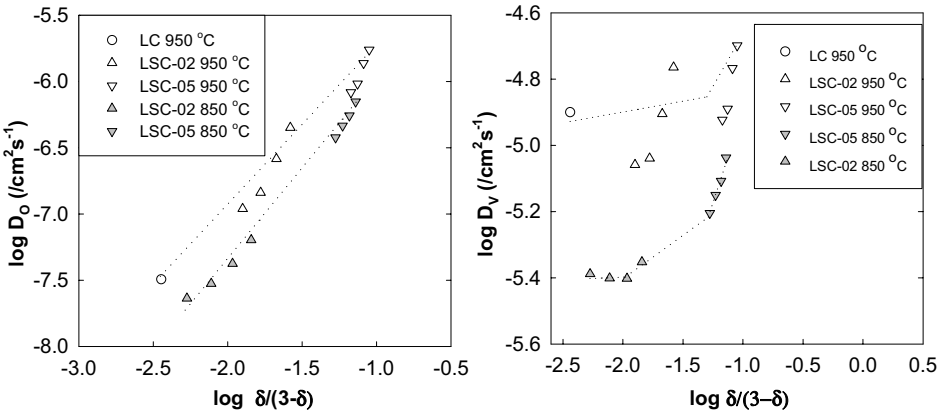

a) b)

Fig. 17. a) D_O versus δ/(3-δ) b) D_V versus δ/(3-δ).

The vacancy diffusion coefficient, D_V, show a tendency of being independent of the vacancy concentration (plateau) at low populations of oxygen vacancies (Fig. 17 b)), consistent with the behaviour of dilute solutions as previously pointed out. However, as the population of oxygen vacancies increase a rather pronounced increase in D_V is observed at both 850 °C and 950 °C. To the authors knowledge, an increasing D_V with increasing vacancy concentration has not been reported in the literature. Intuitively, one would expect the vacancy diffusion coefficient to decrease with increasing population of vacancies, both due to interactions between vacancies (associations) or tendency to order. The oxygen nonstoichiometry in the samples where the observed increase takes place corresponds to δ = 0.27- 0.30. This corresponds to every eleventh or tenth oxygen site being vacant. At these high vacancy concentrations possible interactions between vacancies may occur. To rule out possible error sources inherently associated with conductivity relaxation methods, the transport coefficients should also be assessed by other methods, e.g. thermogravimetry and oxygen isotopic (^{18}O) exchange.

From Fig. 17 a) it can be seen that D_O exhibit an almost linear dependency with the ratio between oxygen vacancies and oxygen ions. The observed behaviour is consistent with Eq (3), giving a linear dependency between D_O and the ratio between vacant and occupied oxygen sites, given a vacancy independent D_V. However, as pointed out above, the non-constant behaviour of D_V at high defect concentrations will also affect D_O and give a more pronounced dependency as observed in Fig. 17 a).

An analytical expression for the vacancy diffusion coefficient is given by Kingery et al. [24]

$$D_V = \gamma \lambda^2 \upsilon_{vac} e^{-\frac{E_a}{RT}} \quad (25)$$

where λ is the jumping distance, ν_{vac} is the frequency of lattice vibrations, E_a is the activation energy for the jump to occur and γ is a so called geometric factor. An increasing D_V with vacancy concentration should in principle correspond to a similar change in one or more of the quantities given in Eq. (25): γ includes the number of nearest-neighbor jump sites and the probability that the atom will jump back into its original position [24]. For vacancies an occupied site is a possible jump site, and accordingly γ should decrease with increasing vacancy concentration, ruling out γ as the factor of importance with respect to the increasing D_V. The minute increase in jumping distance λ with the oxygen vacancy concentration is far to small to account for the several order of magnitude increase in D_O and is accordingly ruled out. The frequency of the lattice vibrations, ν, will be about 10^{13}/seconds for solids [24]. It is reasoned that the frequency might decrease with increasing vacancy concentration, due to an average decrease in bonding strength as oxygen is pulled out. If so, D_V should rather decrease than increase with vacancy concentration. Thus, based on the arguments given above we are left with the activation energy, E_a, as the possible source affecting the behaviour of D_V. Based on Eq. (25) it is apparent that the diffusion coefficient is rather sensitive to the activation energy. E.g. assuming an activation energy around 100 kJ/mol a decrease in E_a of less than 10% is consistent with an increase in D_V corresponding to a factor 2. Using the activation energy argument E_a should decrease with increasing nonstoichiometry (decreasing P_{O2}), which is not evident from Fig. 14 and 15. However, taking into account the substantial uncertainty in the E_a values, we cannot rule out the variation in activation energy as being the main reason for the increasing D_V with increasing nonstoichiometry.

The effect of microstructure on transport properties.

In Fig. 1 the microstructure for all compositions are given. It was concluded that the microstructure was conserved during the experiments, i.e. grain growth was not significant. The range of grain sizes among the different samples are 4-9μm for LC, 1-4 μm for LSC-02 and 2-5 μm for LSC-05, respectively. Differences are due to variation in composition, and sintering conditions.

In the present work there is an open question whether grain boundary diffusion play any major role. Normally, one expects that the rate of diffusion of an atom along a grain boundary, D_{gb}, is higher compared to

bulk diffusion, D_O. However, in order to see the effect of grain boundaries, experiments on samples with identical composition and a large variation in microstructure would be necessary. Preferably, the variation in grain size should be between one and two orders of magnitude. Moreover, the effect of grain boundaries are far better characterized by other methods, e.g. isotopic exchange combined with SIMS (secondary ion mass spectroscopy).

In conclusion, the variation in microstructures for all the samples are too small to give any significant information, and, moreover, electrical conductivity relaxation as a method is not capable of deconvoluting the effect of grain boundaries in any straight forward way.

CONCLUSION

The activation energies for the component diffusion coefficient, D_O, varies from 279 kJ/mol for LC to 174-222 kJ/mol for LSC-02 and 90-105 kJ/mol for LSC-05. The activation energies decrease with increasing Sr-content. The activation energies for the vacancy diffusion coefficient, D_V, are smaller than for D_O corresponding to 77 kJ/mol for LC, 85 kJ/mol for LSC-02 and 75 kJ/mol for LSC-05, in effect almost independent of the Sr-content.

The apparent enthalpies of vacancy formation decreases with increasing Sr content. The values are 206 kJ/mol for LC, 75 kJ/mol for LSC-02 and 15 kJ/mol for LSC-05, respectively.

The D_V coefficients show a somehow unexpected behaviour for some compositions. For low vacancy concentrations in LC and LSC-02, D_V is virtually constant. However, at some high vacancy concentration, corresponding to every eleventh or tenth oxygen site being vacant, there is a pronounced increase in D_V with increasing nonstoichiometry. The behaviour might be related to an ever decreasing activation energy for vacancy jumping with increasing nonstoichiometry. The component diffusion coefficient, D_O, shows a linear increase with increasing oxygen vacancy concentration regardless of which composition is studied. At high vacancy concentrations, an increase in the slope is observed, consistent with the theoretical correlation between D_O and D_V.

ACKNOWLEDGEMENTS

Dr.Ing. Ivar Wærnhus is acknowledged for many inspiring discussions, Dr. Ing Hilde Lea Lein for synthesising the powder samples for the LSC-05 composition. They are both at Department of Materials Science and Engineering, NTNU, Trondheim. Thanks to Norsk Hydro ASA for financial support.

APPENDIX

The chemical potential of oxygen in the gas phase is given by [41]

$$\mu_{O_2}^{gas} = \mu_{O_2}^{0,gas} + RT \ln\left(P_{O_2}\right)$$

$$\mu_{O_2}^{0,gas} = RT(n_1 + n_2 / T + n_3 \ln(T) + n_4 \ln\left(1 - e^{\frac{n_5}{T}}\right) \quad (26)$$

where T is in Kelvin and P_{O2} is in atmospheres and
n_1= -1.225
n_2= -1.045· 10^3 K
n_3= -3.500
n_4=1.013
n_5= 2.242 ·10^3 K

REFERENCES

1. Mizusaki, J.,Tabuchi, J.,Matsuura, T., Yamauchi, S. and Fueki, K., "Electrical conductivity and Seebeck coefficient of nonstoichiometric $La_{1-x}Sr_xCoO_{3-\delta}$", J. Eletrochem. Soc. 144, No.7, (1989), 2082-2088.
2. Teraoka, Y., Zhang, H.M., Furukawa, S. and Yamazoe, N., "Oxygen Permeation through perovskite-type oxides", Chem.Lett. (1985), 1743-46.
3. Voorhoeve, R.J.H. *in* "Advanced Materials in Catalysis" (J.J. Burton and R.L. Garten, Eds.), 1977.
4. Gellings, P. and Bouwmeester, H.J.M., "Ion and mixed conducting oxides as catalysts", Cat.Today. 12, (1992), 1-105.
5. Ohno, Y., Nagata, S., and Sato, H., "Effect of electrode materials on the properties of high temperature solid electrolyte fuel cells", Solid State Ionics, 3/4 , (1981), 439.

6. Seppännen , M., Kytö, M., and Taskinen, P., "Stability of the Ternary phases in the La-Co-O System", Scand.J.Metallurgy 8, (1979), 199-204
7. Seppännen , M., Kytö, M., and Taskinen, P., "Defect structure and nonstoichiometry of $LaCoO_3$", Scand.J.Metallurgy 9, (1980), 3-11.
8. van der Haar, L.M., den Otter, M.W., Morskate, M., Bouwmeester, H.J.M. and Verweij, H., Chemical diffusion and oxygen surface transfer of $La_{1-x}Sr_xCoO_{3-\delta}$ studied with electrical conductivity relaxation", J.Electrochem.Soc. 149, No.3, (2002), J41-J46.
9. Nowotny, J, and Rekas, M., "Defect disorder of undoped and Sr-doped $LaCoO_{3-\delta}$", Bulletin of the Polish Academy of Sciences Chemistry", 50, No.1, (2002), 93-108.
10. Ishigaki, T., Yamauchi, S., Mizusaki, J., Fueki, K. and Tamura, H., "Tracer diffusion coefficient of oxide ions in $LaCoO_3$ Single crystal", J.Solid State Chem., 54**,** (1984), 100-107.
11. Ishigaki, T., Yamauchi, S., Kishio, K., Mizusaki, J., and Fueki, K., "Diffusion of oxide ion vacancies in perovskite-type oxides", J.Solid State Chem., 73**,** (1988), 179-187.
12. Lankhorst, M.H.R. and Bouwmeester, H.J.M., "Determination of oxygen nonstoichiomtery and diffusivity in mixed conducting oxides by oxygen coulometric titration, I. Chemical diffusion in $La_{0.8}Sr_{0.2}CoO_{3-\delta}$", J.Electrochem Soc. 144, No.4, (1997), 1261-1267.
13. Watterud, G., Wiik, K. and Julsrud, S., "Oxygen Transport in $La_{1-x}Sr_xCoO_{3-\delta}$ (x=0, 0.2 and 0.5) assessed with electrical conductivity relaxation. Part II: The mechanisms of oxygen surface exchange.". Paper II in this thesis.
14. Wærnhus, I.," Defect Chemistry, Conductivity and mass transport properties of $La_{1-x}Sr_xFeO_{3-\delta}$ (x=0 and 0.1)" , Thesis, Norwegian University of Science and Technology, (2003). b) Paper 4 in that thesis
15. Mizusaki, J., Yoshihiro, M., Yamauchi, S. and Fueki, K., "Nonstoichiometry and defect structure of the perovskite-type oxides oxides $La_{1-x}Sr_xFeO_{3-\delta}$", J.Solid State Chem. 58, (1985), 257-266.
16. Mizusaki, J., Mima, Y., Yamauchi, S, Fueki, K., and Tagawa, H., "Nonstoichiometry of the Perovskite-type oxides $La_{1-x}Sr_xCoO_{3-\delta}$", J.Solid State Chem. 80, (1989), 102-111.
17. Petrov, A.N., Cherepanov, V.A., Kononchuk, O.F. and Gavrilova, L.Ya., "Oxygen nonstoichiometry of $La_{1-x}Sr_xCoO_{3-\delta}$ $(0< x \leq 0.6)$", J.Solid State Chem. 87, (1990), 69-76.
18. Lankhorst, M.H.R., Bouwmeester, H.J.M. and Verweij, H., "High-temperature coulometric titration of $La_{1-x}Sr_xCoO_{3-\delta}$: Evidence for the effect of electronic band structure on nonstoichiometric behaviour", J.Solid State Chem 133, (1997), 555-567.
19. Lankhorst, M.H.R. and Bouwmeester, H.J.M., "Determination of oxygen nonstoichiomtery and diffusivity in mixed conducting oxides by

oxygen coulometric titration, II. Oxygen nonstoichiometry and defect model for $La_{0.8}Sr_{0.2}CoO_{3-\delta}$", J.Electrochem Soc. 144, No.4, (1997), 1268-1273.

20. Lankhorst, M.H.R, Bouwmeester, H.J.M. and Verweij, H., "Thermodynamics and transport of Ionic and electronic defects in crystalline oxides", J.Am.Ceram.Soc. 80 [9], (1997), 2175-2198.
21. Lankhorst, M.H.R, Bouwmeester, H.J.M. and Verweij, H., "Use of the rigid band formalism to interpret the relationship between O chemical potential and electron concentration of $La_{1-x}Sr_xCoO_{3-\delta}$", Phys.Rev.Lett. 77, No.14. (1996), 2989-2992.
22. Tai,L.-W., Nasrallah, M.M., Naderson, H.U., Sparlin, D.M. and Sehlin, S.R., " Structure and electrical properties of $La_{1-x}Sr_xCo_{1-y}Fe_yO_3$. Part 1. The system $La_{1-x}Sr_xCo_{1-y}Fe_yO_3$", Solid State Ionics 76, (1995), 259-271.
23. Kröger, F.A., "The chemistry of inperfect crystals Vol. 2.", North-Holland Pub. (1974).
24. Kingery, W.D, Bowen, H.K and Uhlmann, D.R., "Introduction to ceramics", Wiley-Interscience, (1976).
25. Kofstad, P., "Nonstoichiometry, Diffusion and electrical conductivity in binary metal oxides", John Wiley and Sons (1972).
26. Schmalzried, H. , "Solid State reactions", Academic Press Inc., (1974).
27. Weppner, W. and Huggins, R.A., "Determination of the kinetic parameters of mixed conducting electrodes and application to the system Li_3Sb", J. Electrochem.Soc. 124, No. 10, (1977), 1569-1578.
28. Maier, J, "Physical chemistry of ionic materials: Ions and electrons in solids", John Wiley & Sons (2004).
29. ten Elshof, J.E., Lankhorst, M.H.R. and Bouwmeester, H.J.M, " Oxygen exchange and diffusion coefficients of strontium doped lanthanum ferrites by electrical conductivity relaxation", J.Electrochem.Soc. 144, No. 3, (1997), 1060-1067.
30. Kleveland, K., Einarsrud, M.-A., Grande, T.," Sintering of $LaCoO_3$ – based ceramics", J.Eur.Ceram.Soc. 20 , (2000), 185-193.
31. Lein, H.L. and Grande, T., unpublished results (2003).
32. Hansen, J.R., Poulsen, F.W. and Hendriksen, P.V., "Determination of oxygen diffusion coefficients by conductivity relaxation", Proc. 6th Eur. Ceram. Soc. Conf., (1999)
33. den Otter, M.W., Bouwmeester, H.J.M, Boukamp, B.A. and Verweij, H., "Reactor flush time correction in relaxation experiments", J.Electrochem.Soc. 148, (2001), J1.
34. Crank, J., "The Mathematics of Diffusion", 2nd Ed. , Oxford Science Publications, (1975).
35. Yasuda, I and Hikita, T. , "Precise determination of the chemical diffusion coefficient of calcium doped lanthanum chromite by means of

electrical conductivity relaxation", J.Electrochem.Soc. 141, No. 5, (1994), 1268-1273.
36. MATLAB ver. 13.1 , The MathWorks Inc. Internet : http://www.mathworks.com
37. den Otter, M.W., Bouwmeester, H.J.M, Boukamp, B.A. and Verweij, H., "Reactor flush time correction in relaxation experiments", J.Electrochem.Soc. 148, (2001), J1.
38. Kharton, V.V., Naumovich, E.N., Kovalevsky, A.V., Viskup, A.P., Figueieredo, F.M., Bashmakov, I.A., Marques, F.M.B., "Mixed electronic and ionic conductivity of $LaCo(M)O_3$ (M=Ga, Cr, Fe or Ni). IV. Effect of preperation method on oxygen transport in $LaCoO_{3-\delta}$", Solid State Ionics 138, (2000), 135-148.
39. Carter, S., Selcuk, A., Chater, R.J., Kajda, J., Kilner, J.A. and Steele, B.C.H., "Oxygen transport in selected nonstoichiometric perovskite-structure oxides", Solid State Ionics 53-56, (1992), 597-605.
40. Katsuki, M., Wang, S., Dokiya, M. and Hashimoto, T., "High temperature properties of $La_{0.6}Sr_{0.4}Co_{0.8}Fe_{0.2}O_{3-\delta}$ oxygen nonstoichiometry and chemical diffusion coefficient", Solid State Ionics 156, (2003), 453-461.
41. IUPAC, Commission on thermodynamics, "Oxygen, International Thermodynamic tables of the fluid state-9 ", Blackwell Scientific, Oxford, (1987).

OXYGEN TRANSPORT IN $La_{1-x}Sr_xCoO_{3-\delta}$ (x=0, 0.2 and 0.5) ASSESSED WITH ELECTRICAL CONDUCTIVITY RELAXATION. Part II: The mechanisms of oxygen surface exchange.

Geir Watterud[a], Stein Julsrud[b] and K. Wiik[*a],
[a]Department of Materials Science and Engineering
Norwegian University of Science and Technology
N-7491 Trondheim, Norway.
[b]Scanwafer AS, N-3907 Porsgrunn, Norway

ABSTRACT

Chemical surface exchange coefficients, k_{chem}, were derived from electrical conductivity relaxations. Utilising thermodynamic factors, surface exchange coefficients, k_0, were calculated for the compositions $La_{0.8}Sr_{0.2}CoO_{3-\delta}$ (LSC-02) and $La_{0.5}Sr_{0.5}CoO_{3-\delta}$ (LSC-05) in the P_{O2} range $2\cdot10^{-1}$ and $2\cdot10^{-3}$ atm, however, only at the lowest oxygen partial pressures for $LaCoO_3$ (LC) due to experimental difficulties.

The activation energy for k_0 for the three compositions are 206 kJ/mol for LC, 110-130 kJ/mol for LSC-02 and 95-120 kJ/mol for LSC-05, and they are in good agreement with values reported in literature.

By relating the k_0 and the equilibrium oxygen exchange flux, j_{ex}^0, different reaction pathways are put forward, aiming at modeling the P_{O2} dependency of the k_0 parameter by means of possible rate-determining steps for the oxygen exchange. A total of four different reaction pathway schemes were considered. The model which suggested a direct installation of an (un)charged oxygen molecule in two vacancies as the rate-determining step gave the best fit for the P_{O2} dependency for k_0 against measured values for oxidation in both LSC-02 and LSC-05. For the reduction the best model suggested an association of oxygen species for LSC-02, while for LSC-05 no model could be fitted to experimental results. The P_{O2} dependency for k_0 became less pronounced with increasing P_{O2} and was dependent on temperature and composition. This could indicate a change in the rate-determining step or a change in the surface reaction pathway. However,

---

Corresponding author: Kjell Wiik, Department of Materials Technology, Norwegian University of Science and Technology, N-7491 Trondheim, Norway, e-mail: kjell.wiik@material.ntnu.no, Telephone no.: +47 73 59 40 82, fax no:+47 73 59 08 60

further studies in this partial pressure and temperature interval is required to verify the reaction mechanism in question.

By examining the values of k_0 in strontium substituted lanthanum coboltites from this work and lanthanum ferrites from literature, a distinct trend of an increasing k_0 with increasing oxygen vacancy concentration in the materials has been observed. Thus, oxygen vacancies are believed to play a major role in the surface exchange of oxygen.

Keywords:
$La_{1-x}Sr_xCoO_{3-\delta}$, Electrical conductivity relaxation, Elementary reactions, Surface exchange coefficient

INTRODUCTION

Lanthanum coboltites, pure and substituted with strontium, are characterised by their ability to permit relatively high concentrations of oxygen vacancies at elevated temperatures. This fact combined with the relative high mobility of the vacancies causes this material to exhibit high oxygen ion conductivity. Together with the high electronic conductivity [1], which is metallic-like at high temperatures, these materials are permeable for oxygen gas. This makes them attractive candidates for oxygen separation membranes [2], oxidation catalysts [3,4] and electrodes in solid oxide fuel cells and oxygen sensors [5].

The oxygen transport in oxide based mixed conductors may be divided in two inherently different processes comprising surface exchange processes and solid-state oxygen ion diffusion in the bulk phase, respectively.

van der Haar et al. [6] have studied the oxygen diffusion and oxygen surface exchange in $La_{1-x}Sr_xCoO_{3-\delta}$ (x=0.2, 0.5 and 0.7) in the temperature range 600-850 °C with electrical conductivity relaxation. They observed that both D_{chem} and k_{chem} increase with P_{O2} for all compositions. For the composition with x=0.2 the activation energies for k_{chem} at different oxygen partial pressures were measured to be in the range 166-216 kJ/mol, whilst for x=0.5 in the range 97-147 kJ/mol.

van Doorn et al. [7] have studied the surface oxygen exchange in $La_{0.3}Sr_{0.7}CoO_{3-\delta}$ with dynamic SIMS measurements. They reported an activation energy for the surface exchange parameter k_0 to be 28 ±5 kJ/mol. It was also observed a P_{O2} dependency for k_0 corresponding to k_0 $P_{O2}^{0.41\pm0.02}$. This P_{O2} dependency has been explained by a rate-determining step involving an adsorbed oxygen specie and an oxygen vacancy, viz.

$$O_{ad} + V_O^{\bullet\bullet} \rightarrow O_O^x + 2h^{\bullet} + S_{ad} \qquad (1)$$

The oxygen partial pressure dependency for k_{chem} and/or k_0 is also reported elsewhere for a number of different compositions: Fe doped $SrTiO_3$ [8], $LaGaO_3$ doped with Sr and Mg [9], Wærnhus et al. [10 b)] for the compound $La_{0.9}Sr_{0.1}FeO_3$ and ten Elshof et al. [11] for $La_{0.9}Sr_{0.1}FeO_3$ and $La_{0.6}Sr_{0.4}FeO_3$. The reported P_{O2} dependencies vary. Common for these studies [8-11] is that the rate of surface exchange is discussed with respect to possible reaction mechanisms.

Bouwmeester et al. [12] have discussed the surface exchange kinetics for different mixed conducting oxides, giving a theoretical approach to decide to what extent the surface exchange processes control the rate of oxygen permeation through the oxides in competition with the contribution from the solid state diffusion. Utilising oxygen nonstoichiometry data from previous studies [13] on oxygen permeation experiments for $La_{0.8}Sr_{0.2}CoO_{3-\delta}$, they found that the oxygen flux changed its P_{O2} dependency with decreasing sample thickness. This change was interpreted in terms of surface reactions becoming rate controlling. The given approach [12] was used to distinguish between surface exchange and bulk diffusion, respectively, being rate limiting with respect to the oxygen transport. By introducing a so-called characteristic thickness, L_c ($=D_O/k_0$) the regimes for surface- and bulk control could be defined. The same approach has partly been used in the present study.

Maier [14,15] approached the surface exchange processes in a phenomenological manner. The surface exchange coefficients were categorised according to three different types of experiments: Chemical experiments, tracer experiments and electrical conductivity experiments. The effective surface rate constants from these may differ due to different experimental conditions, but also due to the fact that they may be described by different mechanisms. Correlation factors between the various exchange coefficients are introduced verifying that the rate-determining step determines the effective rate constants.

In this work we investigate the processes of oxygen surface exchange in the system $La_{1-x}Sr_xCoO_{3-\delta}$ (x=0, 0.2 and 0.5). Based on chemical surface exchange coefficients, k_{chem}, reported in Part I of this work[16], the surface kinetics in terms of temperature, P_{O2} and composition will be described. Possible surface exchange mechanisms, both for oxidation and reduction, will be put forward and discussed.

THEORY

Surface exchange

The total reaction describing the the surface exchange of oxygen between ambient atmosphere and solid surface may be written viz. (Kröger-Vink notation [17]):

$$O_2(g) + 2V_O^{\bullet\bullet} + 4e^- = 2O_O^x \qquad (2)$$

Reaction (2) is a total reaction and may consist of a number of elementary reactions, typically involving adsorption, dissociation/association of the oxygen molecule, charge transfer(s), incorporation/excorporation of oxygen ions in/out of the vacancies. Some examples of different elementary reactions are given by Merkle and Maier [8] for Fe-doped $SrTiO_3$, ten Elshof et al. [11] and Wærnhus et al. [10] for various compositions in the system $La_{1-x}Sr_xFeO_3$, and Ishihara et al. [9] in $LaGaO_3$ based perovskite-type oxides.

The oxidation and reduction reaction can be described as a flux of oxygen in or out of the material surface. If a material is in equilibrium with the ambient oxygen pressure at any given temperature, these fluxes are equal. A small change in the ambient oxygen partial pressure (chemical potential) will subsequently result in a net flow of oxygen in or out of the solid surface [12].

$$j_{O_2} \equiv j_{ox} - j_{red} = j_{ex}^0 \frac{\Delta\mu_{O_2}}{RT} \tag{3}$$

Where $\Delta\mu_{O_2}$ is the difference in chemical potential across the surface. In Eq. (3) the oxygen flux is described in terms of molecular oxygen, O_2 and the relationship between a flux of atomic and molecular oxygen is $j_O = 2 \cdot j_{O2}$. The parameter j^0_{ex} describes the surface exchange rate (flux) of molecular oxygen at equilibrium, meaning that the amount of molecular oxygen entering the sample (j_{ox}) equals the amount leaving (j_{red}), thus:

$$j_{ox} = j_{red} = j_{ex}^0 \tag{4}$$

If a small perturbation in the oxygen chemical potential is applied, corresponding to an oxidation, the oxidation flux j_{ox} will increase and the reduction flux j_{red} will decrease, and vice versa for a reduction.

The expression given in Eq (3) can be derived from irreversible thermodynamics [18]. According to Eq. (3) the driving force for the oxygen flux is the difference in chemical potential for molecular oxygen. However, it is possible to express the driving force in several different ways, either by the difference in the chemical potential of atomic oxygen, or the difference in the concentration of atomic oxygen. The latter gives

$$\Delta C_O = C_{actual} - C_{new\,eq} \tag{5}$$

, where C_{actual} is the true concentration of oxygen at the surface at any time and $C_{new\ eq}$ is the equilibrium concentration of oxygen at the surface when $t=\infty$. From the definition of the chemical surface exchange coefficient, k_{chem}, the oxygen flux is given by:

$$j_O = -D_{chem} \left. \frac{dC_O}{dx} \right|_{surface} = k_{chem} \Delta C_O \tag{6}$$

Since $2j_{O2} = j_O$ and $\Delta\mu_{O2} = 2\Delta\mu_O$ the following relationship may be derived based on Eq.(3):

$$\begin{aligned} j_O &= 2 j_{O_2} = 2 j_{ex}^0 \frac{\Delta\mu_{O_2}}{RT} = 4 j_{ex}^0 \frac{\Delta\mu_O}{RT} \\ &= 4 j_{ex}^0 \frac{\Delta\mu_O}{RT} \frac{1}{\Delta \ln C_O} \Delta \ln C_O \\ &= 4 j_{ex}^0 W_O \Delta \ln C_O \\ &= \frac{4 j_{ex}^0 W_O}{C_O} \Delta C_O \end{aligned} \tag{7}$$

Where W_O is the so called thermodynamic factor [16] defined as:

$$W_O = \frac{1}{2} \left(\frac{d \ln P_{O_2}}{d \ln C_O} \right) \tag{8}$$

From the definition of k_{chem} (Eq. (6)) combined with Eq. (7) the following relationship may be derived:

$$\frac{4 j_{ex}^0 W_O}{C_O} = k_{chem} \tag{9}$$

A more descriptive illustration of surface exchange and associated variables and coefficients is given in Fig. 1: Assume a solid sample with thickness L at equilibrium with the ambient oxygen partial pressure. At this condition $\Delta C_O = 0$, and there is no net transport of oxygen through the surface (Fig 1a). At a given time, t=0, a change in ambient oxygen partial pressure is applied. The oxygen concentration at the surface will change corresponding to the new oxygen partial pressure, but the oxygen concentration in the surface will remain at the same value. Now, there is a driving force for transport, and a net flux of oxygen will be established having its peak value at t=0. With time the driving force for surface exchange will decrease, Fig. 1c), and

eventually a new equilibrium will be established and no net transport of oxygen across the surface will take place, Fig. 1d).

In Eq. (9) a relationship between k_{chem} and j^0_{ex} is established. Often when discussing surface exchange kinetics , another surface exchange coefficient, k_0, is introduced:

$$k_{chem} = \frac{4 j^0_{ex} W_O}{C_O} = k_0 W_O \tag{10}$$

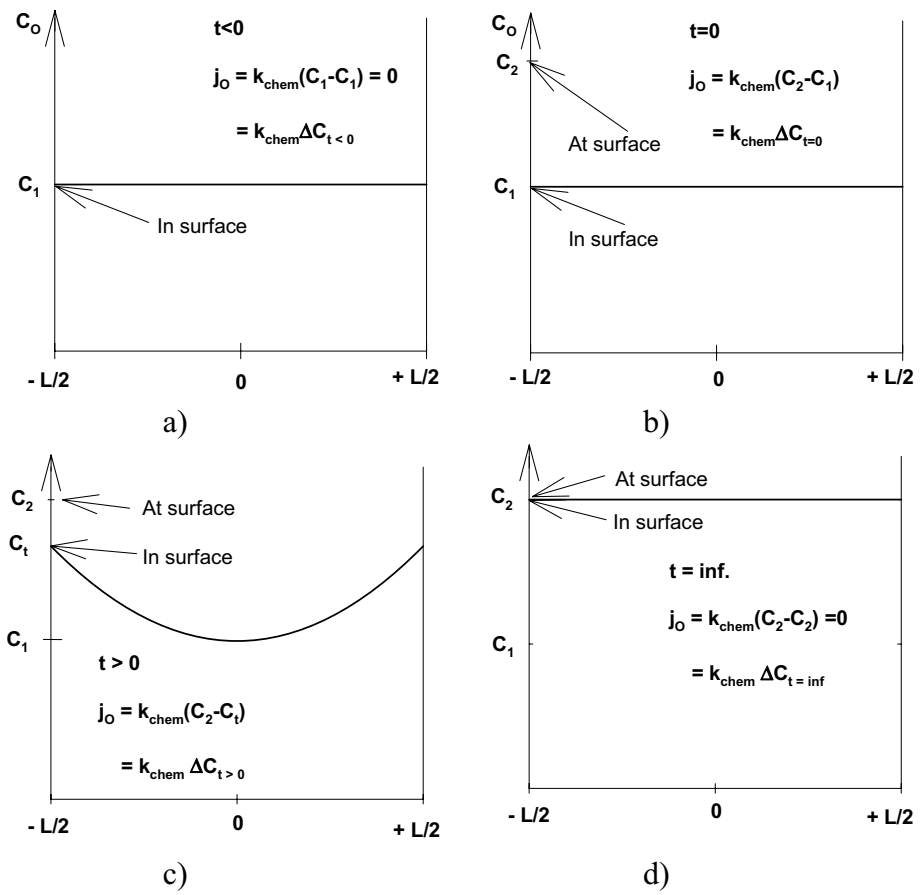

Fig. 1.The oxygen concentration across the surface and through the sample is described as a function of position and at different times. a) Before a change in the oxygen partial pressure, t<0. b) At the time the change is applied, t=0. c) After a given time t. d) When the new equilibrium is established, t=∞.

k_0 is the surface exchange coefficient in the absence of oxygen chemical potential gradients, and can be determined from $^{18}O/^{16}O$ isotopic exchange experiments [11]. The k_0 is sometimes referred to as a tracer surface exchange coefficient k^* [14]. Thus, the relation between the different surface exchange coefficients may be summarised in Eq. (11)

$$j_{ex}^{0} = \frac{1}{4} C_O k_0 = \frac{1}{4} \frac{C_O}{W_O} k_{chem} \tag{11}$$

EXPERIMENTAL

The experimental parts such as material synthesis and measurements of the oxygen transport parameters with electrical conductivity relaxation are thoroughly described in part I [16].

RESULTS AND DISCUSSION

k_{chem} values derived from conductivity relaxation experiments for all compositions are given in part I [16]. Included in part I is also a presentation of oxygen stoichiometry data vs. composition, P_{O2}, and temperature as well as derived thermodynamic factors.

The variation of k_0 with temperature; apparent activation energies.

In Fig 2 the oxygen surface exchange coefficient k_0 are given for pure LC in the temperature interval 950 –1000°C. The figure contains values only from two different oxygen partial pressures, namely $2 \cdot 10^{-2}$ and $2 \cdot 10^{-3}$ atm, because at higher partial pressures no values for k_{chem} could be obtained.

The activation energy for k_0 in LC can be calculated to be 206 ± 25 kJ/mol with no difference between oxidation and reduction values. In part I [16] the activation energy for k_{chem} was calculated to ~0 kJ/mol. According to Eq. (10) the contribution to the activation energies from k_0 and W_O must cancel each other as seen in Eq. (12).

$$E_{a,k_{chem}} = E_{a,W_O} + E_{a,k_0} \tag{12}$$

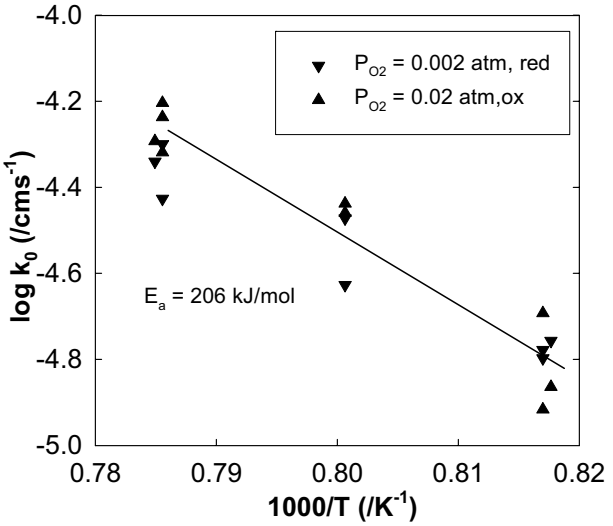

Fig. 2. k_0 for $LaCoO_3$ in the temperature range between 950 and 1000 °C.

In part I [16] the relations between the apparent activation energies for the different diffusion coefficients and the thermodynamic factors were derived. The contribution to the activation energy from the thermodynamic factor W_O in LC was found to be -206 kJ/mol, which is in very good agreement with the measured activation energy for the surface exchange coefficient k_0 in LC.

The surface exchange coefficients, log k_0, derived from k_{chem} values in Part I [16], are plotted against inverse temperature in Fig 3 a,b) for LSC-02 and c,d) for LSC-05, at different partial pressures of oxygen and for both oxidation and reduction processes.

The activation energies are calculated in two different temperature intervals (850-1000 °C) for LSC-02 and (850-950 °C) for LSC-05, because of the observation of a plateau between 950 and 1000 °C in the LSC-05. This plateau was only observed at the lowest oxygen partial pressure in the reduction runs for LSC-02. Further work by Rudberg et al. [20] on the LSC-05 composition confirms the same plateau for k_0 above 950 °C.

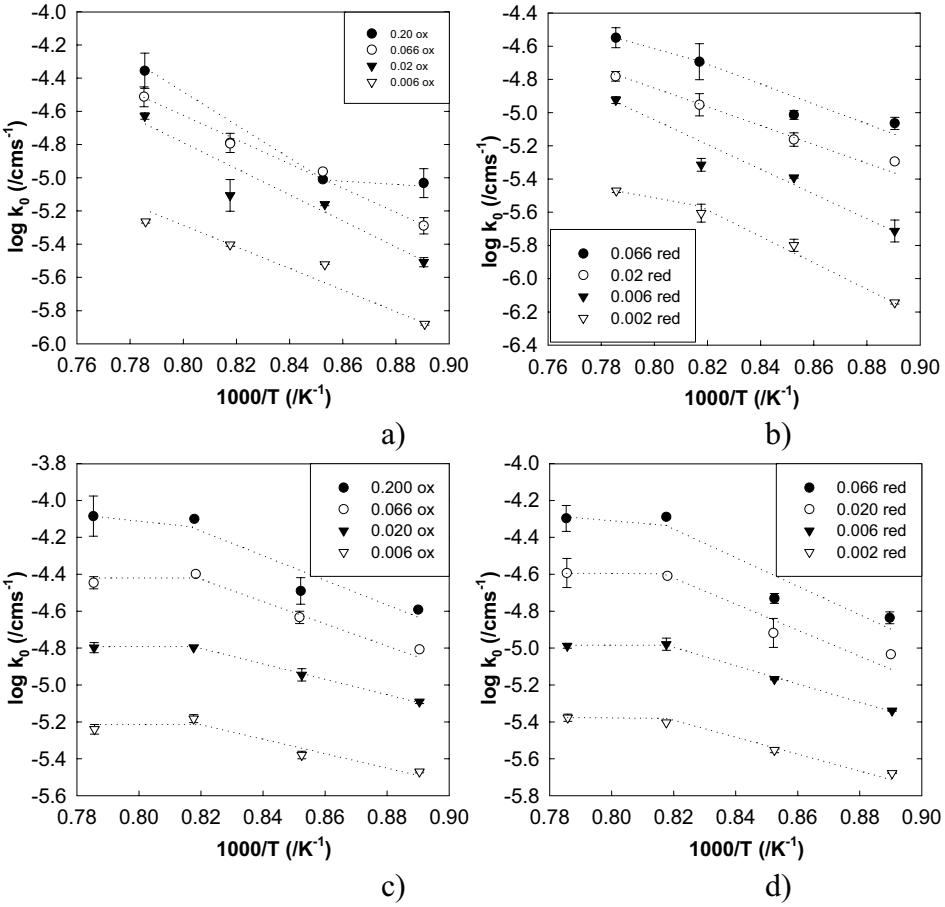

Fig. 3. Average k_0 values with standard deviation versus 1000/T for a) LSC-02 oxidation, b) LSC-02 reduction, c) LSC-05 oxidation and d) LSC-05 reduction. Legend describes the oxygen partial pressure at the end of the relaxation, and whether an oxidation or reduction has occurred. The dotted lines serve as guide to the eye.

In Figs 3a) and b) the log k_0 values for LSC-02 from oxidation and reduction are given versus reciprocal temperature. In both cases these values follow a temperature dependency, which corresponds to the activation energy for the surface exchange coefficient from reduction runs of (95-135) ± 15 kJ/mol, and (105 – 145) ± 15 kJ/mol for the oxidation runs. Values for log k_0 for LSC-05 versus reciprocal temperature are given in Fig. 3 c) and d), for oxidation and reduction respectivelly. At low temperatures a pronounced temperature dependency at all isobars is evident corresponding to apparent activation energies between 75 kJ/mol and 140 kJ/mol

The activation energy for k_0 in LSC-02 is approx. 132 kJ/mol in air for an oxidation process. This value is quite close to 127 ± 8 kJ/mol, which is the activation energy reported for the tracer surface exchange coefficient, k^*, by De Souza and Kilner [21] for the composition $La_{0.8}Sr_{0.2}CoO_{3-\delta}$ measured at 1 atm O_2. The same authors [21] reports the activation energy for the tracer surface exchange coefficient, k^*, for the composition $La_{0.5}Sr_{0.5}CoO_{3-\delta}$ to be 78 ± 4 kJ/mol at 1 atm O_2 between 600 –800 °C, nearly half the value observed at high P_{O2}´s in the present work. This was measured with the $^{18}O/^{16}O$ Isotope Exchange Depth Profile experimental technique, and in a temperature interval between 600 and 800 °C [21] (In this work 850-1000 °C).

Van der Haar et al [6] reported the activation energy for k_{chem} obtained from reduction experiments for the compound $La_{0.8}Sr_{0.2}CoO_{3-\delta}$ measured between 600 and 800 °C with conductivity relaxation to be in the interval 166-216 kJ/mol, while for $La_{0.5}Sr_{0.5}CoO_{3-\delta}$ activation energies for reduction k_{chem} were in the interval 97-147 kJ/mol measured between 750–850 °C. The activation energies of k_{chem} can be compared to the activation energies for k_0 by using the approach of Eq.(12) and the fact that the thermodynamic factor for oxygen ions contribute to the apparent activation energy with –43 kJ/mol (for LSC-02) and -13 kJ/mol for LSC-05 [16]. This gives activation energies for k_0 from van der Haar et al [6] in the interval 209-259 kJ/mol for LSC-02 and 110 - 160 kJ/mol for LSC-05. Values for LSC-02 is almost twice the magnitude observed in this work. No apparent reason for the discrepancy has been found. The values of LSC-05 are fairly close to values obtained in this work.

In Fig 4 the activation energies for k_0 are plotted together with the apparent enthalpy for vacancy formation. In the figure the error bars give a hint of the variation of the k_0 for each composition, and the standard deviation in ΔH_V from [16]. Included in Fig 4 are literature values for k^* from refs [7] and [21] and values for k_0 from [6].

From Fig. 4 it is seen that there is a general trend of a decreasing activation energy with increasing level of Sr. Since the concentration of vacancies will increase with increasing Sr-level, the oxygen vacancies obviously play an important role. This will be further discussed in a later section.

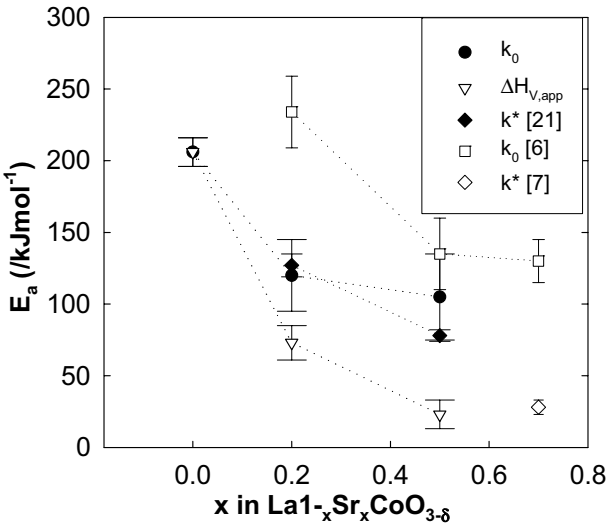

Fig. 4. Activation energy, E_a, for k_0 and the apparent enthalpy of vacancy formation, ΔH_V against level of Sr-substitution. Inserted in the figure is also values for k* from [7,21] measured in air and temperatures 600[21]/700 [7] and 1000°C and k_0 from [6] measured between 600-850 and 1-10^{-4} bar. To distinguish between the errors in the different works, different width on the end of the error bars are used.

The variation of k_0 with P_{O2}

In Fig 5 the k_0 parameter obtained from both oxidation and reduction experiments are plotted versus P_{O2} at all temperatures for LSC-02 and LSC-05, respectively. These are the same values as given in Fig 3. For the case of LC the P_{O2} dependency for k_0 is not further investigated due to difficulties with obtaining surface exchange data at more than two oxygen partial pressures. This is due to the small changes in oxygen vacancy concentrations and electrical conductivity at the given temperatures, which results in a high uncertainty in the derived transport coefficients [1,13].

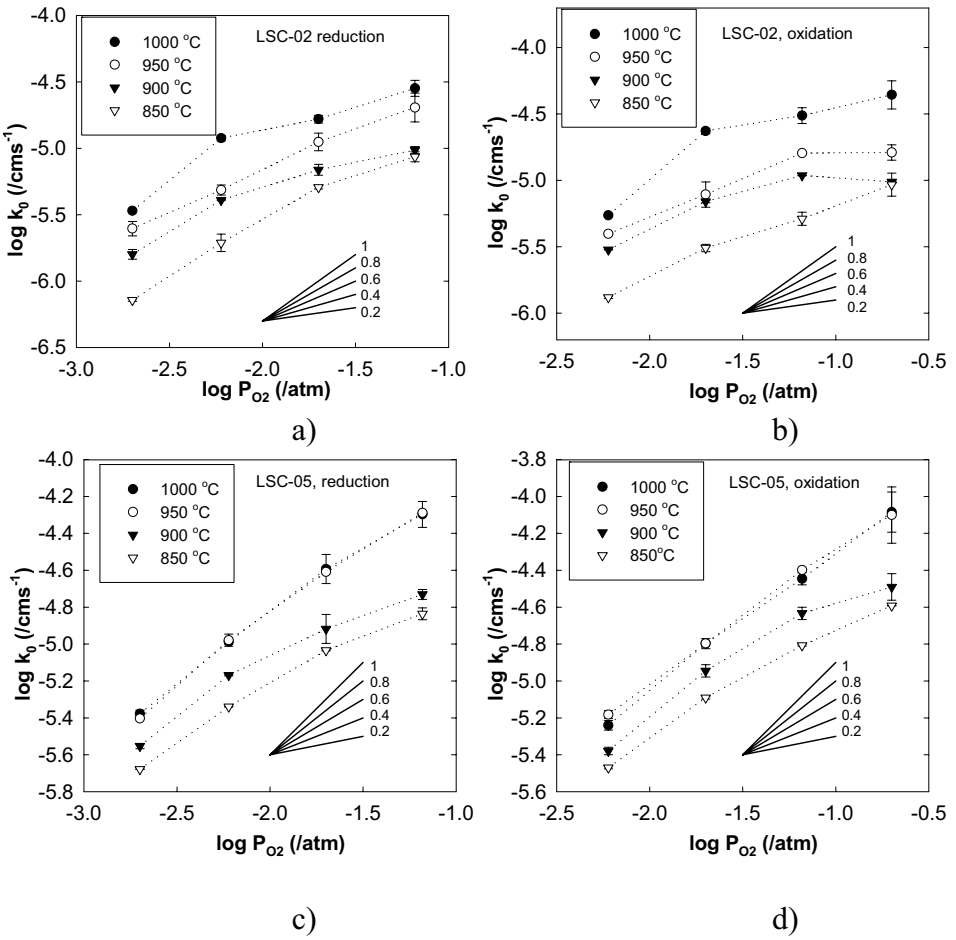

Fig. 5. Values for k_0 obtained in reduction: a) LSC-02 and c) LSC-05 and oxidation: b) LSC-02 and d) LSC-05. The lines wit variable slopes are included to indicate the P_{O2} dependency. Lines serve as guides to the eye.

In Fig 5 the k_0 values deduced from oxidation and reduction experiments are reported separately for LSC-02 and LSC-05, respectively. Included in Fig. 5 are also lines with slopes between 0.2 and 1, to give an indication of possible P_{O2} dependencies. The k_0 values all increases with increasing P_{O2} at all temperatures and for both oxidation and reduction. However, a less pronounced dependency is observed with increasing P_{O2} for both compositions at all temperatures. This might reflect changes in reaction mechanisms or the rate-determining step.

Methods for deriving possible reaction mechanisms based on observed P_{O2} dependencies.

The various transport coefficients which describe the surface exchange of oxygen k_0, k_{chem}, j^0_{ex}, and the relations between them were established in the introduction. The flux of oxygen through a surface when either oxygen is incorporated or released from a solid oxide can be described by the overall reaction given in Eq. (1). The overall reaction may be divided into a number of elementary reactions, and, given that all reactions are taking place in a serial manner, one single elementary reaction may in principle control the overall rate. That is, monitoring the variation in oxygen flux with P_{O2}, temperature and composition might reveal possible rate controlling elementary reactions. This subject is treated extensively in a large number of publications, e.g. Vogler [22].

Assuming j^0_{ex} to be proportional to the actual oxygen flux (reaction rate) the following relationship may be derived based on Eq. (11):

$$reaction\ rate \propto j^0_{ex} = \frac{1}{4} C_O k_0 = \frac{1}{4}\left(\frac{3-\delta}{N_A a^3} \right) k_0 \tag{13}$$

where a is the cubic cell parameter and N_A is the Avogadro constant ($6.023 \cdot 10^{23}$ mol^{-1}). Others have reported a small P_{O2} dependency for the unit cell parameter, a [23], but for all practical purposes this is taken as constant. However, the oxygen stoichiometry (3-δ), vacancy concentration (δ) and concentration of electronic species (n or p) are all important properties of significance to the surface exchange kinetics. The P_{O2} dependencies for these quantities are given in Tab. 1 for both LSC-02 and LSC-05 at all temperatures. The estimates are based on data presented in Part I. It is obvious from Fig. 5 that k_0 is strongly dependent on P_{O2}, and since the dependency of (3-δ) on P_{O2} (Cf. Tab. 1: $0.0030<n<0.0064$) is correspondingly weak, Eq. (13) may be simplified:

$$\text{reaction rate} \propto j^o_{ex} \propto k_O \tag{14}$$

That is, the surface exchange flux is proportional with k_0, and the variation in k_0 with P_{O2} might give significant information with respect to possible rate controlling elementary reactions. A similar approach has also been utilised by Merkle and Maier [8].

Table 1. Tabulated P_{O2} dependencies for the material parameters δ, and (3-δ) (P_{O2}^{n}). Values are calculated from oxygen nonstoichiometry data given in part I [16].

	LSC-02			LSC-05		
Temp.	δ P_{O2}^{n}	(3-δ) P_{O2}^{n}	$[e']-[e']^0$ P_{O2}^{n}	δ P_{O2}^{n}	(3-δ) P_{O2}^{n}	$[e']-[e']^0$ P_{O2}^{n}
1000 °C	-0.165	0.0048	-0.0825	-0.065	0.0064	-0.032
950 °C	-0.188	0.0043	-0.094	-0.068	0.0061	-0.034
900 °C	-0.217	0.0037	-0.108	-0.070	0.0058	-0.035
850 °C	-0.255	0.0030	-0.128	-0.074	0.0054	-0.037

As outlined earlier, the surface exchange reaction in an oxidation step must involve adsorption, charge transfer, dissociation, additional charge transfer and an installation into a vacancy; all steps with respect to oxygen species. For a reduction the same steps in the opposite direction must be applied. From these steps a large number of possible reaction pathways can be put forward. A general equation describing the surface exchange reaction for both oxidation and reduction is given in Eqs. (15)-(16).

$$rate \propto k_{ox} P_{O2}^{a} n^{b} \left[V_O^{\bullet\bullet} \right]^{c} \tag{15}$$

For the reduction this can be written as

$$rate \propto k_{red} n^{x} \left[V_O^{\bullet\bullet} \right]^{y} \left[O_O^{x} \right]^{z} \tag{16}$$

k_{ox} and k_{red} denotes the overall rate constants for oxidation and reduction respectively, while n is the electron concentration. The exponents a,b,c and x,y,z in Eqs (15) and (16) are the reaction order for the given specie and depends on the actual mechanism. All of the defect species in Eqs (15) and (16) will have a P_{O2} dependency, and the P_{O2} dependency of the modelled rate determining step (RDS) will be the sum of all defect P_{O2} dependencies.

In Tabs 2 - 3 a total of four different reactions mechanisms, A-D, are suggested, both for oxidation and reduction. Each reaction mechanism comprises a unique set of elementary reactions. Also included is a simplified rate equation for all elementary reaction, as well as the estimated P_{O2} dependency for k_0 (j^0_{ex}) given that the overall rate is controlled by the reaction in question.

RDS:	Comp	A	B	C	D
Step 1		$O_2(g)+S_{ad}=O_{2,ad}$	$O_2(g)+S_{ad}=O_{2,ad}$	$O_2(g)+S_{ad}=O_{2,ad}$	$O_2(g)+S_{ad}=O_{2,ad}$
		$\propto P_{O2}$	$\propto P_{O2}$	$\propto P_{O2}$	$\propto P_{O2}$
	LSC-02	1.00 / 1.00 / 1.00 / 1.00	1.00 / 1.00 / 1.00 / 1.00	1.00 / 1.00 / 1.00 / 1.00	1.00 / 1.00 / 1.00 / 1.00
	LSC-05	1.00 / 1.00 / 1.00 / 1.00	1.00 / 1.00 / 1.00 / 1.00	1.00 / 1.00 / 1.00 / 1.00	1.00 / 1.00 / 1.00 / 1.00
Step 2			$O_{2,ad}+e^-=O_{2,ad}^-$	$O_{2,ad}+2e^-=O_{2,ad}^{2-}$	$O_{2,ad}+2e^-=O_{2,ad}^{2-}$
			$\propto P_{O2}n$	$\propto P_{O2}n^2$	$\propto P_{O2}n^2$
	LSC-02		0.92 / 0.91 / 0.89 / 0.87	0.84 / 0.81 / 0.78 / 0.74	0.84 / 0.81 / 0.78 / 0.74
	LSC-05		0.97 / 0.97 / 0.96 / 0.96	0.94 / 0.93 / 0.93 / 0.92	0.94 / 0.93 / 0.93 / 0.92
Step 3		$O_{2,ad}+2V_O^{\bullet\bullet}=2O_O^{\bullet\bullet}+S_{ad}$	$O_{2,ad}^-+2V_O^{\bullet\bullet}=O_O^{\bullet}+O_O^{\bullet\bullet}+S$	$O_{2,ad}^{2-}+2V_O^{\bullet\bullet}=2O_O^{\bullet}+S_{ad}$	$O_{2,ad}^{2-}+S_{ad}=2O_{ad}^-$
		$\propto P_{O2}\delta^2$	$\propto P_{O2}n\delta^2$	$\propto P_{O2}n^2\delta^2$	$\propto P_{O2}n^2$
	LSC-02	0.67 / 0.62 / 0.56 / 0.49	0.59 / 0.53 / 0.46 / 0.36	0.51 / 0.43 / 0.35 / 0.23	0.84 / 0.81 / 0.78 / 0.74
	LSC-05	0.87 / 0.86 / 0.86 / 0.85	0.84 / 0.83 / 0.83 / 0.82	0.81 / 0.80 / 0.79 / 0.77	0.94 / 0.93 / 0.93 / 0.92
Step 4					$O_{ad}^-+e^-=O_{ad}^{2-}$
					$\propto \sqrt{P_{O2}}\, n^2$
	LSC-02				0.34 / 0.31 / 0.28 / 0.24
	LSC-05				0.44 / 0.43 / 0.43 / 0.42
Step 5		$O_O^{\bullet\bullet}+2e^-=O_O^x$	$\left\{\begin{array}{l} O^{\bullet}+e^-=O_O^x \\ O^{\bullet\bullet}+2e^-=O_O^x \end{array}\right\}$	$O_O^{\bullet}+e^-=O_O^x$	$O_{ad}^{2-}+V_O^{\bullet\bullet}=O_O^x+S_{ad}$
		$\propto \sqrt{P_{O2}}\, n^2\delta$	$\propto \sqrt{P_{O2}}\, n^2\delta$	$\propto \sqrt{P_{O2}}\, n^2\delta$	$\propto \sqrt{P_{O2}}\, n^2\delta$
	LSC-02	0.17 / 0.12 / 0.08 / -0.01	0.17 / 0.12 / 0.08 / -0.01	0.17 / 0.12 / 0.08 / -0.01	0.17 / 0.12 / 0.08 / -0.01
	LSC-05	0.37 / 0.36 / 0.36 / 0.35	0.37 / 0.36 / 0.36 / 0.35	0.37 / 0.36 / 0.36 / 0.35	0.37 / 0.36 / 0.36 / 0.35

Table 2. Possible reaction mechanisms, A-D, for the oxidation. The numbers in the shaded area corresponds to the calculated P_{O2} dependency for k_0 ($P_{O2}{}^n$) at the step at temperatures 1000 °C / 950 °C / 900 °C / 850 °C for the given composition.

RDS:	Comp	A	B	C	D
Step 1		$O_O^x = O_O^{\bullet\bullet} + 2e^-$	$\left\{\begin{array}{l} O_O^x = O_O^{\bullet} + e^- \\ O_O^x = O_O^{\bullet\bullet} + 2e^- \end{array}\right\}$	$O_O^x = O_O^{\bullet} + e^-$	$O_O^x + S_{ad} = O_{ad}^{2-} + V_O^{\bullet\bullet}$
		$\propto (3-\delta)$	$\propto (3-\delta)$	$\propto (3-\delta)$	$\propto (3-\delta)$
	LSC-02	0.00 / 0.00 / 0.00 / 0.00	0.00 / 0.00 / 0.00 / 0.00	0.00 / 0.00 / 0.00 / 0.00	0.00 / 0.00 / 0.00 / 0.00
	LSC-05	0.01 / 0.01 / 0.01 / 0.01	0.01 / 0.01 / 0.01 / 0.01	0.01 / 0.01 / 0.01 / 0.01	0.01 / 0.01 / 0.01 / 0.01
Step 2					$O_{ad}^{2-} = O_{ad}^{-} + e^-$
					$\propto (3-\delta)/\delta$
	LSC-02				0.17 / 0.19 / 0.22 / 0.26
	LSC-05				0.07 / 0.07 / 0.08 / 0.08
Step 3		$2O_O^{\bullet\bullet} + S_{ad} = O_{2,ad} + 2V_O^{\bullet\bullet}$	$O_O^{\bullet\bullet} + O_O^{\bullet} + S_{ad} = O_{2,ad}^{-} + 2V_$	$2O_O^{\bullet} + S_{ad} = O_{2,ad}^{2-} + 2V_O^{\bullet\bullet}$	$2O_{ad}^{-} = O_{2,ad}^{2-}$
		$\propto (3-\delta)^2 n^{-4}$	$\propto (3-\delta)^2 n^{-3}$	$\propto (3-\delta)^2 n^{-2}$	$\propto ((3-\delta)/\delta)^2\, n^{-2}$
	LSC-02	0.34 / 0.38 / 0.44 / 0.52	0.26 / 0.29 / 0.33 / 0.39	0.17 / 0.20 / 0.22 / 0.26	0.51 / 0.57 / 0.66 / 0.77
	LSC-05	0.14 / 0.15 / 0.15 / 0.16	0.11 / 0.11 / 0.12 / 0.12	0.07 / 0.08 / 0.08 / 0.08	0.21 / 0.22 / 0.22 / 0.23
Step 4			$O_{2,ad}^{-} = O_{2,ad} + e^-$	$O_{2,ad}^{2-} = O_{2,ad} + 2e^-$	$O_{2,ad}^{2-} = O_{2,ad} + 2e^-$
			$\propto ((3-\delta)/\delta)^2\, n^{-3}$	$\propto ((3-\delta)/\delta)^2\, n^{-2}$	$\propto ((3-\delta)/\delta)^2\, n^{-2}$
	LSC-02		0.59 / 0.67 / 0.77 / 0.90	0.51 / 0.57 / 0.66 / 0.77	0.51 / 0.57 / 0.66 / 0.77
	LSC-05		0.24 / 0.25 / 0.25 / 0.27	0.21 / 0.22 / 0.22 / 0.23	0.21 / 0.22 / 0.22 / 0.23
Step 5		$O_{2,ad} = O_2(g) + S_{ad}$	$O_{2,ad} = O_2(g) + S_{ad}$	$O_{2,ad} = O_2(g) + S_{ad}$	$O_{2,ad} = O_2(g) + S_{ad}$
		$\propto ((3-\delta)/\delta)^2\, n^{-4}$	$\propto ((3-\delta)/\delta)^2\, n^{-4}$	$\propto ((3-\delta)/\delta)^2\, n^{-4}$	$\propto ((3-\delta)/\delta)^2\, n^{-4}$
	LSC-02	0.67 / 0.76 / 0.87 / 1.02	0.67 / 0.76 / 0.87 / 1.02	0.67 / 0.76 / 0.87 / 1.02	0.67 / 0.76 / 0.87 / 1.02
	LSC-05	0.27 / 0.28 / 0.29 / 0.31	0.27 / 0.28 / 0.29 / 0.31	0.27 / 0.28 / 0.29 / 0.31	0.27 / 0.28 / 0.29 / 0.31

Table 3. Possible reaction mechanisms, A-D, for the reduction. Numbers in the shaded area corresponds to the calculated P_{O2} dependency for k_0 ($P_{O2}^{\ n}$)at the step at temperatures 1000 °C / 950 °C / 900 °C / 850 °C for the given composition

The first step in an oxidation run is the adsorption of an oxygen molecule. This step can most probably be ruled out as the rate-determining step for the surface exchange, since the number of gas-solid collisions at elevated temperatures are quite high, and the subsequent number of adsorptions should be sufficient. A situation where the adsorption of oxygen is the RDS can occur when the supply of oxygen is very small, i.e. at low P_{O2} or at high temperatures where the amount of adsorbed oxygen will decrease with increasing temperature.

Surface diffusion of the different oxygen species may also be a possible elementary step, and hence a possible RDS (rate determining step). However, the distance from an active adsorption point to the nearest vacancy is probably so small that surface diffusion may be ruled out as an elementary step, and are therefore not included in Tabs 2 and 3. Oxygen species are treated as adsorbed and Merkle and Maier [8] have given a summary of which oxygen species that have been observed at the surface with the various experimental techniques. Both O_2^- and O^- have been observed frequently as adsorbed species on different kinds of surfaces, while the O_2^{2-} specie has been observed even though there are fewer analytical methods available [8], and thus more difficult to observe.

The differences in the mechanisms A-C given in Tab. 2, are whether a none-, single- or doubly-charged oxygen molecule directly interacts (collide) with two vacancies, followed by charge transfer reactions finally giving O^{2-} ionic species installed in the lattice. The mechanism named D consists of a charge transfer to yield an adsorbed O_2^{2-}, followed by dissociation and another charge-transfer before the adsorbed O^{2-} is installed into a vacancy. This mechanism was successfully applied to describe the oxygen surface exchange in $La_{0.9}Sr_{0.1}FeO_3$ [10], with the dissociation/association reaction given in Step 3 in Tabs 2 and 3, as the rate-determining reaction in the surface exchange process for the given material. For the possible reaction mechanisms for the reduction process given in Tab 3, the elementary reactions are reversed in relation to those of the oxidation in Tab 2.

Rate controlling reaction for oxidation and reduction

In this section, we will combine the information given in Tabs. 2-3 with the k_0 behaviour reported in Fig. 5. Similar P_{O2}-dependencies should point to which elementary reactions are probable rate-controlling reactions, given that the relevant elementary reactions are included in Tabs. 2-3. We will discuss oxidation and reduction separately.

Oxidation

With reference to Fig. 5b it is obvious that we should hardly expect one unambiguous rate controlling reaction describing the surface kinetics at all temperatures and oxygen partial pressures. Based on the elementary reactions given in Tab. 2 the surface kinetics is reasonably well described by reaction A3, that is a direct interaction between a surface adsorbed oxygen specie and two oxygen vacancies, viz.:

$$O_{2,ad} + 2V_O^{\bullet\bullet} = 2O_O^{\bullet\bullet} + S_{ad} \tag{17}$$

with the corresponding rate law:

$$k_0 \propto rate = k_{ox} P_{O_2} \delta^2 \tag{18}$$

where δ represents the concentration of oxygen vacancies and k_{ox} is an Arrhenius rate constant.

In this case the rate (k_0) should be proportional to P_{O2}^n where n change from 0.49 to 0.67 as the temperature changes from 850 to 1000°C (Cf. Tab. 2). Except from the highest oxygen partial pressure at 900 and 950°C there is a fair fit between model and experimental data, supporting the assumption that reaction (17) is a probable RDS for the oxidation of $La_{0.8}Sr_{0.2}CoO_3$ at the conditions given. Now, assuming that reaction (17) also describes the oxidation surface kinetics for $La_{0.5}Sr_{0.5}CoO_3$ (LSC-05) we should expect the rate to be proportional to P_{O2}^n where n should increase from 0.85 to 0.87 as the temperature increase from 850 to 1000°C. This proportionality is reasonably well fulfilled except at the highest oxygen partial pressure at 850 and 900°C. Hence, it is suggested that for the oxidation process the rate controlling surface exchange reaction is best described by reaction (18) both for 20 and 50% Sr-doped $LaCoO_3$. This statement points out the important role of vacancies with respect to surface kinetics.

Reduction

Based on the suggested reaction pathways given in Tab. 3, interpretation of the reduction surface kinetics seems to be more complex. It should also be recalled that the uncertainty in k_0 derived from reduction relaxations might be higher than oxidation k_0 due to reasons discussed in Part I of this work [16] where the procedure of obtaining data from the relaxation experiments were discussed.

For $LaCoO_3$ with 20% Sr (LSC-02) we suggest that reaction (D3) gives the best description at low oxygen partial pressures (Fig. 5a):

$$2O_{ad}^{-} = O_{2,ad}^{2-} \tag{19}$$

with the following rate equation:

$$k_0 \propto rate = k_{red}\left(\frac{3-\delta}{\delta}\right)^2 \frac{1}{n^2} \tag{20}$$

With reference to Tab. 3 the "P_{O2}-exponent", n, should decrease from 0.77 to 0.51 with increasing temperature from 850 to 1000 °C in fair accordance with the experimental data reported in Fig. 5a). Wærnhus et al. [10] have also suggested reaction (D3) to be rate controlling for Sr-doped $LaFeO_3$ ($La_{0.9}Sr_{0.1}FeO_3$). Furthermore, in particular at 850 and 900 °C and the highest oxygen partial pressure, there is a less pronounced P_{O2} dependency, suggesting a possible shift in mechanism, however, data are too sparse to suggest any probable reaction.

Now, increasing the Sr-content in $LaCoO_3$ to 50% (Fig. 5c) we face an even more challenging assignment in terms of suggesting a viable reaction mechanism. Generally, the observed P_{O2}-dependancy (Cf. Fig. 5c) is more pronounced than any of the reactions given in Tab. 3 , with exception of the lowest temperature at the highest P_{O2} where the proportionality approach n=0.3 and thus pointing towards a desorption reaction being rate controlling, viz.:

$$O_{2,ad} = O_2(g) + S_{ad} \tag{21}$$

with the corresponding rate equation:

$$k_0 \propto rate = k_{red}\left(\frac{3-\delta}{\delta}\right)^2 \frac{1}{n^4} \tag{22}$$

As seen in Figs 3c) and d) k_0 in the LSC-05 composition showed very small thermal activation above 950 °C, corresponding to activation energies ranging from 5 kJ/mol to 15 kJ/mol. The increase in k_0 with P_{O2} is also significant in the whole temperature range (Figs 5c) and d)).

The change in activation energy might reflect a shift in the rate controlling elementary reaction taking place at the surface. The high activation energies observed at low temperatures are probably associated with rate controlling reactions involving formation of oxygen vacancies and/or breaking of chemical bonds, as seen in the previously discussed mechanisms. However, the major shift to smaller apparent activation energy at higher temperatures point in the direction of an adsorption type of mechanism becoming rate controlling, e.g. corresponding to:

$$O_2(g) + S_{ad} \rightarrow O_{2,ad} \tag{23}$$

Both a low activation energy as well as a pronounced P_{O2} dependency should result from a process controlled by reaction (23). If adsorption/desorption is the rate-controlling mechanism in this case, a measured P_{O2} dependency of ~1 should be measured at these temperatures, which is not far away from observations as can be seen in Figs 5c) and d).

Finally, we should recall that conclusions drawn above are not absolute and depends on a number of assumptions. First of all it should be emphasised that firm conclusions with respect to possible rate controlling reactions depends on reliable oxygen flux data. With reference to the k_0 values reported in Fig. 5 there is a high uncertainty in rate data, probably inherently asociated with the method of deriving fundamental kinetic data from conductivity relaxation experiments. Secondly, the reaction pathways given in Tabs. 2-3 may not give the complete picture with respect to all possible elementary reactions. Still, other reaction pathways including other elementary reactions may also be possible. At last, the tabulated reaction mechanisms assumes that all elementary reactions take place in a serial (consecutive) manner, with one single reaction typically being the RDS and consequently controlling the total rate. It should be kept in mind that reactions also may take place in parallell giving a total rate resulting from two or more reactions. Such a situation is not easilly modelled by the simple approach described above.

Surface exchange coefficient, k_0, and the role of vacancies

In Fig 6 values for log k_0 obtained for $LaCoO_3$ with 20 (LSC-02) and 50% Sr (LSC-05) are given in terms of reciprocal temperature at 0.20 atm (oxidation). Included are also values for k^* for $LaCoO_3$ at 0.045 atm [28], $LaFeO_3$ at 0.065 atm [29], $La_{0.9}Sr_{0.1}FeO_{3-\delta}$ at 0.065 atm [30] and $La_{0.75}Sr_{0.25}FeO_{3-\delta}$ at 0.065 atm [30].

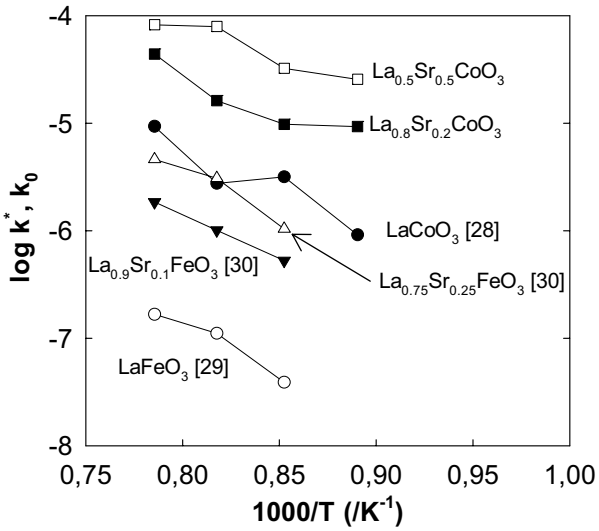

Fig. 6. Surface exchange coefficients k_0 and tracer surface exchange coefficients k^*, plotted against temperature and P_{O2} given; $LaCoO_3$ at 0.045 atm [28], $LaFeO_3$ at 0.065 atm [29], $La_{0.9}Sr_{0.1}FeO_{3-\delta}$ at 0.065 atm [30], $La_{0.75}Sr_{0.25}FeO_{3-\delta}$ at 0.065 atm [30], $La_{0.8}Sr_{0.2}CoO_{3-\delta}$ at 0.20 (ox) atm and $La_{0.5}Sr_{0.5}CoO_{3-\delta}$ at 0.20 (ox) atm from this work.

Due to a high inaccuracy in k_0 values obtained in this work for $LaCoO_3$ it has been chosen to use k_0 values reported by Ishigaki et al. [28]. The electronic conductivity for the cobaltites ($La_{1-x}Sr_xCoO_3$) is typically 4-5 orders of magnitude higher compared with the ferrites ($La_{1-x}Sr_xFeO_3$), a difference which is not reflected in Fig. 6 and thus indicates that the surface exchange rate is not controlled by the electronic conductivity.

However, there seems to be a trend in Fig. 6: The oxygen vacancy concentration increases with increasing Sr-content, and the vacancy concentration is also general higher in the coboltites than in ferrites. The figure obviously shows that at a given temperature the surface exchange coefficients, k_0 (or k*), increases with increasing population of oxygen vacancies. Even though this is only a semi quantitative approach, Fig. 6 emphasise the importance of vacancies and also comply well with the oxidation surface exchange kinetics derived in the present work.

CONCLUSION

The oxygen surface exchange parameter k_0, calculated from the thermodynamic factors and k_{chem} are reported for the partial pressure range $2 \cdot 10^{-3}$ – $2 \cdot 10^{-1}$ atm and in the temperature interval 850 (950 for x= 0) to 1000 °C for the compositions x = 0.2 and 0.5 (in $La_{1-x}Sr_xCoO_{3-\delta}$), and only the lowest oxygen partial pressures for $LaCoO_3$. The activation energy for k_0 in the three compositions are 206 kJ/mol for x=0, 110-130 kJ/mol for x=0.2 and 95-120 kJ/mol for LSC-05, and they are in good agreement with values reported in literature, for the compositions x=0.2 and 0.5. For the x = 0.5 composition the thermal activation of k_0 showed a plateau above 950 °C, maybe owing to a gas adsorption/desorption mechanismtaking place at the surface and corresponding to an activation energy of ~15 kJ/mol.

The P_{O2} dependency for k_0 has been investigated with respect to possible reaction mechanisms and the identification of possible rate determining steps. A total of four different reaction pathway schemes were proposed and their theoretical P_{O2} dependencies calculated. The main differences between these models are in which order the oxygen molecule is dissociated and ionised.

The model which suggested a direct installation of an (un)charged oxygen molecule in two vacancies as the rate-determining step gave the best fit for the P_{O2} dependency for k_0 against measured values, for both LSC-02 and LSC-05 in oxidation experiments. In reduction experiments a rate-determining step involving an association of two charged atomic oxygen is suggested for LSC-02, while for LSC-05 no P_{O2} dependency for k_0 against measured values could be assigned to a specific rate determining step. The P_{O2} dependency became less pronounced with increasing P_{O2} in both LSC-02 and LSC-05, possibly indicating a change in the rate-determining step or a change in the surface reaction pathway. However, further studies in this partial pressure and temperature interval is required to identify this potential change.

By examining the values of k_0 in strontium substituted lanthanum coboltites from this work and lanthanum ferrites from literature, it can be seen that k_0 increases with increasing oxygen vacancy concentration. Thus, oxygen vacancies are believed to play a major role in the surface exchange of oxygen.

ACKNOWLEDGEMENTS

Dr.Ing. Ivar Wærnhus is acknowledged for many inspiring discussions, Dr. Ing Hilde Lea Lein for synthesising the powder samples for the LSC-05 composition, both at Department of Materials Science and Engineering, NTNU, Trondheim. Thanks to Norsk Hydro ASA for financial support.

REFERENCES

1. Mizusaki, J.,Tabuchi, J.,Matsuura, T., Yamauchi, S. and Fueki, K., "Electrical conductivity and Seebeck coefficient of nonstoichiometric $La_{1-x}Sr_xCoO_{3-\delta}$", J. Eletrochem. Soc. 144, No.7, (1989), 2082-2088.
2. Teraoka, Y., Zhang, H.M., Furukawa, S. and Yamazoe, N., "Oxygen Permeation through perovskite-type oxides", Chem.Lett. (1985), 1743-46.
3. Voorhoeve, R.J.H. *in* "Advanced Materials in Catalysis" (J.J. Burton and R.L. Garten, Eds.), 1977.
4. Gellings, P.J. and Bouwmeester, H.J.M., "Ion and mixed conducting oxides as catalysts", Catalysis Today 12, (1992), 1-105.
5. Ohno, Y., Nagata, S., and Sato, H., "Effect of electrode materials on the properties of high temperature solid electrolyte fuel cells", Solid State Ionics, 3/4 , (1981), 439.
6. van der Haar, L.M., den Otter, M.W., Morskate, M., Bouwmeester, H.J.M. and Verweij, H., Chemical diffusion and oxygen surface transfer of $La_{1-x}Sr_xCoO_{3-\delta}$ studied with electrical conductivity relaxation", J.Electrochem.Soc. 149, No.3, (2002),J41-J46.
7. van Doorn, R.H.E., Fullarton, I.C., de Souza, R.A., Kilner, J.A., Bouwmeester, H.J.M. and Burggraaf, A.J., "Surface oxygen exchange of $La_{0.3}Sr_{0.7}CoO_{3-\delta}$", Solid State Ionics 96, (1997), 1-7.
8. Merkle, R. and Maier, J., " Oxygen incorporation into Fe-doped $SrTiO_3$: Mechanistic interpretation of the surface reaction", Phys.Chem.Chem.Phys 4, (2002), 4140-4148.
9. Ishihara, T., Kilner, J.A., Honda, M., Sakai, N., Yokokawa, H. and Takita, Y., "Oxygen surface exchange and diffusion in $LaGaO_3$ based perovskite type oxides", Solid State Ionics 113-115, (1998), 593-600.
10. Wærnhus, I.," Defect Chemistry, Conductivity and mass transport properties of $La_{1-x}Sr_xFeO_{3-\delta}$ (x=0 and 0.1)" , Thesis, Norwegian University of Science and Technology, (2003). b) Paper 4 in that thesis
11. ten Elshof, J.E., Lankhorst, M.H.R. and Bouwmeester, H.J.M, " Oxygen exchange and diffusion coefficients of strontium doped lanthanum ferrites by electrical conductivity relaxation", J.Electrochem.Soc. 144, No. 3, (1997), 1060-1067.

12. Bouwmeester, H.J.M., Kruidhof, H. and Burggraaf, A.J., "Importance of the surface exchange kinetics as rate limiting step in oxygen permeation through mixed-conducting oxides", Solid State Ionics 72, (1994), 185-194.
13. Mizusaki, J., Mima, Y., Yamauchi, S, Fueki, K., and Tagawa, H., "Nonstoichiometry of the Perovskite-type oxides $La_{1-x}Sr_xCoO_{3-\delta}$", J.Solid State Chem. 80, (1989), 102-111.
14. Maier, J., "On the correlation of macroscopic and microscopic rate constants in solid state chemistry", Solid State Ionics 112 (1998), 197-228.
15. Maier, J., "Interaction of oxygen with oxides: How to interpret measured effective rate constants?", Solid State Ionics 135 (2000), 575-588.
16. Watterud, G., Wiik, K. and Julsrud, S., "Oxygen transport in $La_{1-x}Sr_xCoO_{3-\delta}$ (x=0, 0.2 and 0.5) assessed with electrical conductivity relaxation. Part I: Bulk Diffusion and k_{chem}". Part I of this thesis.
17. Kröger, F.A., "The chemistry of inperfect crystals Vol. 2.", North-Holland Pub. (1974).
18. Prigogine, I., "Thermodynamics of irreversible processes", 2nd Ed., John Wiley & Sons, (1961).
19. Weppner, W. and Huggins, R.A., "Determination of the kinetic parameters of mixed conducting electrodes and application to the system Li_3Sb", J. Electrochem.Soc. 124, No. 10, (1977), 1569-1578.
20. Rudberg, E., Wiik, K., Nisancioglu, K. and Svennson, A.-M., Unpublished Work, (2004).
21. De Souza, R.A. and Kilner, J.A., "Oxygen transport in $La_{1-x}Sr_xMn_{1-y}Co_yO_{3\pm\delta}$ perovskites. Part II: Oxygen surface exchange.", Solid State Ionics 126, (1999), 153-161.
22. Vogler, H.S. , "Elements of chemical reaction engineering",2nd Ed., Prentice-Hall (1992).
23. Lein, H.L. and Grande, T., unpublished results (2003).
24. Barin, I., "Thermochemical data for pure substances", VCH, Verlagsgesellschaft mBH, Weinheim, Deutschland, (1989).
25. Mizusaki, J., Yoshihiro, M., Yamauchi, S. and Fueki, K., "Nonstoichiometry and defect structure of the perovskite-type oxides oxides $La_{1-x}Sr_xFeO_{3-\delta}$", J.Solid State Chem. 58, (1985), 257-266.
26. Petrov, A.N., Cherepanov, V.A., Kononchuk, O.F. and Gavrilova, L.Ya., "Oxygen nonstoichiometry of $La_{1-x}Sr_xCoO_{3-\delta}$ ($0< x \leq 0.6$)", J.Solid State Chem. 87, (1990), 69-76.
27. Lankhorst, M.H.R., Bouwmeester, H.J.M. and Verweij, H., "High-temperature coulometric titration of $La_{1-x}Sr_xCoO_{3-\delta}$: Evidence for the effect of electronic band structure on nonstoichiometric behaviour", J.Solid State Chem 133, (1997), 555-567.

28. Ishigaki, T., Yamauchi, S., Mizusaki, J., Fueki, K. and Tamura, H., "Tracer diffusion coefficient of oxide ions in $LaCoO_3$ Single crystal", J.Solid State Chem., 54, (1984), 100-107.
29. Ishigaki, T., Yamauchi, S., Mizusaki, J., Fueki, K. and Tamura, H., "Diffusion of oxide ions in $LaFeO_3$ single crystal", J.Solid State Chem., 55, (1984), 50-53.
30. Ishigaki, T., Yamauchi, S., Kishio, K., Mizusaki, J., and Fueki, K., "Diffusion of oxide ion vacancies in perovskite-type oxides", J.Solid State Chem., 73, (1988), 179-187.

OXYGEN TRANSPORT IN PURE AND Al-DOPED $SrTiO_3$ MEASURED WITH ELECTRICAL CONDUCTIVITY RELAXATION. Part I: In O_2/N_2 mixtures

Geir Watterud[a], Stein Julsrud[b] and K. Wiik[*a],
[a]Department of Materials Science and Engineering
Norwegian University of Science and Technology
N-7491 Trondheim, Norway.
[b]Scanwafer AS, N-3907 Porsgrunn, Norway

ABSTRACT

Oxygen transport in $SrTiO_3$ (ST), $SrTi_{0.98}Al_{0.02}O_3$ (STA-02) and $SrTi_{0.95}Al_{0.05}O_3$ (STA-05) have been investigated with electrical conductivity relaxation in O_2/N_2 mixtures in the temperature interval 850-1000 °C.

Measurements of the electrical conductivity in both O_2/N_2 and CO/CO_2 mixtures were consistent with the defect chemistry derived for pure $SrTiO_3$ while the two Al- substituted compositions showed an unexpected P_{O2} dependency in CO_2 rich atmospheres. This might be related to phase transitions or segregation of Al on the grain boundaries. However, we were not able to describe the conductivity behaviour in terms of defect chemistry at these conditions, thus unabling the calculation of thermodynamic factors and subsequent derivation of more fundamental transport coefficients. Therefore this work is mainly concerned with the chemical transport coefficients, D_{chem} and k_{chem}.

D_{chem} for ST and STA-02 in O2/N2 mixtures, and k_{chem} for STA-02 and STA-05 in O_2/N_2 mixtures are reported. Values for the component diffusion coefficient, D_O, and the vacancy diffusion coefficient, D_V, are reported at 950 °C. The values for the diffusion coefficients and the corresponding activation energies are in good agreement with literature data.

Corresponding author: Kjell Wiik, Department of Chemistry, Norwegian University of Science and Technology, N-7491 Trondheim, Norway, e-mail: kjell.wiik@material.ntnu.no, Telephone no.: +47 73 59 40 82, fax no:+47 73 59 08 60

Values for D_{chem} are reported for ST and STA-02 and are along with their corresponding activation energies (187 and 104-180 kJ/mol, respectively) in good agreement with values from literature. Values for k_{chem} in STA-02 and STA-05 are reported, and show pronounced P_{O2} dependencies. The activation energy in STA-05 was in the interval 90-105 kJ/mol. The activation energy for STA-02 could not be calculated due to experimental uncertainty.

Keywords:
$SrTiO_3$, Al doped, Electrical conductivity relaxation, k_{chem}, D_{chem}.

INTRODUCTION

$SrTiO_3$ is a technologically important mixed-conducting electroceramic [1], and also serve as an excellent model material for studying defect chemistry and oxygen transport/exchange [2]. Strontium titanate based materials have been proposed as candidate materials for use as sensors (oxygen), photoelectrodes and varistors amongst others [3]. Due to its role as a model material, an enormous amount of research has been performed on this material and its related compounds [4].

$SrTiO_3$ adopts the cubic perovskite structure above 105 K [1]. Studying the binary phase diagram of SrO and TiO_2 [5] it can be seen that the material may have a limited amount of excess SrO and thus form a solid solution at T<1580 °C. However, the range of solid solution with excess TiO_2 is very narrow. Maier et al. reported no secondary phases in a sample with nominal composition $SrTi_{1.005}O_3$ [6]. The excess TiO_2 was assumed to be compensated by formation of vacancies on the Sr-site. $SrTiO_3$ may also be substituted at both A- and B-site to form solid solutions with specific material properties. Common substituents are La and Ba on the A-site, while Fe, Zr and Al may be substituted on the B-site [1]. In some cases the substituted solid solutions will deviate from cubic symmetry.

The electronic conductivity in pure, acceptor and donor doped $SrTiO_3$ are measured and described in detail by many authors [7-13]. From these works a reliable and quantitative defect model has been established. The defect model will be presented later in this work.

The ionic transport of oxygen in perovskites can in general be divided into two different processes, the surface exchange of oxygen between the material surface and the ambient atmosphere and the solid state bulk diffusion, respectively. The transport coefficients associated with the two processes, are the diffusion coefficient D, and the surface exchange coefficient k. These parameters can be obtained by three phenomenologically different methods; stationary conductivity measurements, tracer experiments and chemical diffusion experiments [14,15,16]. A more thorough discussion on the correlation between the transport coefficients are given in Ref. [14].

Bulk diffusion

The solid state diffusion of oxygen measured with different techniques is reported and discussed in a large number of publications, covering a wide

range of temperatures and oxygen partial pressures. Müller and Härdtl [17] studied the transient change in electrical conductivity with changing oxygen partial pressure, and applied an ambipolar diffusion model to assess data for the chemical diffusion coefficient. (This model is almost equal to a conductivity relaxation model, see e.g. [18]) They reported D_{chem} for oxygen ions to be in the range $2 \cdot 10^{-5}$ -$2 \cdot 10^{-6}$ $cm^2 s^{-1}$ at temperatures between 850 and 1000 °C and P_{O2} corresponding to air and nearby.

Walters and Grace [19] reported data for the oxygen vacancy diffusion coefficient D_V obtained in H_2/H_2O mixtures, using the conductivity relaxation method. Paladino studied the chemical diffusion by a thermogravimetrical method [20]. Later Schwarz and Anderson [21] used a capacitance manometric method to calculate D_V in $SrTiO_3$ finding values in agreement with Paladino[20].

Common for [19,20] is that the level of impurities is unknown and thus not taken into consideration while discussing the values for the chemical diffusion coefficient D_{chem}.

Claus et al. [2] have performed tracer experiments and reported diffusion coefficients for oxygen transport for a specimen with known levels of acceptor impurities originating from iron. The absolute values for the chemical diffusion coefficients are in the same range as those obtained by Müller and Härdtl [17].

Noll et al. [22] have used an optical technique to measure the chemical diffusion in the temperature range 177-727 °C (450 - 1000 K) finding results which corresponds well with values obtained from chemical polarization experiments [13], optical adsorption [23,24] and conductivity experiments [25]. Schlüter et al. [26] adds chemical diffusion coefficients obtained from permeation experiments to the results given in Refs.[13,22-25], and shows that all these methods give similar results for the chemical diffusion coefficients. In all the mentioned references, the $SrTiO_3$ materials examined have well defined levels of (acceptor) impurities originating from iron.

The values for D_{chem} in $SrTiO_3$ from refs [17, 19-23, 25, 26] are compiled into Fig 1 and it can be seen that the scattering is considerable.

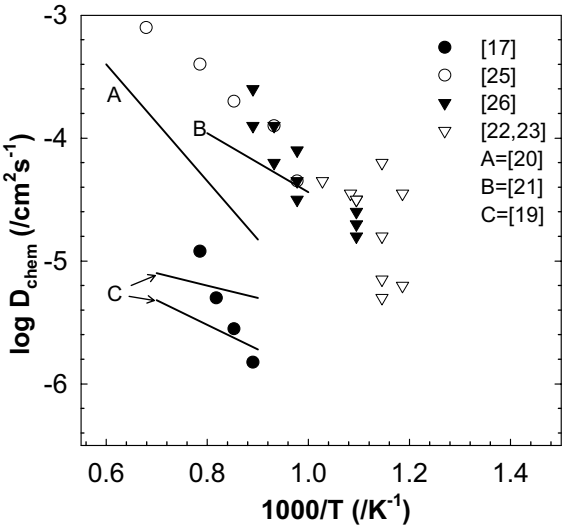

Fig. 1. Values for D_{chem} in $SrTiO_3$ from references given in the legend of the figure.

There are no literature data for the chemical diffusion coefficients of oxygen in Al-substituted $SrTiO_3$. However, the oxygen ionic conductivity is measured at 1000 °C for $SrTi_{0.9}Al_{0.1}O_3$ at P_{O2}´s ranging from 10^{-17} to 1 atm [27]. The values for the σ_{O2-} increased from 10^{-3} S/cm to ~$3 \cdot 10^{-3}$ S/cm at the lowest oxygen partial pressure. By introducing the Nernst-Einstein equation (e.g. Ref. [28]) one obtains an oxygen component diffusion coefficient of ~$4 \cdot 10^{-9}$ cm^2s^{-1}, which is approximately similar to the component diffusion coefficient given by Paladino [20] in pure $SrTiO_3$. However, Widerø et al. [27] reported a density of only 73% of the theoretical value, and adjustments due to high porosity were not performed.

Song and Yoo [29-32] have examined the chemical diffusivity in $BaTiO_{3-\delta}$ (pure and with acceptor doping) with electrical conductivity relaxation at both sides of and in the mixed regime of the n and p-type conductivity. Results and trends from this material will be discussed in relation to the $SrTiO_3$ system from this work.

Surface exchange processes

For the surface exchange coefficients Maier [15,16] have given a theoretical treatment of the coefficients originating from different experimental set-ups; stationary conductivity, tracer diffusion and chemical diffusion experiments. The theoretical treatment is given in terms of irreversible thermodynamics

and relates the surface exchange coefficients originating from tracer diffusion and chemical diffusion, respectively, with the thermodynamic factor. This will be treated more thoroughly in the subsequent sections.

The surface exchange processes in $SrTiO_3$ are studied and understood to a certain extent. Merkle and Maier [33] have performed a mechanistic interpretation of the oxygen incorporation in Fe-doped $SrTiO_3$, and put forward a probable reaction pathway for the transport of oxygen from atmosphere to bulk. The models were compared to experimental values obtained by using the same optical method as described by Bieger et al. [24]. Plausible rate-determining steps (RDS) were suggested. Two conclusions were made; the RDS in an oxidation process contains an O_2^{n-} molecular oxygen specie (n = 0, 1 or 2), and tan electron participates before or in the RDS.

Leonhardt et al. [3] have examined the surface exchange reaction in Fe doped $SrTiO_3$ by performing relaxation experiments monitored with a modified optical technique from [34], and tracer experiments analysed by SIMS. They report an increasing surface exchange coefficient from tracer experiments, k^*, with increasing content of iron impurities, as well as an increasing surface exchange parameter from relaxation experiments, k_{chem}, with increasing oxygen partial pressure. The effects of adding thin metal or metal oxide films on the $SrTiO_3$ materials were also studied, showing enhanced values for k^*, but no change in the activation energy.

Schlüter et al [26] have studied the chemical surface exchange coefficient with permeation, and report values in accordance with values obtained by other methods, e.g. Bieger et al [23]

There are no literature data for the surface exchange coefficient in Al-substituted $SrTiO_3$. However, Yoo et al. [34] have studied the chemical surface exchange coefficient (and diffusion) for $BaTiO_3$ substituted with 1.8 mol % Al, showing an increasing k_{chem} with increasing P_{O2} at high oxygen partial pressures (O_2/N_2 –mixtures). This is also observed in many previous works in other material systems such as $La_{0.9}Sr_{0.1}FeO_3$ [36] and $La_{0.5}Sr_{0.5}CoO_{3-\delta}$ [18,37]. In CO/CO_2-mixtures the k_{chem} seemingly increases with increasing content of CO, a development also reported in [36] at conditions where $P_{CO} < P_{CO2}$.

In a previous work [37,38], the oxygen diffusion and surface exchange coefficients have been investigated in the system $La_{1-x}Sr_xCoO_{3-\delta}$ (x=0, 0.2 and 0.5). This material system exhibits metallic-like conductivity with high concentrations of electrons and oxygen vacancies. The conductivity in

$SrTiO_3$ is several orders of magnitude lower and also the concentration of oxygen vacancies in $SrTiO_3$ is significantly lower. This work will focus on the assessment of oxygen diffusion- and surface exchange coefficients in the electron poor $SrTiO_3$-material, both nominally pure and substituted with 2 and 5 % aluminium. In Part II [39] oxygen transport coefficients will be assessed in CO/CO_2-mixtures.

THEORY

Defect Chemistry of SrTiO3

Many authors have studied the defect chemistry in $SrTiO_3$ [7-13] and from these works a quantitative defect model for $SrTiO_3$ is established. The defect model is based on a localised electron model. At very low oxygen partial pressures, the reduction process will dominate and this can be described by Eq. (1).

$$O_O^x = \frac{1}{2}O_2 + V_O^{\bullet\bullet} + 2e' \tag{1}$$

using the notation for defect species given by Kröger and Vink [40].
Eq. (1) gives rise to a n-type conductivity regime, since four electrons are "liberated" for every oxygen molecule "leaving" the oxide. At very high P_{O2}´s the incorporation of oxygen (oxidation) will dominate, and the material will show p-type conductivity, viz.:

$$\frac{1}{2}O_2 + V_O^{\bullet\bullet} = O_O^x + 2h^{\bullet} \tag{2}$$

If excess TiO_2 is present this will result in vacancies on the Sr-site, as reported by Maier et al. [6], and additional oxygen vacancies. This can be described by

$$TiO_2 \overset{SrTiO_3}{\rightleftharpoons} Ti_{Ti}^x + 2O_O^x + V_{Sr}^{''} + V_O^{\bullet\bullet} \tag{3}$$

With an incorporation of acceptor impurities such as Al_2O_3, the Al will enter the Ti –sites in the structure, with subsequent formation of an oxygen vacancy

$$Al_2O_3 \overset{SrTiO_3}{\rightleftharpoons} 2Al_{Ti}^{'} + 3O_O^x + V_O^{\bullet\bullet} \tag{4}$$

Assuming charge neutrality, charge balance gives:

$$2\left[V_O^{\bullet\bullet}\right] + p = 2\left[V_{Sr}^{''}\right] + \left[A_{Ti}^{'}\right] + n \tag{5}$$

where p≡[h$^{\bullet}$]and n≡[e′]. [$A_{Ti}{}'$] represent the net acceptor content, occurring from both added material and contamination. Additionally, equilibrium between electrons and holes is assumed to be established through:

$$nill = e^{'} + h^{\bullet} \tag{6}$$

All defect parameters are now introduced in Eq. (1) to (4), and in combination with charge neutrality, mass conservation and the relevant equilibria it is possible to describe the variation in population of defect species with e.g. P_{O2}. This is given in Fig 2.

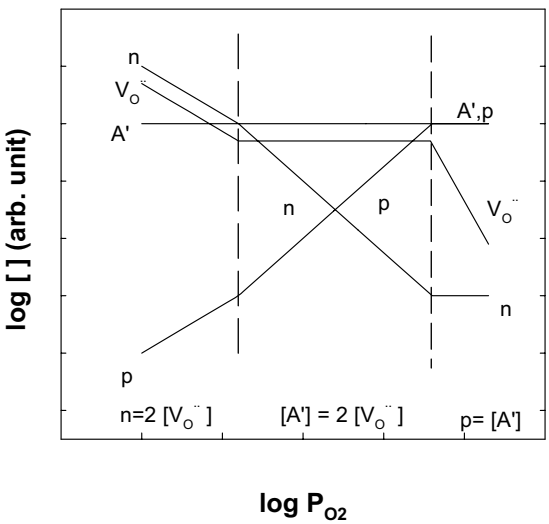

Fig 2. Schematic representation of equilibrium defect model for acceptor doped $SrTiO_3$. Figure is adapted and redrawn from Chan et al. [8] and Eror and Balachandran [9].

A more detailed presentation of the defect chemistry is given in [7-13], while a short derivation of the electrical conductivity behaviour is given below.
The general formula for the total electrical conductivity is given by

$$\sigma_{tot} = \sum_i c_i z_i e \mu_i \tag{7}$$

C_i is the concentration of the specie i, z_i is the number of elementary charges, e is the elementary charge and μ_i is the mobility of specie i. The conductivity will in general be a function of the concentration of the electrons and electron holes, since their mobility is much greater than the ionic species. However, at the conductivity minimum ("interception" between n and p, Fig. 1) the ionic contribution to the total conductivity can often not be neglected. For the case of undoped $BaTiO_3$, Song and Yoo [30] reported the electronic transference number, t_{el}, to be around 0.5 at the electronic conductivity minimum at 800 °C.

At low partial pressures, electrons and oxygen vacancies will be the major defects. The charge balance for Eq. (1) can in this case be written as :

$$2\left[V_O^{\bullet\bullet}\right] \approx n \tag{8}$$

By introducing this into the mass-action expression of Eq. (1) one obtains

$$n \propto P_{O2}^{-1/6} \tag{9}$$

Thus at the lowest oxygen partial pressures, the conductivity will (theoretically) be proportional to $P_{O2}^{-1/6}$.

At medium oxygen partial pressures, the amount of oxygen vacancies will be defined by the population of acceptor impurities, giving a constant $[V_O^{\bullet\bullet}]$ in this region. This means that the charge neutrality condition can be written as

$$2\left[V_O^{\bullet\bullet}\right] \approx 2\left[V_{Sr}^{''}\right] + \left[A_{Ti}^{'}\right] \approx \left[A_{Ti}^{'}\right] \tag{10}$$

It is assumed that the concentration of vacancies on the Sr-site is much lower than the concentration of oxygen vacancies. The constant oxygen vacancy concentration in this region can be introduced into the mass action laws for Eq.(1) and (2), giving

$$n \propto P_{O2}^{-1/4} \quad and \quad p \propto P_{O2}^{+1/4} \tag{11}$$

This means that the conductivity will change its proportionality with P_{O2} from (–1/4) to (+1/4) with increasing oxygen partial pressure in this region.

At even higher oxygen partial pressures, the amount of acceptor impurities will define the population of electronic holes. Thus the charge neutrality condition will in this case be

$$\left[A_{Ti}^{'}\right] \approx p \tag{12}$$

This means that the conductivity will be independent of P_{O2} at the highest oxygen partial pressures. By using the charge neutrality condition one obtains a $P_{O2}^{-1/2}$ dependency for the oxygen vacancy concentration in this region.

Solid State Diffusion

As pointed out earlier, it is possible to define several different types of diffusion coefficients, and all are related to each other. A thorough discussion of the different diffusion coefficients is given in Ref. [14]. A shorter review of the different diffusion coefficients have been given elsewhere [37], thus only a brief presentation will be given here.

The component diffusion coefficient of oxygen D_O, is related to the vacancy diffusion coefficient, D_V, by means of their respective concentrations [41].

$$C_O D_O = C_V D_V \tag{13}$$

The chemical diffusion coefficient, D_{chem}, is related to the D_O and D_V parameters via the thermodynamic factors for ions and vacancies, viz. [42]:

$$\begin{aligned} D_{chem} &= \left(\frac{1}{2}\frac{\partial \ln P_{O_2}}{\partial \ln C_O}\right) D_O = W_O D_O \\ &= -\left(\frac{1}{2}\frac{\partial \ln P_{O_2}}{\partial \ln C_V}\right) D_V = W_V D_V \end{aligned} \tag{14}$$

where W_O and W_V are the thermodynamic factors for oxygen ions and vacancies respectively.

Surface exchange coefficients

The transport coefficients associated with surface exchange of oxygen have previously been treated elsewhere [38], thus only the most important equations will be presented here.

The oxidation and reduction reaction can be described as a flux of oxygen in or out of the material. If a material is in equilibrium with the oxygen pressure in the surroundings at any given temperature, these fluxes are equal. If the oxygen activity in the ambient is changed by a small amount, oxygen will flow in or out of the sample as described in Eq. (15) [43].

$$j_{O_2} \equiv j_{ox} - j_{red} = j_{ex}^0 \frac{\Delta\mu_{O_2}}{RT} \tag{15}$$

The parameter j^0_{ex} describes the surface exchange rate (flux) of molecular oxygen at equilibrium. Thus at equilibrium:

$$j_{ox} = j_{red} = j_{ex}^0 \tag{16}$$

The expression given in Eq (15) can be derived by means of irreversible thermodynamics [15,44].

Similarly, as for the chemical diffusion coefficient, a chemical surface exchange coefficient, k_{chem}, can be defined, relating the flux with a concentration difference. Also, a surface exchange coefficient, k_0, can be defined, describing the surface exchange when there are no oxygen chemical potential gradients present. These two are related to the equilibrium flux j^0_{ex}, and the thermodynamic factor for oxygen ions and the relation is given in Eq. (17) [38].

$$j_{ex}^0 = \frac{1}{4} C_O k_0 = \frac{1}{4} \frac{C_O}{W_O} k_{chem} \tag{17}$$

EXPERIMENTAL

Polycrystalline samples with composition $SrTiO_3$ (ST), $Sr_{0.98}Al_{0.02}TiO_3$ (STA-02) and $Sr_{0.95}Al_{0.05}TiO_3$ (STA-05) were prepared through a solid state route. Stoichiometric amounts of $SrCO_3$ (BDH Laboratory Supplies, >98.5%), TiO_2 (Merck, >99%) and γ-Al_2O_3 (Merck, >99.5%) were mixed in a boron carbide mortar and pressed to pellets. The pellets were fired at

1400 °C for a total of 200 h divided into a total of 4 different cycles. Between each firing the pellets were crushed and mixed in a boron carbide mortar approx. 20 min. pr. grams of material and then pressed again. The firing temperature was chosen in accordance with the reported phase relations in the system SrO –TiO_2 [5], showing a eutectic melt at 1440^{o}C on the TiO_2 excess "side". Subsequent to heat treatments all three compositions were subjected to X-ray powder diffraction (XRD) (Cu K_{α}, Phillips PW1730/10) and showed single-phase composition for all samples. The single phase powders were uniaxially pressed into slabs at 15 MPa followed by isostatical pressing at 200 MPa and 25 °C. All compositions were sintered at 1520 °C for 12 h.

Bulk densities for the sintered slabs were measured using the Archimedean method, and all samples were sintered to densities higher than 95 % of the crystallographic density for $SrTiO_3$, which is 5.118 g/cm^3 [45]. For the 2 and 5% aluminium doped compositions, the crystallographic densities are believed to be slightly lower than for the undoped one. Open porosities in the materials were in the interval 0.5-1.1 %. In order to perform conductivity relaxation experiments to measure the transport properties of the bulk material, the bulk material needs to have closed porosity. During the sintering pores starts closing when the total porosity is ~15 % and are closed at a total porosity of around 5 % [46]. Thus, the materials in this work have sufficient density. XRD analysis of the sintered samples showed single-phase material. The samples were cut and polished to give slabs that were of the size of about 7.5mm x 2.5 mm x 23 mm.

Oxygen surface exchange and diffusion were measured by the electrical conductivity relaxation technique. This method and the theory behind have been extensively described by many authors [18,29,36,37,47,48].

RESULTS AND DISCUSSION

Measured electrical conductivity

The measured time independent ("equilibrium") electrical conductivities for ST, STA-02 and STA-05 are given in Figs 3a-c) respectively.

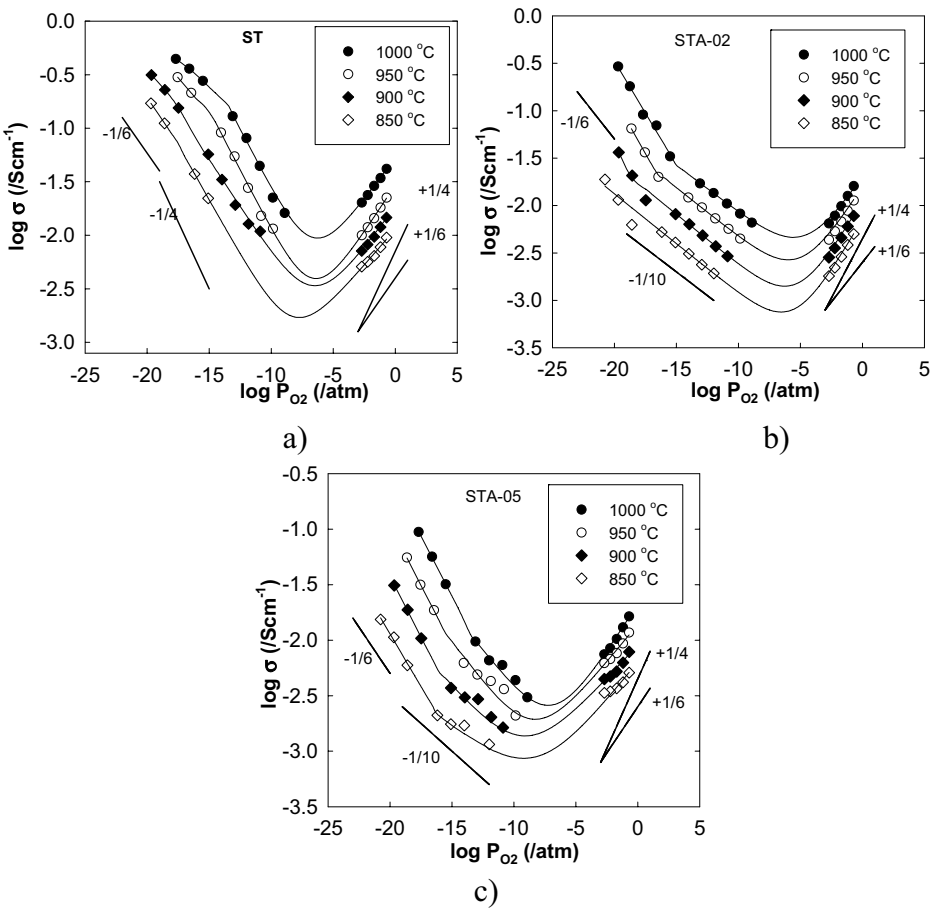

Fig. 3. Measured electrical conductivities in materials a) ST, b) STA-02 c) STA-05. Lines are regressions based on measured values.

The solid lines in Fig 3 are regressions based on measured values and also give an indication on probable conductivity behaviour at intermediate P_{O2}´s.

From Fig 3 it can be seen that there are three different regions at each temperature for all compositions, in which the log conductivity is a linear function with log P_{O2}, however with different proportionality factors. The

reciprocals of these values, m (corresponding to $P_{O2}^{1/m}$), are given in Tab. 1. The conductivity also increases with temperature for all compositions, consistent with a semiconductor.

Table 1. Reciprocal values for the measured P_{O2} dependencies for the electrical conductivity in all samples at the given temperatures.

Sample, Temp	High P_{O2}, p-type $\sigma \quad P_{O2}^{(1/m)}$	Med. P_{O2}, n-type $\sigma \quad P_{O2}^{(1/m)}$	Low P_{O2}, n-type $\sigma \quad P_{O2}^{(1/m)}$
ST, 1000 °C	6.3735	-4.4444	-10.6383
ST, 950 °C	5.6529	-4.4643	-7.5075
ST, 900 °C	6.4103	-5.6529	-7.0771
ST, 850 °C	7.4019	-4.8497	-5.8651
STA-02, 1000 °C	5.0659	-10.0604	-4.5579
STA-02, 950 °C	4.8450	-9.6154	-4.2753
STA-02, 900 °C	4.5641	-9.3721	-4.3159
STA-02, 850 °C	4.4643	-9.5057	-4.5455
STA-05, 1000 °C	5.7837	-6.9541	-4.6189
STA-05, 950 °C	7.3206	-6.5402	-4.5977
STA-05, 900 °C	8.2034	-7.8493	-4.5683
STA-05, 850 °C	7.1685	-11.8064	-5.2798

From Tab 1, and also in Fig 3, it can be seen that the measured P_{O2} dependencies for all three compositions is different from the proportionalities derived in the introduction. Similar behaviour have been reported by Eror and Balachandran [9], reporting "m-values" between 1/4.36 and 1/6.07 in the p-type region for $SrTiO_3$ with ≤ 1-% Al and temperatures between 850 and 1050 °C. The variation in conductivity for ST given in Fig 3a is similar to those obtained by Chan et al. [8] and Eror and Balachandran [9]. For the other two compositions, no literature data are available. However, Eror and Balachandran [9] reported the conductivity for $SrTiO_3$ with 1 % Al to be larger than pure $SrTiO_3$ with a factor of about 3 in the p-type regime. A reversed behaviour was observed in the n-type regime showing the conductivity for pure $SrTiO_3$ almost 3 times larger than the 1 % Al doped. Thus, according to [9] the conductivity minima shift to lower P_{O2}´s with dopant level of Al.

The electrical conductivity behaviour of $SrTiO_3$ with P_{O2} (Fig. 3a) corresponds to the theoretical derivations presented in the introduction. For STA-02 and STA-05 this is not the case. It can be seen from Fig 3b and c,

and from the dependencies in Tab 1 that at the highest P_{O2}'s and at the lowest P_{O2}'s, the dependencies are close to the expected values of +1/4 and –1/4 respectively. In the middle region the P_{O2} dependency is less pronounced (~ -1/10), and deviates substantially from the expected (+1/4). This behaviour can not be described by a defect model. The observed behaviour might be due to the presence of impurities, or it could be related with the Al-doping. If Al starts to precipitate to another phase below a certain oxygen partial pressure, this will influence the total conductivity. However, the measurements of electrical conductivity were reproducible and with rather short equilibration times, so the reason for the unexpected behaviour can not be due to any slow processes working in the background such as cation diffusion or the formation of Schottky defects, as seen in $LaFeO_3$ [36]. If, for any reason, Al-precipitation takes place the corresponding diffusion path must be extraordinary small, corresponding to a spinodal type of phase separation.

In Fig 4a the measured electrical conductivites are plotted at 1000 and 850 °C in the p-type regime. It can be seen that the introduction of aluminium, both for STA-02 and STA-05, give a decrease in conductivity with a factor of around 1/3. In Fig 4b the measured electrical conductivities are plotted at 1000 °C with the partial pressures of oxygen corresponding to air composition (in the typical p-type conductivity regime), and at $P_{CO} = 0.002$ atm and 0.20 atm, corresponding to $P_{O2} = 10^{-8.7}$ and $10^{-12.9}$ atm, respectively (in the n-type conductivity regime). It is seen that the measured electrical conductivity decreases with the introduction of Al, regardless of whether the conductivity shows p-type or n-type. For the measurements in the n-type region the observation of decreasing conductivity with the introduction of Al is consistent with Eror and Balachandran [9], while the behaviour in the p-type regime show a reversed trend compared with [9], that is, a decreasing conductivity with Al-level.

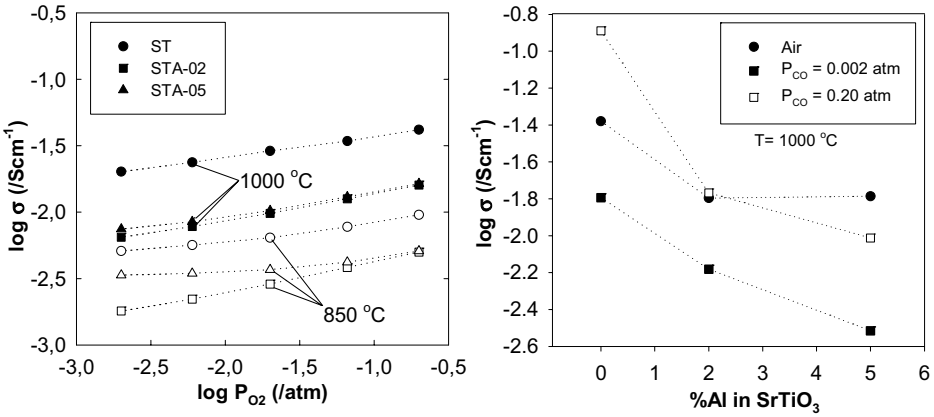

a) b)

Fig. 4. a) Measured electrical conductivites for all three compositions in O_2/N_2 mixtures, with closed symbols denoting 1000 °C, while open symbols denotes 850 °C. b) Measured electrical conductivites at 1000 °C and at different partial pressures as a function of atomic % of Al in the sample.

The main purpose of the present work is to study oxygen surface exchange, and oxygen bulk diffusion. From conductivity relaxation measurements it is possible to obtain so called chemical values, D_{chem} and k_{chem}. However, a complete discussion also involves an evaluation of derived coefficients such as component/vacancy diffusion coefficients and tracer diffusion exchange coefficients. These variables may be deduced if the thermodynamic factors (W_O and W_V) or oxygen nonstoichiometry data are available, which they only are for pure $SrTiO_3$ at 950°C [49]. For the remaining compositions and temperatures W_O and W_V are not available. Thus, our discussion will basically be confined to the chemical transport coefficients, D_{chem} and k_{chem}.

On the limitations and restrictions associated with transport coefficient calculations

The conductivity relaxation experiments for ST, STA-02 and STA-05 gave not easily interpretable data for D_{chem} and k_{chem}. The challenge was generally associated with transport coefficients not converging in the numerical fitting procedure between experimental results and the model for oxygen transport. The phenomena of non-converging transport coefficients are illustrated in Fig 5.

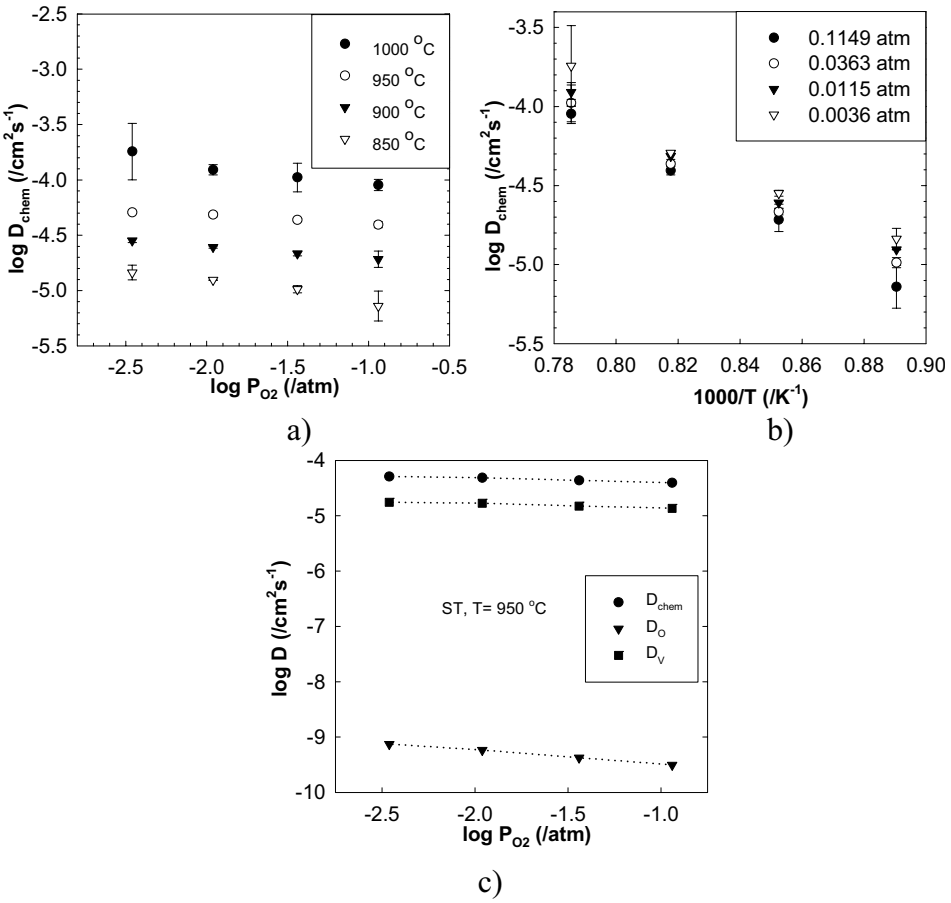

Fig. 6. D_{chem} for $SrTiO_3$ plotted versus a) P_{O2} ,b) Temperature and c) D_O, D_V and D_{chem} plotted versus P_{O2} at 950 °C.

From Fig 6a it can be seen that the D_{chem} parameter increases with decreasing P_{O2} following a dependency of $\sim P_{O2}^{-0.14\pm0.05}$ in the near-air oxygen partial pressures for all examined temperatures. The absolute value of D_{chem} fits well with values from Tragut and Härdtl [25]. The latter work does, however, not provide any values for the oxygen partial pressures under which the measurements were performed.

From Fig 6b it can be seen that the temperature dependency for D_{chem} is almost the same regardless of the mean oxygen partial pressure. This gives an activation energy for D_{chem} of 187 ± 17 kJ/mol. This value is in good agreement with data reported by Müller and Härdtl [17] who obtained an activation energy of ~190 kJ/mol for D_{chem} in the same temperature interval.

Schwarz et al. [49] measured the oxygen nonstoichiometry in $SrTiO_3$ to follow a $\delta \quad P_{O2}^{-0.17}$ dependency at 954 °C. From these oxygen nonstoichiometry values thermodynamic factors for oxygen ions, W_O, and vacancies, W_V, can be calculated, and thus enable the calculation of the component diffusion coefficient D_O and vacancy diffusion coefficient D_V for $SrTiO_3$ at 950 °C according to Eq. (14) ($W_O \sim 10^5$ and $W_V \sim 3$). The values for D_O and D_V in $SrTiO_3$ are given in Fig 6c. Both the oxygen component diffusion coefficient and vacancy diffusion coefficient from this plot agree with those obtained by Schwarz and Anderson [21]. It has been shown earlier [37] that the thermodynamic factors for ions and vacancies, W_O and W_V, have a temperature dependence, and thus contribute to an apparent activation energy. Hence, the activation energy for the component and vacancy diffusion coefficients, D_O and D_V respectively, will not be equal to the one for chemical diffusion. However, since oxygen nonstoichiometry data are available at only one temperature, the activation energies for D_O and D_V cannot be obtained.

The diffusion coefficient D_{chem} obtained from experiments in O_2/N_2 mixtures for STA-02 is given in Fig 7a versus P_{O2} and in Fig 7b versus temperature.

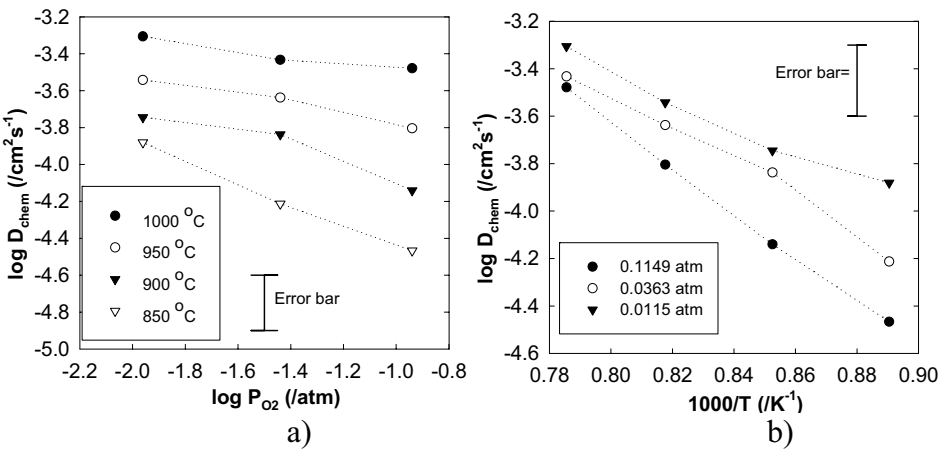

Fig. 7. Average values of D_{chem} for $SrTi_{0.98}Al_{0.02}O_3$ plotted versus a) P_{O2} and b) Temperature. The standard deviation for D_{chem} in each plot is between 0.10 and 0.20 (log_{10} scale), shown as an example error bar in the figures. Lines are guide to the eye.

In Fig 7a) it can be seen that the P_{O2} dependency for the D_{chem} for STA-02 is stronger than compared with ST. It can also be seen that the P_{O2} dependency is less pronounced with increasing temperature. By assuming a constant D_V

at a given temperature, this can be discussed in terms of the thermodynamic factor for vacancies W_V and its variation with P_{O2}. The P_{O2} dependency of W_V becomes less pronounced with increasing temperature and thus increased concentration of oxygen vacancies, thus the P_{O2} dependency for W_V will give the P_{O2} dependency for D_{chem}.

In Fig 7b) the D_{chem} for STA-02 is plotted versus temperature. It can be seen that the activation energy for D_{chem} increases with P_{O2}, varying from 104 ± 22 kJ/mol to 180 ± 20 kJ/mol at the highest P_{O2}. The same behaviour for the activation energy has also been observed for $La_{0.9}Sr_{0.1}FeO_3$ by Wærnhus et al. [36], with an increasing activation energy with increasing P_{O2}. In both materials this is consistent with the introduction of more oxygen vacancies when decreasing the P_{O2} or introducing an aliovalent cation, and a decrease in the activation energy is expected. In comparison to the ST-composition the activation energy for D_{chem} in STA-02 is lower than in the ST, and the same was observed in $LaFeO_3$ / $La_{0.9}Sr_{0.1}FeO_3$ by Wærnhus [36].

In Fig 8 D_{chem} values for ST and STA-02 are given at 1000 °C along with data for undoped [29] and 1.8 % Al-doped [32] $BaTiO_3$ and $CaTiO_3$ [51].

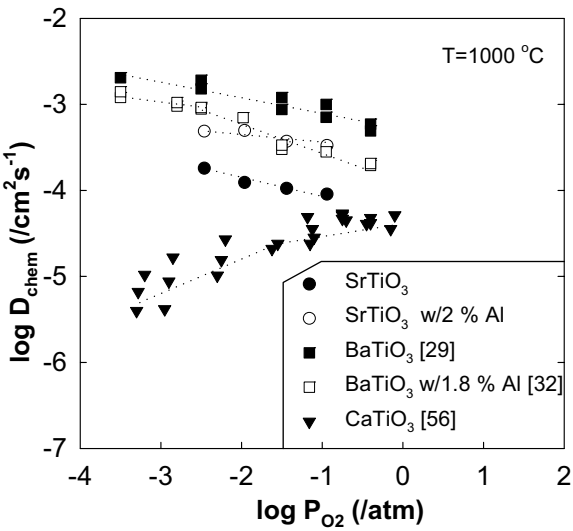

Fig. 8. Comparison plot of D_{chem} at 1000 °C in ST and STA-02, compared with values of un-doped [29] and 1.8 % doped [32] $BaTiO_3$ and $CaTiO_3$ [51]. Lines in the plot serve as guides to the eye.

By comparing the absolute values for D_{chem} for STA-02 and ST it can be seen that the introduction of 2 % Al increases D_{chem} with about half an order of magnitude. For $BaTiO_{3-\delta}$ [29,32] the reverse trend is observed, decreasing

D_{chem} while introducing Al. The reason for the decreasing behaviour has not been discussed by the authors [29,32].

In Fig 8 it can be seen that D_{chem} for the undoped alkaline earth titanates increases with increasing atomic number: $CaTiO_3 < SrTiO_3 < BaTiO_3$. The oxygen vacancy concentration is expected to decrease in the same order at fixed temperatures and P_{O2}´s. This is because the basicity increase with atomic number [52] and thus stabilises the 4-valent Ti and the vacancy concentration decreases. Thus, for a given change in partial pressure at a given temperature the change in oxygen stoichiometry, $\Delta\delta$, should decrease with increasing basisity, while the corresponding thermodynamic factor for vacancies should increase since it is inversely proportional with the vacancy concentration as seen in Eq. (19)

$$W_V = -\frac{1}{2}\frac{\partial \ln P_{O_2}}{\partial \ln C_V} \tag{19}$$

Thus, assuming the D_V to be almost the same for the three compositions, the D_{chem} should increase with increasing atomic number Ca < Sr < Ba in accordance with Eq (19).

Even though the materials in Fig 8 show high values for D_{chem}, the flux through these materials in an oxygen partial pressure gradient will not be very high. This is due to the inherent small variation in oxygen nonstoichiometry with P_{O2} for these materials. Thus, the concentration gradient will be small, as will the flux according to Fick's law of diffusion.

Surface exchange of oxygen

In Fig 9, average chemical surface exchange coefficients from oxidation and reduction experiments are plotted for STA-02 versus oxygen partial pressure at 1000 °C. At temperatures below 1000 °C, the determination of k_{chem} resulted in a mixture of converging and non-converging parameters in the iterations in the numerical procedure. The converging parameters were also highly scattered, hence, no exchange data below 1000 °C are reported.

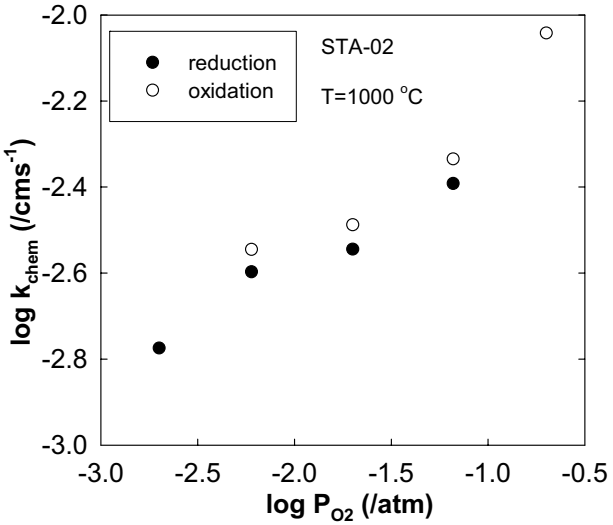

Fig. 9. Values for k_{chem} in STA-02 plotted versus oxygen partial pressure at 1000 °C

The k_{chem} from reduction is proportional with $P_{O2}^{0.24\pm0.05}$, while from oxidation the proportionality is $P_{O2}^{0.19\pm0.06}$. These proportionalities are smaller than those reported by Merkle and Maier [33], who reported $k_{chem} \propto P_{O2}^{0.33}$ for $SrTiO_3$ with ~3 ‰ Fe for both oxidation and reduction runs. These measurements were also performed at temperatures between 650 and 730 °C, giving quite different conditions compared with this work.

In Fig 10, the chemical surface exchange coefficients from oxidation and reduction experiments are plotted for STA-05 versus oxygen partial pressure and inverse temperature, respectively.

In Fig 10a and 10b values for k_{chem} versus P_{O2} originating from reduction and oxidation are plotted. The P_{O2} dependency for k_{chem} follows a $k_{chem} \propto P_{O2}^{n}$ for both oxidation and reduction. For the reduction n is between 0.09 and 0.13, while for the oxidation n ranges between 0.14 and 0.23. In both cases n increases with temperature. The dependency was slightly higher in STA-02, thus adding Al seemingly gives a smaller P_{O2} dependency.

In Fig 10c and 10d values for k_{chem} versus temperature originating from reduction and oxidation are plotted. The apparent, average activation energies for k_{chem} from the reduction are between 80 and 100 kJ/mol, and

for oxidation between 90 and 114 kJ/mol. Schlüter et al. [26] measured the activation energy for k_{chem} to 60 ± 20 kJ/mol for 0.22 % Fe doped $SrTiO_3$ at temperatures below ~840 °C.

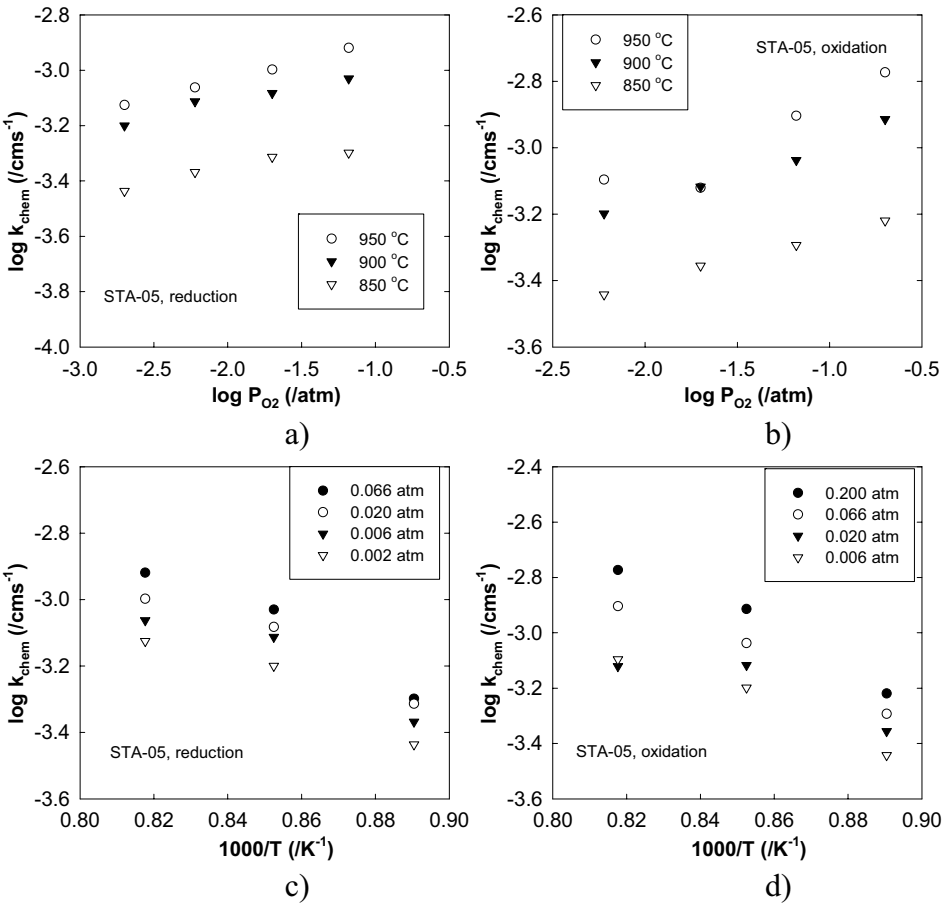

Fig. 10. Values for k_{chem} in STA-05 plotted versus oxygen partial pressure in a) from reduction, b) from oxidation, and versus temperature in c) from reduction and d) from oxidation.

Values for k_{chem} in ST could not be obtained, due to non-converging coefficients.

Comparison between different material systems

In an earlier work [37,38] the transport properties of $La_{1-x}Sr_xCoO_{3-\delta}$ (x= 0, 0.2 and 0.5) was investigated with electrical conductivity relaxation. This

system has metallic-type of electrical conductivity (~1000 S/cm) at elevated temperatures, and also high concentrations of oxygen vacancies [53], except for pure $LaCoO_3$ [54]. In $SrTiO_3$, pure and Al substituted, the conductivity is ~0.01 S/cm, i.e. a difference of 5 orders of magnitude at elevated temperatures, and a concentration of oxygen vacancies which is much lower than for the lanthanum coboltite system.

For both of the non-substituted materials, $LaCoO_3$ and $SrTiO_3$, there were problems with non-converging values for k_{chem}, while values for D_{chem} converged. For $LaCoO_3$, values of k_{chem} were only obtained at oxygen partial pressures below 0.02 atm [37], while no data for k_{chem} were obtained for $SrTiO_3$.

This can be discussed in light of Eq. (18). From this work and others [36,37,38], it has been established that D_{chem} increases with decreasing P_{O2}, while k_{chem} increases with P_{O2}. Thus the value L_α given in Eq. (18) will increase with increasing P_{O2}, since the P_{O2} dependency is more pronounced for k_{chem} than for D_{chem}. This means that at high P_{O2} the value of L_α will be large and only D_{chem} can be determined from experiment. Similarly at very low P_{O2}'s L_α is low and only k_{chem} can be determined. Furthermore, there is a medium P_{O2} range where both coefficients can be determined. The extent of this range for L_α where both parameters are obtainable, depends on the material, as reported for $LaCoO_3$ [37] and $SrTiO_3$ materials, that is, due to the ratio between D_{chem} and k_{chem}.

For materials where aliovalent substitutions are introduced, values for k_{chem} are reported for many compositions. Values for k_{chem} in the materials Al-doped $SrTiO_3$ (this work), Sr in $LaFeO_3$ [36], Sr in $LaCoO_{3-\delta}$ [37,38] and Al in $BaTiO_3$ [35] have been measured with electrical conductivity relaxation. k_{chem} for these materials at 1000 °C are given in Fig 11a. All materials included in Fig 11a show p-type conductivity in the given oxygen partial pressure interval.

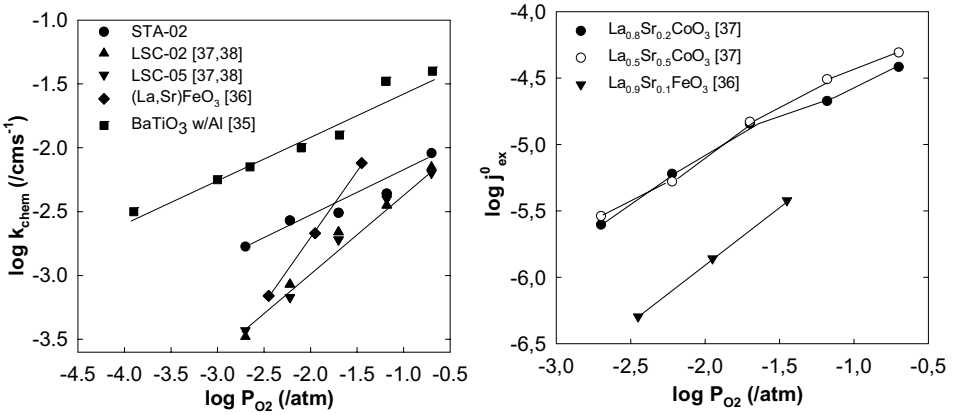

a) b)

Fig. 11. a) Literature data for k_{chem} at 1000 °C. STA-02 is taken from this work. LSC-02 and LSC-05 correspond to the compositions $La_{0.8}Sr_{0.2}CoO_{3-\delta}$ and $La_{0.5}Sr_{0.5}CoO_{3-\delta}$ [37,38]. Data for $La_{0.9}Sr_{0.1}FeO_3$ is taken from [36] while 1.8 % Al doped $BaTiO_3$ is taken from [35]. b) Calculated equilibrium flux j^0_{ex} for $La_{0.8}Sr_{0.2}CoO_{3-\delta}$ and $La_{0.5}Sr_{0.5}CoO_{3-\delta}$ [37] and $La_{0.9}Sr_{0.1}FeO_3$ [36]. Lines are guide to the eye.

From Fig 11a it can be seen that the k_{chem} only varies with about 1 order of magnitude between the materials reported. The electrical conductivity of the materials ranges from ~10^{-2} S/cm for $BaTiO_3$ [32,35] and $SrTiO_3$ (this work), via 10^{-1} S/cm for the $La_{0.9}Sr_{0.1}FeO_3$ [36] to 1000 S/cm for Sr in $LaCoO_{3-\delta}$ [37,38], that is, at least 5 orders of magnitude. Fig. 11a indicates that materials with the highest electrical conductivity result in the lowest k_{chem} values at 1000 °C (e.g. Sr-doped $LaCoO_3$). These materials also exhibit the highest oxygen nonstoichiometry, δ and the most pronounced P_{O2} dependency for k_{chem}. The material with the lowest electrical conductivity and the expected lowest oxygen nonstoichiometry is the material with the highest values for k_{chem}, and k_{chem} for that material has the least pronounced P_{O2} dependency. This can be seen in light of the previous discussion; it seems that the k_{chem} will be relatively much higher than the D_{chem} in materials with small oxygen vacancy concentrations. This incomplete discussion also emphasize the need for the thermodynamic factors, which would enable us to discuss more fundamental transport coefficients such as D_o, D_v and k_o.

In an earlier work [38] a comparison of the values of the surface exchange coefficient k_0, in the materials $La_{1-x}Sr_xFeO_3$ and $La_{1-x}Sr_xCoO_3$ at (almost) equal P_{O2} has been examined between 850-1000 °C. It was seen that k_0 increased with increasing Sr content, and thus more oxygen vacancies, over

the whole examined temperature interval. The k_0 was also higher in the coboltites than in the ferrite system. In this work an analytical expression for k_0 was put forward, proposing k_0 proportional with the oxygen vacancy concentration.

k_0 and k_{chem} are related via the thermodynamic factor for oxygen ions, W_O, and given in Eq. (17)

$$k_{chem} = W_O k_0 \tag{20}$$

From the observations in Fig 11a) and earlier work [38] it can be seen that between the compared materials it is the $La_{1-x}Sr_xFeO_3$ that has the highest k_{chem} and smallest k_0 and vice versa for $La_{1-x}Sr_xCoO_3$. Thus it seems that W_O is the main contributor to the high k_{chem} values. Generally, the more stable a compound is, the smaller the change in oxygen vacancy concentration (and thus the same for the oxygen ion concentration) will be at a given step in P_{O2} and thus a higher W_O (Eq. (14)). Calculations of W_O for $La_{1-x}Sr_xFeO_3$ [36,47] show that W_O is higher in the ferrites than in the $La_{1-x}Sr_xCoO_3$ system [37]. This generalisation can also be applied to the even more stable compounds $BaTiO_3$ and $SrTiO_3$, where high values of k_{chem} are measured, but due to the low oxygen vacancy concentration, low values of k_0 and thus for j^0_{ex} are expected.

In Fig 11b) the equilibrium surface exchange flux j^0_{ex} (Eq. (17)) is calculated for $La_{0.8}Sr_{0.2}CoO_{3-\delta}$, $La_{0.5}Sr_{0.5}CoO_{3-\delta}$ [37] and $La_{0.9}Sr_{0.1}FeO_3$ [36], and it can be seen that the highest equilibrium exchange flux, j^0_{ex}, corresponds to the materials with the highest oxygen nonstoichiometry.

CONCLUSION

The equilibrium electrical conductivities were measured in O_2/N_2 - and CO/CO_2- mixtures. For the $SrTiO_3$ composition the conductivity changed corresponding to theoretical derivations. For $SrTiO_3$ with 2 and 5 % Al a simple defect model could explain the conductivity behaviour at low and high P_{O2}'s, while deviations were observed at medium P_{O2}'s. The deviation may be due to phase separation involving precipitation of a Al-rich phase.

D_{chem} for ST and STA-02 and k_{chem} for STA-02 and STA-05 are reported. Additionally, values for the component diffusion coefficient, D_O, and the vacancy diffusion coefficient, D_V, are reported at 950 °C, where oxygen vacancy concentrations are provided from the literature. The values for the diffusion coefficients and the corresponding activation energies are in good agreement with literature. Values for k_{chem} in STA-02 and STA-05 are reported, and show pronounced P_{O2} dependencies. The activation energy could only be calculated for STA-05 , giving 90-105 kJ/mol, due to the large scattering of k_{chem} in STA-02.

Literature studies of the chemical diffusion coefficients indicates that D_{chem} increases with increasing atom-number in the series of $CaTiO_3$, $SrTiO_3$ and $BaTiO_3$.

Literature studies also indicates that materials with low oxygen vacancy concentrations exhibit larger values for k_{chem} than those with high vacancy concentrations. The equilibrium oxygen exchange coefficient, k_0, increase with increasing oxygen nonstoichiometry which suggests that the oxygen vacancy concentration plays a major role in the surface exchange of oxygen.

ACKNOWLEDGEMENTS

Norsk Hydro ASA is acknowledged for financial support to the experimental work.

REFERENCES

1. De Souza, R.A., Fleig, J., Merkle, R. and Maier, J., "$SrTiO_3$: a model electroceramic", Z.Metallkd. 94, No.3, (2003), 218-225.
2. Claus, J., Leonhardt, M. and Maier, J., "Tracer diffusion and chemical diffusion in acceptor doped $SrTiO_3$", J.Phys.Chem.Solids 61, (2000), 1199-1207.
3. Leonhardt, M., De Souza, R.A., Claus, J. and Maier, J., "Surface kinetics of oxygen incorporation into $SrTiO_3$", J. Electrochem Soc. 146, No.2, (2002), J19-J26.
4. A search for $SrTiO_3$ as a keyword on the ISI Web of Knowledge, http://isiknowledge.com in Dec 2004, resulted in more than 7000 hits.
5. Cocco, A. and Massazza,F., Ann.Chim. (Rome), 53, (1963), 892. *Reprinted in* : Levin, E.M., Robbins, C.R. and McMurdie,H.F., " Phase diagrams for ceramists", American ceramic society, Columbus (1964), Supplement Fig no 2334.
6. Maier J., Scwitzgebel, G. and Hagemann, H.-J., "Electrochemical investigations of conductivity and chemical diffusion in pure and doped cubic $SrTiO_3$ and $BaTiO_3$", J.Solid State Chem 58, (1985), 1-13.
7. Walters, L.C. and Grace, R.E., "Formation of point defects in Strontium titanate", J.Phys.Chem.Solids 28, (1967), 239-244.
8. Chan, N.-H., Sharma, R.K. and Smyth, D.M., "Nonstoichiometry in $SrTiO_3$", J.Electrochem Soc 128, No. 8, (1981), 1762-1769.
9. Eror, N.G. and Balachandran, U., "High-Temperature defect structure of acceptor doped strontium titanate", J.Am.Ceram.Soc. 65, No. 9, (1982), 426-431.
10. Waser, R., "Bulk conductivity and defect chemistry of acceptor doped strontium titanate in the quenched state", J.Am.Ceram.Soc. 74, No. 8, (1991), 1934-1940.
11. Choi, G.M. and Tuller, H., Defect structure and electrical properties of Single crystal $Ba_{0.03}Sr_{0.97}TiO_3$, J.Am.Ceram.Soc. 71, No. 4, (1988), 201-205.
12. Moos, R. and Härdtl, K.H., "Defect chemistry of donor doped and undoped Strontium titanate ceramics between 1000° and 1400 °C, J.Am.Ceram.Soc., 80, No. 10, (1997), 2549-62.
13. Denk, I., Münch, W. and Maier, J., "Partial conductivities in $SrTiO_3$: Bulk Polarization experiments, oxygen concentration cell measurements, and defect-chemical modelling", J.Am.Ceram.Soc. 78, No. 12, (1995), 3265-3272.
14. Maier, J., "Physical chemistry of ionic materials: Ions and electrons in solids", John Wiley & Sons (2004).

15. Maier, J., “On the correlation of macroscopic and microscopic rate constants in solid state chemistry”, Solid State Ionics 112 (1998), 197-228.
16. Maier, J., “Interaction of oxygen with oxides: How to interpret measured effective rate constants?”, Solid State Ionics 135 (2000), 575-588.
17. Müller, A. and Härdtl, K.H., ”Ambipolar diffusion phenomenain $BaTiO_3$ and $SrTiO_3$”, Apll.Phys. A, 49, (1989), 75-82.
18. van der Haar, L.M., den Otter, M.W., Morskate, M., Bouwmeester, H.J.M. and Verweij, H., “Chemical diffusion and oxygen surface transfer of $La_{1-x}Sr_xCoO_{3-\delta}$ studied with electrical conductivity relaxation”, J.Electrochem.Soc. 149, No.3, (2002),J41-J46.
19. Walters, L.C. and Grace, R.E, “Diffusion of point defects in strontium titanate”, J.Phys.Chem.Solids, 28, (1967), 245-248.
20. Paladino, A.E., “Oxidation kinetics of single-crystal $SrTiO_3$”, J.Am.Ceram.Soc 48, No. 9, (1965), 476-478.
21. Schwarz, D.B. and Anderson, H.U., “Determination of oxygen chemical diffusion coefficients in single crystal $SrTiO_3$ by capacitance manometry”, J.Electrochem.Soc 122, No. 5, (1975), 707-710.
22. Noll, F., Münch, W., Denk, I. and Maier, J., “ $SrTiO_3$ as a prototype of a mixed conductor: Conductivities, oxygen diffusion and boundary effects”, Solid State Ionics 86-88, (1996), 711-717.
23. Bieger, T., Maier, J. and Waser, R., “Optical investigation of oxygen incorporation in $SrTiO_3$”, Solid State Ionics 53-56, (1992), 578-582.
24. Bieger, T., Maier, J. and Waser, R., “Kinetics of oxygen incorporation in $SrTiO_3$: An optical investigation”, Sens.Act. B, 7, (1992), 763-768.
25. Tragut, Ch., Härdtl, K.H., “Kinetic behaviour of resistive oxygen sensors”, Sens.Act. B, 4, (1991), 425-429.
26. Schlüter, H.-J., Barsoum, M. and Maier, J., “Kinetic studies of oxygen incorporation in $SrTiO_3$ by permation experiments, Solid State Ionics 101-103, (1997), 509-515.
27. Widerø, M., Munch, W., Larring, Y. and Norby, T., “Proton and apparent hydride ion conduction in Al-substituted $SrTiO_3$”, Solid State Ionics 154-155, (2002), 669-677.
28. Bouwmeester, H.J.M. and Burggraaf, A.J. in “Dense Ceramic Membranes for oxygen separation” in “The CRC Handbook of the Solid State Electrochemistry”, P.J. Gellings and H.J.M. Bouwmeester Eds., CRC Press Inc., (1997).
29. Song, C.-R. and Yoo, H.-I., “Chemical diffusivity of $BaTiO_{3-\delta}$: I: Experimental determination”, Solid State Ionics 120, (1999), 141-153.
30. Song, C.-R. and Yoo, H.-I., “Chemical diffusivity of $BaTiO_{3-\delta}$: II Defect chemical analysis”, Phys.Rev. B. 61, No. 6, (2000), 3975-3982.

31. Song, C.-R. and Yoo, H.-I., "Chemical diffusivity of $BaTiO_{3-\delta}$: III Conductivity-nonstoichiometry (δ) correlation in a mixed n/p regime", Solid State Ionics 124, (1999), 289-299.
32. Song, C.-R. and Yoo, H.-I., "Chemical diffusivity of $BaTiO_{3-\delta}$: IV Acceptor doped case", J.Am.Ceram.Soc. 83, No.4, (2000), 773-779.
33. Merkle, R. and Maier, J., "Oxygen incorporation into Fe-doped $SrTiO_3$: Mechanistic interpretation of the surface reaction", Phys.Chem.Chem.Phys 4, (2002), 4140-4148.
34. Denk, I., Noll, F. and Maier, J., "*In situ* profiles of oxygen diffusion in $SrTiO_3$: Bulk behaviour and boundary effects", J.Am.Ceram.Soc 80, No. 2, (1997), 279-285.
35. Yoo, H.I., Song, C.-R., Lee, Y.-S. and Lee, D.-K., "Surface reaction kinetics in oxygen nonstoichiometry re-equilibration of $BaTiO_{3-\delta}$", Solid State Ionics 160, (2003), 381-387.
36. Wærnhus, I.," Defect Chemistry, Conductivity and mass transport properties of $La_{1-x}Sr_xFeO_{3-\delta}$ (x=0 and 0.1)" , Thesis, Norwegian University of Science and Technology, (2003).
37. Watterud, G., Wiik, K. and Julsrud, S., "Oxygen transport in $La_{1-x}Sr_xCoO_{3-\delta}$ (x=0, 0.2 and 0.5) assessed with electrical conductivity relaxation. Part I: Bulk Diffusion and k_{chem}". Part I of this thesis.
38. Watterud, G., Wiik, K. and Julsrud, S., "Oxygen Transport in $La_{1-x}Sr_xCoO_{3-\delta}$ (x=0, 0.2 and 0.5) assessed with electrical conductivity relaxation. Part II: The mechanisms of oxygen surface exchange." Part II of this thesis
39. Watterud, G., Wiik, K. and Julsrud, S., "Oxygen Transport in pure and Al doped $SrTiO_3$ measured with electrical conductivity relaxation. Part II: in CO/CO_2 mixtures". Part IV of this thesis.
40. Kröger, F.A., "The chemistry of inperfect crystals Vol. 2.", North-Holland Pub. (1974).
41. Schmalzried, H. , "Solid State reactions", Academic Press Inc., (1974).
42. Weppner, W. and Huggins, R.A., "Determination of the kinetic parameters of mixed conducting electrodes and application to the system Li_3Sb", J. Electrochem.Soc. 124, No. 10, (1977), 1569-1578.
43. Bouwmeester, H.J.M., Kruidhof, H. and Burggraaf, A.J., "Importance of the surface exchange kinetics as rate limiting step in oxygen permeation through mixed-conducting oxides", Solid State Ionics 72, (1994), 185-194.
44. Prigogine, I., "Thermodynamics of irreversible processes", 2nd Ed., John Wiley & Sons, (1961).
45. Howard, S.A., Yau, J.K. and Anderson, H.U., "Structural characterisation of $Sr_{1-x}La_xTiO_{3\pm\delta}$ as a function og oxygen partial pressure at 1400 °C", J.Appl.Phys, 65, (1989), p. 1492.

46. German, R.M., “Sintering theory and practice”, J.Wiley & Sons, (1996), Chap 3.
47. ten Elshof, J.E., Lankhorst, M.H.R. and Bouwmeester, H.J.M, “ Oxygen exchange and diffusion coefficients of strontium doped lanthanum ferrites by electrical conductivity relaxation”, J.Electrochem.Soc. 144, No. 3, (1997), 1060-1067.
48. Hansen, J.R., Poulsen, F.W. and Hendriksen, P.V., “Determination of oxygen diffusion coefficients by conductivity relaxation”, Proc. 6th Eur. Ceram. Soc. Conf., (1999)
49. Schwarz, D.B., Conger, G.J. and Anderson, H.U., “Measurements of nonstoichiometry in $SrTiO_3$ and $BaTiO_3$”, Proc. of the Intl. Conf. on Sr Containing Compounds, p. 161, ed. T.J. Gray, Nat. Res. Council, Ottawa, Canada (1973).
50. den Otter, M.W., Bouwmeester, H.J.M, Boukamp, B.A. and Verweij, H., “Reactor flush time correction in relaxation experiments”, J.Electrochem.Soc. 148, (2001), J1.
51. Bak, T., Nowothy, J. and Sorrel, C.C., “Chemical diffusion in calcium titanate”, J.Phys.Chem.Solids 65, (2004), 1229-1241.
52. Huheey, J.E., Keiter, E.A. and Keiter, R.L., “Inorganic chemistry: Principles of structure and reactivity”, 4th Ed., HarperCollins College Publishers, (1993)
53. Mizusaki, J.,Tabuchi, J.,Matsuura, T., Yamauchi, S. and Fueki, K., “Electrical conductivity and Seebeck coefficient of nonstoichiometric $La_{1-x}Sr_xCoO_{3-\delta}$”, J. Eletrochem. Soc. 144, No.7, (1989), 2082-2088
54. Seppännen , M., Kytö, M., and Taskinen, P., “Defect structure and nonstoichiometry of $LaCoO_3$”, Scand.J.Metallurgy 9, (1980), 3-11.

OXYGEN TRANSPORT IN PURE AND Al-DOPED $SrTiO_3$ MEASURED WITH ELECTRICAL CONDUCTIVITY RELAXATION. Part II: In CO/CO_2 mixtures

Geir Watterud[a], Stein Julsrud[b] and K. Wiik[*a],
[a]Department of Materials Science and Engineering
Norwegian University of Science and Technology
N-7491 Trondheim, Norway.
[b]Scanwafer AS, N-3907 Porsgrunn, Norway

ABSTRACT

Chemical oxygen transport coefficients (D_{chem} and k_{chem}) have been measured for $SrTi_{1-x}Al_xO_3$ (ST: x=0, STA-02: x=0.02 and STA-05: x=0.05) by means of electrical conductivity relaxation experiments. Measurements have been done in CO/CO_2-mixtures at temperatures between 850 and 1000°C.

D_{chem} are reported for ST and STA-02 while k_{chem} are reported for ST, STA-02 and STA-05. The D_{chem} showed a P_{O2}-dependency, which can be explained by the variation in the thermodynamic factors. The introduction of Al in the sample increases the value of D_{chem}, probably due to the introduction of more oxygen vacancies. STA-02 showed a discrete step in D_{chem} in CO-rich atmospheres. This may be due to a phase transition at P_{O2} $\sim 10^{-17}$ atm.

The k_{chem} showed a maximum at $P_{CO}/P_{CO2} = 1$ for STA-02 and STA-05. This behaviour corresponds well with a rate controlling reaction involving a charged and adsorbed CO_2 molecule. The same maximum is also seen in $BaTiO_3$ (literature) undoped and substituted with 1.8 % Al.

Both $SrTiO_3$ and $BaTiO_3$ (literature) show a decreasing k_{chem} with increasing substitution level of Al, probably due to a decreasing thermodynamic factor.

Corresponding author: Kjell Wiik, Department of Chemistry, Norwegian University of Science and Technology, N-7491 Trondheim, Norway, e-mail: kjell.wiik@material.ntnu.no, Telephone no.: +47 73 59 40 82, fax no:+47 73 59 08 60

Keywords:
$SrTiO_3$, Pure and Al-substituted, Electrical conductivity relaxation, CO/CO_2 mixtures, Rate determining step, D_{chem}, k_{chem}

INTRODUCTION

In Part I of this work [1], a more general introduction to the electrical and ionic (oxygen) transport properties, including solid state diffusion and surface exchange, of $SrTiO_3$ was given. These properties make $SrTiO_3$ an important mixed-conducting electroceramic for various applications [2], and it also serve as an excellent model material for studying defect chemistry, diffusion in perovskites and mixed conductors [3]. Strontium titanate based materials have been discussed as a candidate material for use as a sensor, photoelectrode or varistor amongst others [4].

In the literature there are only a few works that are related to $SrTiO_3$ in mixtures of CO/CO_2, most of these are mainly concerned with defect modelling based on conductivity measurements, e.g. [5,6]. No data on diffusion or surface exchange for $SrTiO_3$ in mixtures of CO/CO_2 have been found in the literature. However, Walters and Grace [7] reported data for the oxygen vacancy diffusion coefficient, D_V, obtained by conductivity relaxation in H_2/H_2O mixtures and temperatures between 900 and 1200°C, that is, at even lower P_{O2}´s than obtained in CO/CO_2-mixtures. None of the works [5,6,7] reported any decomposition of materials used in the experiments. Thus, the $SrTiO_3$ material is believed to be stable in the range of temperature and P_{O2} used in the present work.

Song and Yoo [8-11] have examined the chemical diffusivity in pure and Al-doped $BaTiO_{3-\delta}$ with electrical conductivity relaxation in mixtures of CO/CO_2. With the introduction of Al in the $BaTiO_3$ structure, they reported a small increase in the electrical conductivity, as opposed to the results presented in Part I of this work [1] where the conductivity was found to decrease when Ti in $SrTiO_3$ was substituted with Al. The values for D_{chem} in both pure and Al-doped $BaTiO_{3-\delta}$ showed an increase with increasing P_{O2}, i.e. increasing P_{CO2}.

There are no literature data for the surface exchange coefficient in Al-substituted $SrTiO_3$. Yoo et al. [12] have studied the chemical surface exchange coefficient (and diffusion) for both pure $BaTiO_3$ and $BaTiO_3$ substituted with 1.8 mol % Al. In the CO/CO_2 mixtures k_{chem} seemingly reaches its maximum value at $P_{CO} = P_{CO2}$. This behaviour was also reported by Wærnhus et al. [13] in the system $LaFeO_3$ doped with Sr. By modelling the oxygen incorporation assuming CO_2 as the main oxygen supplier, the behaviour was rationalised by assuming a rate-determining step consisting of the dissociation of a charged adsorbed CO_2 molecule.

In a previous work [14,15], the oxygen diffusion and surface exchange coefficients have been measured for Sr doped lanthanum coboltites. As opposed to strontium titanate the lanthanum coboltites exhibit both a high electronic conductivity (metallic) and a high population of oxygen vacancies.

THEORY

The defect model for $SrTiO_3$, was given in Part I of this work [1]. A more thorough review of the solid state diffusion parameters and surface exchange parameters and their relations are given elsewhere [1,14,15].

EXPERIMENTAL

Polycrystalline samples with composition $SrTiO_3$ (ST), $Sr_{0.98}Al_{0.02}TiO_3$ (STA-02) and $Sr_{0.95}Al_{0.05}TiO_3$ (STA-05) were prepared by a solid state route, details are given elsewhere [1].

Oxygen surface exchange and diffusion were measured by the electrical conductivity relaxation technique, described in a previous work [14]. The measurements were carried out in the temperature interval between 850-1000 °C, where the samples have been held at experimental temperatures for time periods of about four to six weeks, including the experiments performed in O_2/N_2 mixtures [1].

The oxygen partial pressures used in these experiments were controlled by mixtures of CO diluted in CO_2 and CO_2 diluted in CO, respectively. By regulating the flow ratios between the two gases, the different oxygen partial pressures were defined. The diluted gas component could be varied in the range from 0.20 to 0.002 atm, corresponding to two different P_{O2} regimes. A schematic drawing of the P_{O2}-regimes is given in Fig 1, also including a third regime corresponding to the mechanical O_2/N_2-mixtures from Part I [1]. Switching a four-way valve initialised the conductivity relaxation process, and the change in partial pressure of the diluted gas was half an order of magnitude in every relaxation. The step in CO/CO_2 corresponds to a step in oxygen partial pressure of around one order of magnitude. A more detailed description of the experimental set-up is given in Wærnhus [13].

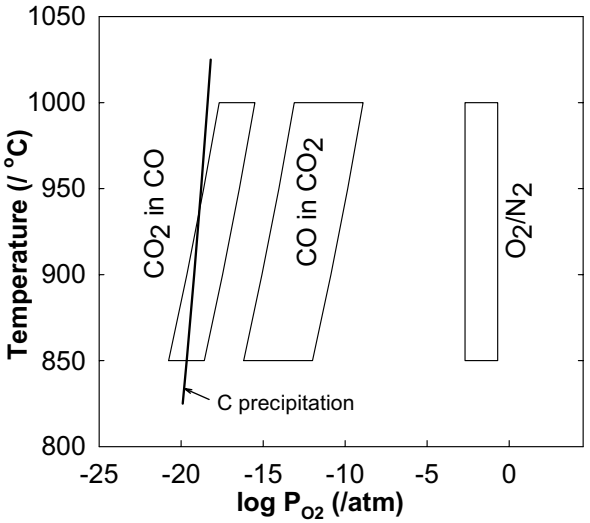

Fig. 1. Schematic drawing of the "P_{O2} window" for the conductivity relaxation measurements.

RESULTS AND DISCUSSION

As pointed out in Part I of this work [1], we were not able to establish a plausible defect chemistry model based on the electrical conductivity measurements for Al substituted $SrTiO_3$. In the absence of a defect model, we were also unable to calculate the thermodynamic factors, W_O and W_V. Although oxygen nonstoichiometry data for pure $SrTiO_3$ is given at 950 °C, they are reported only at the high oxygen partial pressures. Thus, it is not possible to calculate thermodynamic factors on the basis of nonstoichiometry in the CO/CO_2 mixtures. For this reason, the following discussion will only consider the chemical transport parameters, D_{chem} and k_{chem}, respectively.

In the calculations of the transport coefficients the same restrictions as reported in Part I [1] is applied, with respect to which coefficients were possible to calculate. Thus, in some experiments D_{chem} converged in the numerical fitting procedure while in others k_{chem} converged or both converged. For the ST-composition data for D_{chem} were obtained in the temperature interval 850 –950 °C, while data for k_{chem} were obtained at 1000 °C only. For STA-02, values for both D_{chem} and k_{chem} were obtained in the whole temperature range 850 - 1000 °C, while for STA-05 only values for k_{chem} were obtained in the interval between 900 and 1000 °C. Non

reported coefficients at certain temperatures and gas compositions are due to "non converging" values.

CO/CO_2 mixtures and bulk diffusion of oxygen, D_{chem}

In Fig. 2 D_{chem} for ST at all temperatures in CO/CO_2 gas mixtures are plotted versus the oxygen partial pressure.

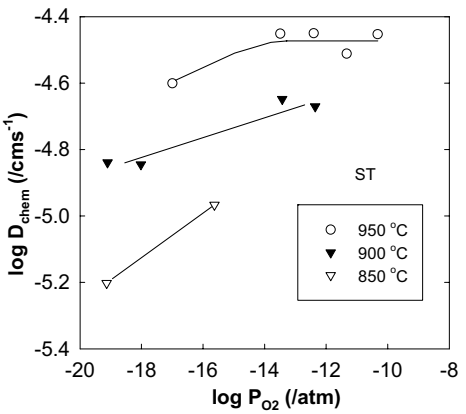

Fig. 2 D_{chem} for ST plotted versus P_{O2} at all temperatures. Solid lines serve as a guide to the eye.

D_{chem} apparently increases both with P_{O2} and temperature, corresponding to an activation energy between 72 and 129 kJ/mol.

In Fig. 3 the chemical diffusion coefficient, D_{chem}, for STA-02 at all temperatures are given as a function of P_{O2} in the CO/CO_2 gas mixture regimes.

It can be seen in Fig. 3a) that the D_{chem} varies, with a tendency to increase with increasing P_{O2}. However, the increase is seen in two different P_{O2} regimes, corresponding to a CO- and CO_2 rich atmosphere, respectively. It can also be seen that the D_{chem} increase in a discrete manner when changing from a CO_2-rich atmosphere to a CO-rich atmosphere (low P_{O2}). This sudden increase may correspond to a phase transition or phase separation at $P_{O2} \sim 10^{-17}$ atm. Obviously, further experimental activities related to $SrTiO_3$, pure and doped, should also involve phase studies in the CO/CO_2 atmospheres in order to identify whether phase transition/separation takes place.

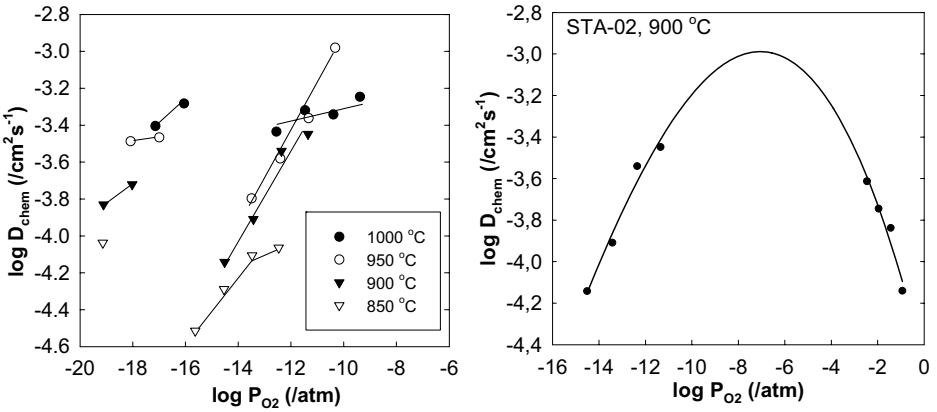

Fig. 3. a) Chemical diffusion coefficient, D_{chem}, for STA-02 measured in CO/CO_2 mixtures. Drawn lines serve as guides to the eye. b) D_{chem} for STA-02 at 900 °C in a P_{O2} interval between 1 -10^{-16} atm. Solid line corresponds to Eq. (2).

A phase transition can affect both the vacancy diffusion coefficient, D_V; and the thermodynamic factor for vacancies, W_V, and give an increase in D_{chem} according to Eq. (1) ([14]). In Eq.(1) the relations between D_{chem} and the component diffusion coefficient D_O and the vacancy diffusion coefficient D_V with their respective thermodynamic factors W_O and W_V are given.

$$D_{chem} = \left(\frac{1}{2} \frac{\partial \ln P_{O_2}}{\partial \ln C_O} \right) D_O = W_O D_O$$
$$= -\left(\frac{1}{2} \frac{\partial \ln P_{O_2}}{\partial \ln C_V} \right) D_V = W_V D_V \qquad (1)$$

We can not rule out that a change in W_v actually takes place based on the measured electrical conductivity for the STA-02 in Part I [1].

Song and Yoo [9,11] have studied the chemical diffusion in pure and 1.8 mol % Al doped $BaTiO_3$. They reported a similar trend for D_{chem} as in this work. The trend may be described as D_{chem} having its peak value at a minimum in the electrical conductivity and declining at "both sides". This behaviour is described in Eq.(2), derived in [9,11].

$$D_{chem} = \frac{D^0_{chem} t_{el}}{\cosh\left(\frac{1}{4}\ln\frac{P_{O_2}}{P^0_{O_2}}\right)} \quad (2)$$

where $P_{O2}{}^0$ is the oxygen partial pressure at the conductivity minimum, $D_{chem}{}^0$ is the corresponding chemical diffusion coefficient and t_{el} is the transport number for electrons. In Fig 3b) it can be seen that Eq. (2) describes the behaviour for D_{chem} in a large P_{O2} interval.

For STA-05 no values for D_{chem} were obtained since D_{chem} were non-converging.

CO/CO_2 mixtures and surface exchange of oxygen, k_{chem}

The chemical surface exchange coefficients, k_{chem}, are plotted against the partial pressure ratio P_{CO}/P_{CO2} for ST at 1000 °C in Fig 4. All other temperatures failed to give k_{chem} since this coefficient did not converge. For STA-02 k_{chem} data are given for temperatures between 850 and 1000°C in Fig. 5, while Fig. 6 shows k_{chem} data for STA-05 between 900 and 1000 °C.

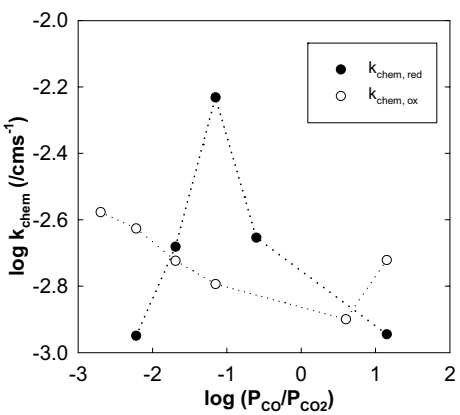

Fig. 4. k_{chem} versus P_{CO}/P_{CO2} at 1000 °C in ST. Dotted line is included as a guide to the eye.

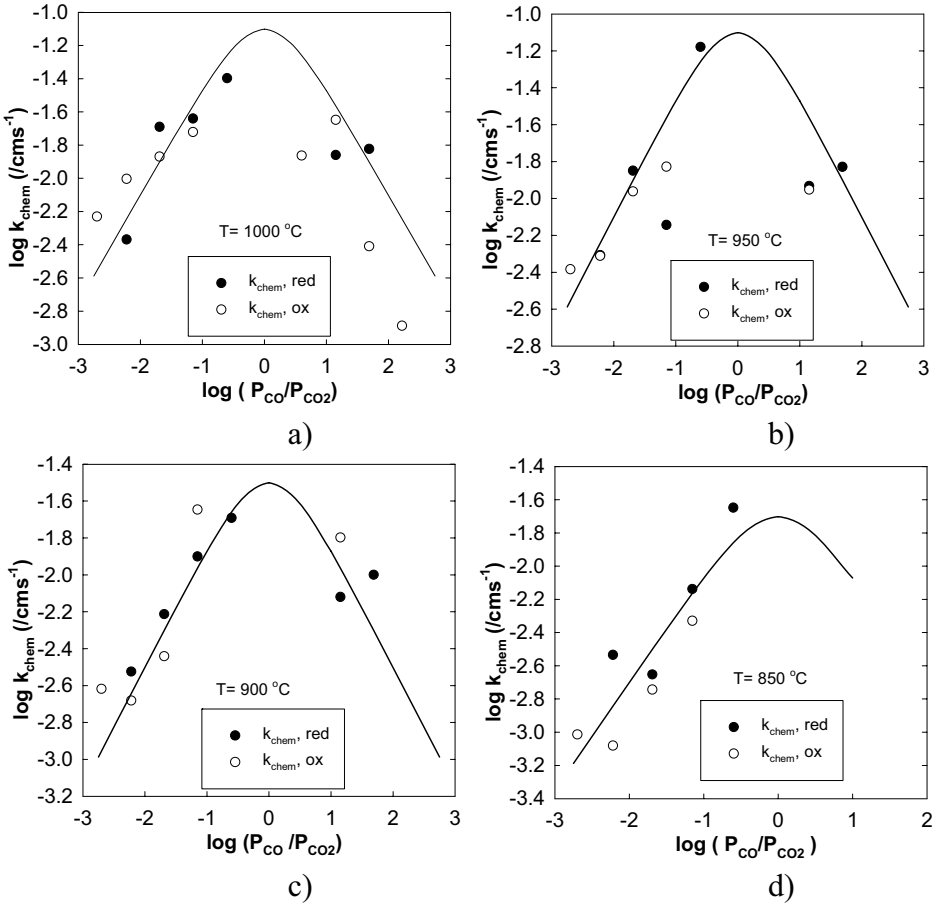

Fig. 5. Chemical surface exchange, k_{chem}, for STA–02 at a) 1000 °C, b) 950 °C, c) 900 °C and d) 850 °C. Solid lines according model proposed by Wærnhus et al. [13].

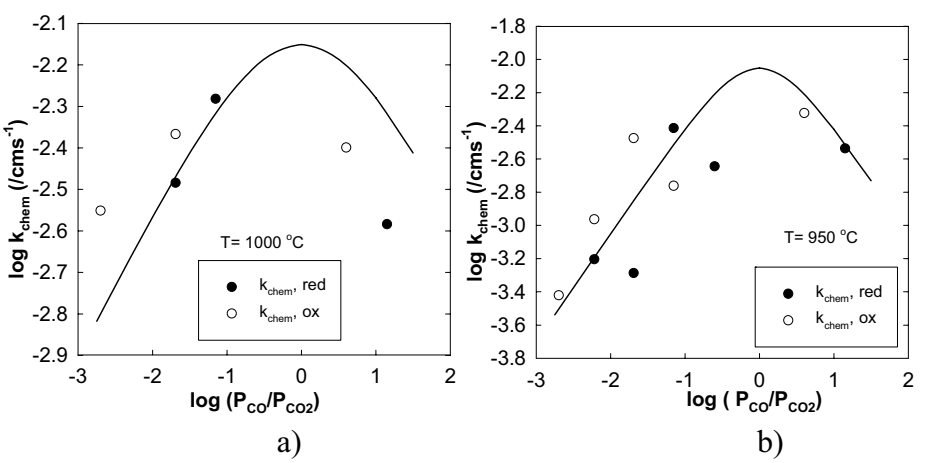

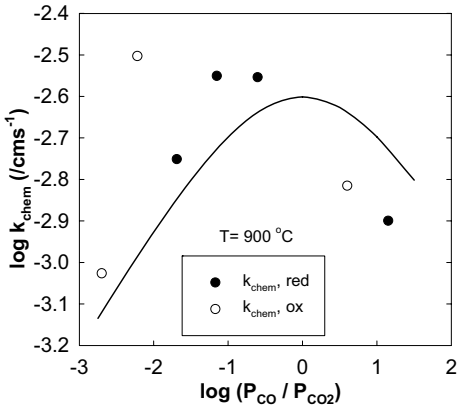

c)

Fig. 6. k_{chem} for STA-05 for a) 1000 °C, b) 950 °C and c) 900 °C .

For ST (Fig. 4) the values that originate from oxidation increases moderately with increasing P_{CO2} in the given pressure range. This can be explained by the fact that even though O_2 molecules are present in a mixture of CO/CO_2, the concentration is very low and most probably it is CO_2 that acts as the major source of oxygen to be incorporated. The value of k_{chem} is proportional to the partial pressure of CO_2, analogous to the P_{O2} dependency seen in O_2/N_2 mixtures. For the values originating from the reduction runs the behaviour is significantly different, with a peak for k_{chem} at some intermediate ratio between CO and CO_2. However, in part I [1], no values for k_{chem} for ST could be obtained at any temperature in O_2/N_2 mixtures since the k_{chem} did not converge in the numerical procedure, the same as for the temperatures below 1000 °C in the mixture of CO/CO_2. Thus, the uncertainty in the values in Fig 4 can be quite high and the apparent peak at the intermediate P_{CO}/P_{CO2} ratio could be an effect of this uncertainty.

For the k_{chem} values reported for STA-02 and STA-05 in Figs. 5 and 6 there is a trend of a maximum where the P_{CO}/P_{CO2} ratio is unity. To clarify this behaviour lines are included as guides to the eye in Figs 5 and 6.

Thus, measurements of k_{chem} for STA-02 and STA-05, and apparently for the reduction values for ST, all display similar behaviour with the P_{CO}/P_{CO2}-ratio. This behaviour for k_{chem} is consistent with observations reported by Wærnhus et al. [13], investigating oxygen surface exchange for $La_{0.9}Sr_{0.1}FeO_3$ in mixtures of CO/CO_2. They found a similar behaviour of transport across the surface in CO/CO_2 mixtures with a peak flux at P_{CO} around 0.5 atm (P_{CO}/ P_{CO2} =1).

Wærnhus et al. [13] investigated the flux in terms of possible rate determining steps and explained this maximum in the flux at $P_{CO}/P_{CO2} = 1$ probably to be due to an elementary reaction which involved the dissociation of a charged adsorbed CO_2 molecule at the surface. The similar behaviour for k_{chem} that were observed for the compositions in the present investigation (STA-02 and STA-05) might imply the same rate-determining step for these materials as in $La_{0.9}Sr_{0.1}FeO_3$. By relating k_{chem} to a set of elementary reactions, Wærnhus et al. [13] pointed out a possible rate-determining step comprising the dissociation of CO_2.

The overall incorporation of oxygen into vacancies in mixtures of CO/CO_2 can be written as

$$CO_2(g) + V_O^{\bullet\bullet} = O_O^x + 2h^{\bullet} + CO(g) \tag{3}$$

with CO_2 as the supplier of oxygen to be incorporated.

The reaction pathway for incorporation of oxygen in mixtures of CO/CO_2 is suggested by Wærnhus et al. [13] and given in Tab 1.

Table 1. The reaction pathway of incorporation of oxygen in mixtures of CO/CO_2 suggested by Wærnhus et al. [13].

	Name	Elementary reaction
1	Adsorption	$CO_2 + S_{ad} = CO_{2,ad}$
2	Charge transfer #1	$CO_{2,ad} = CO_{2,ad}^- + h^{\bullet}$
3	Dissociation	$CO_{2,ad}^- + S_{ad} = CO_{ad} + O_{ad}^-$
4	Charge transfer #2	$O_{ad}^- = O_{ad}^{2-} + h^{\bullet}$
5	Reaction with vacancy	$O_{ad}^{2-} + V_O^{\bullet\bullet} = O_O^x + S_{ad}$
6	Desorption of CO	$CO_{ad} = CO + S_{ad}$

For the reaction pathway scheme given in Tab 1, step no. 3, dissociation, is suggested as the rate-determining step:

$$CO_{2,ad}^- + S_{ad} = CO_{ad} + O_{ad}^- \tag{4}$$

The rate of this reaction will show the same partial pressure dependency as the flux of oxygen entering/leaving the sample [15]. Hence:

$$reaction\ rate \propto j_{ex}^{0} = \frac{1}{4} k_0 C_O = \frac{1}{4} \frac{k_{chem}}{W_O} C_O \tag{5}$$

The comparison between k_{chem} and oxidation/reduction fluxes involves the thermodynamic factor, W_O, as introduced in Eq. (1). With the relations between the thermodynamic factors and their respective concentrations, $C_O W_V = C_V W_O$ [14], this means that the relation between W_O, C_O, k_{chem} and j_{ex}^{0} in Eq. (5) can be written as

$$k_{chem} = \frac{4 j_{ex}^{0} W_O}{C_O} = \frac{4 j_{ex}^{0} W_V}{C_V} \tag{6}$$

If the P_{O2} dependency of the oxygen vacancy concentration is sufficiently low, or if it is cancelled out by the P_{O2} dependency of the W_V, k_{chem} and j_{ex}^{0} will apparently have the same P_{O2} dependency. Thus, the comparison between k_{chem} and the model of Wærnhus et al. [13] originating from fluxes, will be straightforward. However, since numerical values for the thermodynamic factors are unavailable in this work, the comparisons are restricted to the shapes of the curves.

The rate expression for Step 3 in Tab 1, can be written as [13]

$$rate \propto \frac{P_{CO_2}}{p} \tag{7}$$

, where p is the electron hole concentration.

The rate expression in Eq (7) can be found by assuming the remaining elementary steps at equilibrium, which will "eliminate" the intermediates involved in the elementary reactions [13].

Eq (7) only deals with the oxidation part of the model. However, when the probable rate-determining step for the oxidation is identified, the proportionality of the reduction part can be calculated by the equilibrium condition saying that the oxidation and reduction fluxes are equal. This can be done by assuming the same reaction pathway as for the oxidation only in reversed order and with the same rate-determining step. From this the rate for the reduction part will be proportional to

$$rate \propto \frac{p\left[O_O^x\right]}{\left[V_O^{\bullet\bullet}\right]} P_{CO} \tag{8}$$

The rates given in Eqs (7) and (8) is the origin of the curve shape of the model proposed by Wærnhus et al. [13], since Eq. (7) is rate-determining in the high P_{CO} regions and correspondingly for Eq. (8) in the high P_{CO2} regions.

In Figs 5 and 6 solid lines have been included to give guides to the eye and elucidate the k_{chem} dependency in terms of the ratio between CO and CO_2. The similarity in the behaviour for k_{chem} against the P_{CO}/P_{CO2} ratio in STA-02 and STA-05 and the oxidation/reduction fluxes in Sr-doped $LaFeO_3$ is obvious [13]. Thus Eq. (4) suggests a probable rate determining step also for the system of Al substituted $SrTiO_3$.

In Fig 7 average values for k_{chem} are plotted for STA-02 and STA-05 at 1000 °C against the ratio CO/CO_2.

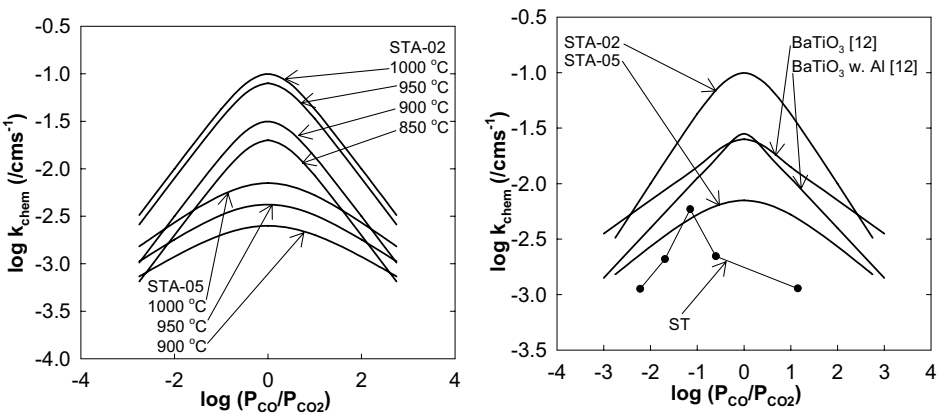

Fig. 7. a) Values for k_{chem} in CO/CO_2 mixtures for STA-02 and STA-05 at all temperatures, b) Values for k_{chem} in CO/CO_2 mixtures for STA-02 and STA-05 at 1000 °C with values for k_{chem} for ST from this work and for $BaTiO_3$ and $BaTiO_3$ with 1.8 mol % Al added, taken from Yoo et al. [12].

In Fig 7a it can be seen that values originating from STA-02 in general are higher than those from STA-05, i.e. increasing the Al content will decrease the k_{chem}. The same is seen in Fig 7b) where values at 1000°C for k_{chem} for pure and 1.8 mol % Al-doped $BaTiO_3$ from Yoo et al. [12] are included, together with reduction k_{chem} values for $SrTiO_3$. The values for k_{chem} in $SrTiO_3$ do not fall in the trend of lowering the k_{chem} with the introduction of Al in the sample. This is most probably due to the high uncertainty in the measurements of k_{chem} in this sample

Another aspect of Fig 7b) is that the $BaTiO_3$-system shows similar behaviour for k_{chem} against the P_{CO}/P_{CO2} as seen in this work and, again, a reasonable rate-determining step might be the dissociation (association) of a CO_2^- - specie as proposed by Wærnhus et al. [13].

CONCLUSION

The D_{chem} in ST and STA-02 showed a dependency on the partial pressure of oxygen, which is suggested to be due to the variation in the thermodynamic factors for oxygen vacancies (and thus for ions) with P_{O2}. This behaviour is also reported previously. The introduction of Al in the sample increases the value of D_{chem}. For STA-02 a sharp increase in the D_{chem} values in the CO-rich atmospheres were observed compared to the CO_2 – rich. This can be due to a phase transition/spearation at P_{O2} ~10^{-17} atm.

The k_{chem} values for STA-02 and STA-05 showed a maximum at a partial pressure of CO corresponding to 0.50 atm at all temperatures. This behaviour of the k_{chem}'s correspond well to a surface exchange reaction of oxygen with a rate determining step involving the dissociation of a charged and adsorbed CO_2 molecule. The same rate-determining step is probably present in $BaTiO_3$ as observed in the literature. From the $SrTiO_3$ and $BaTiO_3$ materials an observation of decreasing k_{chem} with the introduction of Al is evident.

ACKNOWLEDGEMENTS

Norsk Hydro ASA is acknowledged for financial support.

REFERENCES

1. Watterud, G., Julsrud, S. and Wiik, K.," Oxygen Transport in pure and Al-doped $SrTiO_3$ measured with electrical conductivity relaxation. Part I: In O_2/N_2 mixtures", Part III of this thesis
2. De Souza, R.A., Fleig, J., Merkle, R. and Maier, J., "$SrTiO_3$: a model electroceramic", Z.Metallkd. 94, No.3, (2003), 218-225.
3. Claus, J., Leonhardt, M. and Maier, J., "Tracer diffusion and chemical diffusion in acceptor doped $SrTiO_3$", J.Phys.Chem.Solids 61, (2000), 1199-1207.
4. Leonhardt, M., De Souza, R.A., Claus, J. and Maier, J., "Surface kinetics of oxygen incorporation into $SrTiO_3$", J. Electrochem Soc. 146, No.2, (2002), J19-J26.
5. Chan, N.-H., Sharma, R.K. and Smyth, D.M., "Nonstoichiometry in $SrTiO_3$", J.Electrochem Soc 128, No. 8, (1981), 1762-1769.
6. Eror, N.G. and Balachandran, U., "High-Temperature defect structure of acceptor doped strontium titanate", J.Am.Ceram.Soc. 65, No. 9, (1982), 426-431.
7. Walters, L.C. and Grace, R.E, "Diffusion of point defects in strontium titanate", J.Phys.Chem.Solids, 28, (1967), 245-248.
8. Song, C.-R. and Yoo, H.-I., "Chemical diffusivity of $BaTiO_{3-\delta}$: I: Experimental determination", Solid State Ionics 120, (1999), 141-153.
9. Song, C.-R. and Yoo, H.-I., "Chemical diffusivity of $BaTiO_{3-\delta}$: II Defect chemical analysis", Phys.Rev. B. 61, No. 6, (2000), 3975-3982.
10. Song, C.-R. and Yoo, H.-I., "Chemical diffusivity of $BaTiO_{3-\delta}$: III Conductivity-nonstoichiometry (δ) correlation in a mixed n/p regime", Solid State Ionics 124, (1999), 289-299.
11. Song, C.-R. and Yoo, H.-I., "Chemical diffusivity of $BaTiO_{3-\delta}$: IV Acceptor doped case", J.Am.Ceram.Soc. 83, No.4, (2000), 773-779.
12. Yoo, H.I., Song, C.-R., Lee, Y.-S. and Lee, D.-K., "Surface reaction kinetics in oxygen nonstoichiometry re-equilibration of $BaTiO_{3-\delta}$", Solid State Ionics 160, (2003), 381-387.
13. Wærnhus, I.," Defect Chemistry, Conductivity and mass transport properties of $La_{1-x}Sr_xFeO_{3-\delta}$ (x=0 and 0.1)" , Thesis, Norwegian University of Science and Technology, (2003).
14. Watterud, G., Wiik, K. and Julsrud, S., "Oxygen Transport in $La_{1-x}Sr_xCoO_{3-\delta}$ (x=0, 0.2 and 0.5) assessed with electrical conductivity relaxation. Part I: Bulk Diffusion and k_{chem}". Part I of this thesis.
15. Watterud, G., Wiik, K. and Julsrud, S., "Oxygen Transport in $La_{1-x}Sr_xCoO_{3-\delta}$ (x=0, 0.2 and 0.5) assessed with electrical conductivity relaxation. Part II: The mechanisms of oxygen surface exchange." Part II of this thesis

APPENDIX I

The mathematics of oxygen exchange and diffusion

The derivations presented in this appendix is rewritten from an unpublished internal note written by Wærnhus [1].

A response to stepwise change in oxygen activity

Consider a large plane sheet with sides A and thickness $2l_x$ (l_x<<A) in chemical and thermal equilibrium with the surrounding atmosphere. The initial oxygen concentration in the sample is C_0. At a given time, t=0, the oxygen activity (oxygen partial pressure), is changed to a new value which corresponds to a new equilibrium oxygen concentration, C_∞. The change in oxygen pressure causes a mass transport of oxygen into or out of the sample, depending on whether the pressure is increased or decreased. At any given time, t, and position, x ($-l_x < x < l_x$) the oxygen concentration in the sample is given by C(x,t).

By solving Fick's 2.law of diffusion, this concentration can be calculated

$$\frac{\partial C(x,t)}{\partial t} = D_{chem} \frac{\partial^2 C(x,t)}{\partial x^2} \tag{A.1}$$

, where D_{chem} is the chemical diffusion coefficient (with unit $cm^2\ s^{-1}$). Assuming linear interface kinetics, the boundary conditions are described by the oxygen flux through the surface.

$$J_O = \mp D_{chem} \frac{\partial C(x = \pm l_x, t)}{\partial x} = k_{chem} \left(C(x = \pm l_x, t) - C_\infty \right) \tag{A.2}$$

, where k_{chem} (cm s^{-1}) is the apparent surface exchange coefficient. The subscript "chem" denotes that there is a chemical gradient that causes the mass transport. The last boundary condition needed to solve Fick's second law is symmetry through the centre of the sample.

Using the following substitutions

$$C^*(x,t) = C(x,t) - C_0 \tag{A.3}$$

$$\Delta C = C_\infty - C_0 \tag{A.4}$$

the new equation and the new boundary conditions are given as:

$$\frac{\partial C^*(x,t)}{\partial t} = D_{chem} \frac{\partial^2 C^*(x,t)}{\partial x^2} \tag{A.5}$$

$$\mp D_{chem} \frac{\partial C^*(x = \pm l_x, t)}{\partial x} = k_{chem}(C^*(x = \pm l_x - \Delta C) \tag{A.6}$$

Equation (A.5) is solved in the Laplace domain. The Laplace transform L[f(t)]=f(s) of (A.5) gives

$$s\overline{C^*(x,s)} = D_{chem} \frac{\partial^2 \overline{C^*(x,t)}}{\partial x^2} \tag{A.7}$$

The Laplace transform of the boundary conditions given in Equation (A.6) are

$$\mp D_{chem} \frac{\partial \overline{C^*(x = \pm l_x, s)}}{\partial x} = \pm k_{chem} \left[\overline{C^*(x = \pm l_x, s)} - \overline{\Delta C} \right] \tag{A.8}$$

The general solution of Equation (A.7) is

$$\overline{C^*(x,s)} = Ae^{\lambda x} + Be^{-\lambda x}, \lambda = \sqrt{\frac{s}{D_{chem}}} \tag{A.9}$$

Inserting Equation (A.9) into Eq. (A.8) gives the values of A and B.

$$A = B = \frac{\overline{\Delta C}}{\cosh(\lambda l_x) + \frac{D_{chem}\lambda}{k_{chem}} \sinh(\lambda l_x)} \tag{A.10}$$

Backsubstitution of equation (A.10)into Eq.(A.9) leads to the solution in the Laplace domain.

$$\overline{C^*(x,s)} = \frac{\overline{\Delta C}\cosh(\lambda x)}{\cosh(\lambda l_x) + \frac{D_{chem}\lambda}{k_{chem}}\sinh(\lambda l_x)} \tag{A.11}$$

Solving for delta function gas exchange

Suppose the change in the oxygen activity in the ambient (Eq. (A.4)) is time dependent and can be described by the Dirac delta function [2]. This corresponds to a constant oxygen activity interrupted only by a peak of infinite height and zero extension. The change in oxygen activity can be described by Equation ((A.12)).

$$\Delta C(t) = \delta(t) + C_0 \tag{A.12}$$

The laplace transform of Eq (A.12) is

$$\overline{\Delta C} = \overline{\delta(t)} = 1 \tag{A.13}$$

The solution in the time domain of Eq (A.11)is found by a method described in Crank [3].

Suppose

$$\overline{C^*(x,s)} = \frac{f(s)}{g(s)} \tag{A.14}$$

where f(s) and g(s) is the numerator and the denominator of Eq (A.11) respectively. If g(s) = $(s-a_1)(s-a_2)\ldots(s-a_n)\ldots$where an is the solution of $g(a_n)=0$, $C^*(x,t)$ can be described as

$$C^*(x,t) = \sum_{a_n} \frac{f(a_n)}{\frac{dg}{ds}(a_n)} e^{a_n t} \tag{A.15}$$

The equation g(s)=0 can not be solved but the solution must satisfy

$$\Gamma_{n,x} \tan \Gamma_{n,x} = L_x = l_x \frac{k_{chem}}{D_{chem}} \tag{A.16}$$

The relations between a_n, λ and Γ_n is

$$a_n = \lambda^2 D_{chem} = -\frac{\Gamma_{n,x}^2 D_{chem}}{l_x^2}, \lambda = -\frac{i\Gamma_{n,x}}{l_x} \tag{A.17}$$

This gives

$$C^*(x,t) = C(x,t) - C_0 = -\sum_{n=1}^{\infty} \frac{2k\Gamma_{n,x}^2 \cos\left(\Gamma_{n,x} \cdot \frac{x}{l_x}\right)}{l_x \cos\left(\Gamma_{n,x}\right)\left(\Gamma_{n,x}^2 + L_x^2 + L_x\right)} e^{-\frac{\Gamma_{n,x}^2 D_{chem} t}{l_x^2}} \tag{A.18}$$

Solving for gas exchange as a discontious step

Suppose the change in axygen activity can be described by the unit step function also called the Heaviside function [3]

$$f(t) = \Delta C \cdot u(t) + C_0 \tag{A.19}$$

where u(t)= 0 when t<0 and u(t)=1 when t>0.

To solve for this gas exchange process, convolution can be used, since

$$\overline{C^*_{unit\ step}} = \overline{C^*} \cdot \overline{f(t)} \tag{A.20}$$

where C^* is defined in Eq (A.11). This leads to

$$C^*_{unit\ step} = \Delta C\left(C^* * f(t)\right) = \Delta C \int_0^t C^*(t') f(t-t') dt' \tag{A.21}$$

The solution will then be

$$\frac{C^*_{unit\ step}}{\Delta C} = \frac{C(x,t) - C_0}{C_\infty - C_0} = 1 - \sum_{n=1}^{\infty} \frac{2L_x \cos\left(\Gamma_{n,x} \cdot \frac{x}{l_x}\right)}{\cos\left(\Gamma_{n,x}\right)\left(\Gamma_{n,x}^2 + L_x^2 + L_x\right)} e^{-\frac{\Gamma_{n,x}^2 D_{chem} t}{l_x^2}} \tag{A.22}$$

The total change in the oxygen content can be found by integrating the concentration with respect to x across the sample from –l to l, giving

$$\frac{M(t)}{M_\infty} = 1 - \sum_{n=1}^{\infty} \frac{2L_x^2}{\Gamma_{n,x}^2\left(\Gamma_{n,x}^2 + L_x^2 + L_x\right)} e^{-\frac{\Gamma_{n,x}^2 D_{chem} t}{l_x^2}} \tag{A.23}$$

Solving for gas exchange as an exponential step

Suppose the change in oxygen activity can be described by an exponential function

$$f(t) = \Delta C\left(1 - e^{-\frac{t}{\tau}}\right) + C_0 \tag{A.24}$$

This approach has been done by den Otter et al. [4]. With use of the same procedure as for a unit step, the concentration profile can be calculated with convolution integral. In this case the convolution integral is given by

$$\int_0^t e^{-at'}\left(1 - e^{-(t-t')/\tau}\right) dt' = \frac{1}{a}\left(1 - \frac{-e^{at} + a\tau e^{-t/\tau}}{a\tau - 1}\right) \tag{A.25}$$

This gives the solution for the concentration profile

$$\frac{C^*_{\exp step}}{\Delta C} = \frac{C(x,t) - C_0}{C_\infty - C_0} = 1 - \sum_{n=1}^{\infty} \frac{2L_x \cos\left(\Gamma_{n,x} \cdot \frac{x}{l_x}\right)}{\cos\left(\Gamma_{n,x}\right)\left(\Gamma_{n,x}^2 + L_x^2 + L_x\right)} B(t) \tag{A.26}$$

where B(t) equals

$$B(t) = \left[\frac{e^{-\frac{\Gamma_{n,x}^2 D_{chem} t}{l_x^2}} - \frac{\Gamma_{n,x}^2 D_{chem}}{l_x^2}\tau e^{-t/\tau}}{1 - \frac{\Gamma_{n,x}^2 D_{chem}\tau}{l_x^2}}\right] \tag{A.27}$$

The total change in the oxygen content is then found by integrating Eq. (A.26) with the sample dimension as limits.

$$\frac{M(t)}{M_\infty} = 1 - \sum_{n=1}^{\infty} \frac{2L_x^2}{\Gamma_{n,x}^2 \left(\Gamma_{n,x}^2 + L_x^2 + L_x\right)} B(t) \tag{A.28}$$

$\Gamma_{n,x}$ is defined in Eq. (A.16)

An experiment in three dimensions

The process of incorporating oxygen or releasing oxygen in a sample can be given as

$$\frac{1}{2} O_2(g) + V_O^{\bullet\bullet} = O_O^x + 2h^{\bullet} \tag{A.29}$$

with Kröger-Vink notation [5]. In this case the sample is a p-type conductor. As long as the concentration of positive charge carriers (p) is higher than that of negative charge carriers (n) the change in conductivity will be proportional to the change in mass of oxygen. This can be described as [6]

$$\frac{\sigma(t) - \sigma_0}{\sigma_\infty - \sigma_0} = \frac{M(t)}{M_\infty} \tag{A.30}$$

Equation (A.30) relates electrical conductivity to the D_{chem} and k_{chem} given in equation (A.28).

The solution given in equation (A.28) is for one dimension. The solution in three dimensions is given by [3]

$$C(x,y,z,t) = C(x,t) \cdot C(y,t) \cdot C(z,t) \tag{A.31}$$

This leads to the solution in three dimensions

$$\frac{M(t)}{M_\infty} = \frac{M(x,y,z,t) - M_0}{M_\infty - M_0} = 1 - \prod_{j=x,y,z} \sum_{n=1}^{\infty} \frac{2L_j^2}{\Gamma_{n,j}^2 \left(\Gamma_{n,j}^2 + L_j^2 + L_j\right)} B(t) \tag{A.32}$$

The Γ's the and L's are defined in equation (A.16), and B(t) is given in Eq. (A.27). The subscript j means the dimension, instead of x, which gives the solution in the one-dimensional case.

References

1. Wærnhus, I., internal note on the mathematics of conductivity relaxation, NTNU, Trondheim, Norway, (2000).
2. Kreyzig, E., "Advanced Engineering Mathematics", 8th Ed , John Wiley & Sons (1999) pp 278
3. Crank, J., "The Mathematics of Diffusion", 2nd Ed. , Oxford Science Publications, (1975).
4. den Otter, M.W., Bouwmeester, H.J.M, Boukamp, B.A. and Verweij, H., "Reactor flush time correction in relaxation experiments", J.Electrochem.Soc. 148, (2001), J1.
5. Kröger, F.A., "The chemistry of inperfect crystals Vol. 2.", North-Holland Pub. (1974).
6. Yasuda, I and Hikita, T. , "Precise determination of the chemical diffusion coefficient of calcium doped lanthanum chromite by means of electrical conductivity relaxation", J.Electrochem.Soc. 141, No. 5, (1994), 1268-1273.

APPENDIX 2

The chemical potential of oxygen

The chemical potential of oxygen in the gas phase is given by IUPAC [1] and can be calculated with Eq. (A.33)

$$\mu_{O_2}^{gas} = \mu_{O_2}^{0,gas} + RT \ln\left(P_{O_2}\right)$$
$$\mu_{O_2}^{0,gas} = RT(n_1 + n_2 / T + n_3 \ln(T) + n_4 \ln\left(1 - e^{\frac{n_5}{T}}\right) \quad \text{(A.33)}$$

where T is in Kelvin and P_{O2} is in atmospheres and the coefficients n_1-n_5 is equal to
n_1= -1.225
n_2= -1.045· 10^3 K
n_3= -3.500
n_4=1.013
n_5= 2.242 ·10^3 K

References

1. IUPAC, commision on thermodynamics, “Oxygen, International Thermodynamic tables of the fluid state-9 ”, Blackwell Scientific, Oxford, (1987).